STUDY OF RAIN CHARACTERISTICS IN TROPICAL REGION EFFECT TO SATELLITE COMMUNICATION SYSTEMS

PRASIT NAKONRAT

A THESIS SUBMITTED IN PARTIAL FULFILLMENT OF

THE REQUREMENT FOR THE DEGREE OF

MASTER OF ENGINEERING IN ELECTRICAL ENGINEERING

SCHOOL OF GRADUATE STUDIES

KING MONGKUT'S INSTITUTE OF TECHNOLOGY LADKRABANG

2002

ISBN 974-9546-22-9

หัวข้อวิทยานิพนธ์	**การศึกษาลักษณะของฝนในเขตภูมิอากาศแถบร้อนชื้นที่มีผลกระทบต่อระบบการสื่อสารดาวเทียม**
นักศึกษา	**นายประสิทธิ์ นครราช**
รหัสประจำตัว	42061014
ปริญญา	**วิศวกรรมศาสตรมหาบัณฑิต**
สาขาวิชา	**วิศวกรรมไฟฟ้า**
พ.ศ.	2545
อาจารย์ผู้ควบคุมวิทยานิพนธ์	**รศ.ฉรงค์ เหมกรณ์**
อาจารย์ผู้ควบคุมวิทยานิพนธ์ร่วม	Prof. Yoshiaki Moriya

บทคัดย่อ

วิทยานิพนธ์นี้ นำเสนอผลการศึกษาลักษณะของฝนและการลดทอนของสัญญาณดาวเทียม เนื่องจากฝนในเขตพื้นที่ฝนตกชุกในเขตภูมิอากาศแถบร้อนชื้นของประเทศไทย แม้ว่าข้อมูลที่ได้จากการทดลองในภาคสนามนั้นจะเป็นข้อมูลเชิงสถิติระยะสั้นเท่านั้น แต่ในวิทยานิพนธ์ฉบับนี้นั้นนำเสนอไม่ใช่เพียงเฉพาะลักษณะโดยทั่วไปของการวิเคราะห์ข้อมูลแต่ยังนำเสนอการวิเคราะห์ในเชิงสถิติของข้อมูลฝนและการลดทอนเนื่องจากฝนอีกด้วย การกระจายของช่วงเวลาต่อเนื่องที่อัตราการตกของฝนและที่การจางหายของสัญญาณถูกแสดงให้เห็นโดยการวิเคราะห์ข้อมูลที่ได้และเปรียบเทียบกับโมเดลที่ได้มีการนำเสนอมาแล้ว การกระจายแบบมีเงื่อนไขแสดงให้เห็นความน่าจะเป็นของเหตุการณ์ทั้งจำนวนครั้งและเวลาต่อ 1 ปี ในกรณีที่อัตราฝนและค่าการลดทอนของสัญญาณดาวเทียมที่เกินกว่าค่าที่กำหนด นอกจากนี้แล้ว เมื่อพิจารณาที่ข้อมูลอัตราฝนช่วง 1 นาที ที่ได้จากการทดลอง และข้อมูลอัตราฝนช่วง 1 ชั่วโมง ที่ได้จากข้อมูลของกรมอุตุนิยมวิทยาแห่งประเทศไทยซึ่งเป็นข้อมูลเชิงสถิติระยะยาว ดังนั้นแล้วรูปแบบการแปลงข้อมูลสะสมอัตราฝนช่วง 1 ชั่วโมง ไปเป็น อัตราฝนช่วง 1 นาที จะถูกพิจารณาเพื่อให้ได้รูปแบบที่ง่ายและเหมาะสม

Thesis Title	Study of Rain Characteristics in Tropical Region Effect to Satellite Communication Systems
Student	Mr. Prasit Nakonrat
Student ID	42016014
Degree	Master of Engineering
Programme	Electrical Engineering
Year	2002
Thesis Advisor	Assoc.Prof. Narong Hemmakorn
Thesis Co-Advisor	Prof.Yoshiaki Moriya

ABSTRACT

This thesis presents rain and rain attenuation characteristics in high rainfall regions of tropical regions of Thailand. Even though experimental data obtained from experiment sites are short-term statistical data, not only general characteristics but also statistical characteristics of rain and rain attenuation are presented. Distributions of the duration of rain and signal fades are characterized by analyzing obtained data and proposed models. Conditional distributions are illustrated the probability of number and time of events per year of rain intensity and signal attenuation greater than given thresholds. In addition, 1-minute rain rate data available by examining measuring and 1-hour rain rate data obtained by meteorological department of Thailand that are long-term statistical data, proper and simple conversion method of 1-hour rain rate data to 1-minute rain rate distribution are considered.

ACKNOWLEDGEMENTS

Since this thesis was started, many persons have contributed their help and cooperation for the successful completion of it. I would like to take this occasion to express my appreciation to all of them.

Firstly, I would like to express my sincere thanks to my advisor and co-advisor, Assoc.Prof. Narong Hemmakorn and Prof. Yoshiaki MORIYA, respectively, who give me not only many helpful suggestions and useful advice but also cooperation for researching as co-researchers. I also appreciate them attention and stimulating the progress of this research.

I would like to appreciate Assoc.Prof. Nipha Leelaruji for hers helpful suggestion. Also I would like to thank to Prof. Matsuichi YAMADA for helpful suggestion during his short-term expert in KMITL. I am thankful to Assoc.Prof. Prakit Tangtisanon for contributed observation data of Ku band satellite communication at KMITL.

I would like to thank meteorological station staffs at Klong Yai for their cooperation in operating rain and rain attenuation observation experiment and good care for our equipment.

Specially thank to my colleagues in Satellite Communication Laboratory, ReCCIT, especially, Mr.Adit Decharat, Mr.Tikumporn BoonChuck and Miss Khajitphan Makaratut for their helpful in not only researching but also everything during doing master degree in KMITL. Also, thank to Dr. Suthichai Noppanakeepong and his advisees for helpful discussion.

Finally, this thesis is dedicated to everyone in my family, who always supports and encourages me for all in my life.

Prasit Nakonrat

TABLE OF CONTENTS

TABLE OF CONTENTS (to)

TABLE OF CONTENTS (to)

LIST OF FIGURES

LIST OF FIGURES (to)

LIST OF FIGURES (to)

LIST OF FIGURES (to)

LIST OF TABLES

CHAPTER 1

INTRODUCTION

1.1 Literature of Rain Effects

Rain affects the design of any communication or remote sensing system that relies on the propagation of electromagnetic wave through the lowest 10 km of Earth's atmosphere at frequency above 10 GHz. Communication systems may experience a loss of signal due to the attenuation caused by rain on radio link and be temporarily unavailable to use. Radar systems may experience a loss of signal from the target of interest or find the signal from that target to be of smaller amplitude than unwanted signal at the same apparent range produced by scattering from the rain. Scattering by rain may also introduce unwanted or interfering signal into communication system receiver that may mask the desired signal. The problem of system designer is the prediction or forecast of the effects of rain on radar, remote sensing, or communication system located anywhere on or above the surface of the Earth. As yet, the models and information needed to predict the occurrence of a rain event producing attenuation or available are not available covering all over the world. At some time in the future it may be possible to use numerical models for storm development and motion to predict the occurrence time, duration, and magnitude of rain event producing attenuation on a radio link. At the present, all we can do is predict the occurrence statistics of such events for typical month or year.

Communication systems are designed to available time or availability specifications for "any month" or for a typical year. Any month has been interpreted to mean the worst month in a typical year. With the added assumption that the underlying statistics for the rain process do not vary from one year to the next, any year is typical year. Current worry about climate change and climate dynamics would suggest that a temporal in variance in the statistics of rain should not be expected. Observations show that large year-to-year fluctuations occur in the measured time in a year an attenuation or scattered signal level threshold is exceeded. These variations are much larger than can be attributed to climate change. With in the statistical limitation of current observation produced by (1) limited length of record, (2) lack of continuity of record, (3) uncertainty in equipment calibration, and (4) limited equipment dynamics range, the assumption of stationary or invariance with time is justified when time is measured in number of entire years.

On shorter time scales or time intervals not spanning an integral number of year, seasonal effects are important and stationary can not be assumed [1].

Attenuation measurements have been made on terrestrial line-of-sight paths between antennas located on the surface of the Earth or between satellite and Earth terminals (Earth-space or slant paths). Attenuation values may also be inferred from multifrequency radar measurements of the variations in scattering cross section with range or from radiometric measurements of the emission of electromagnetic waves by rain and clouds. To obtain statistics for a path, the durations of the time intervals when the signals are attenuated be preselected amounts are tabulated for each rain occurrence or rain events and for all the rain events in each months and each year. Unfortunately, rain event data are not generally reported and only a small fraction of the monthly observations have been published. Extensive databases of annual and worst-month rain attenuation statistics have been prepared from observations published be the International Radio Consultative Committee [CCIR 1990d].

If a complete descriptions of the rain drop size, shape, orientation, and hydrometeor-type distributions were available for all locations and time, the attenuation and scattering on any path could be calculated for any system. In the absence of such data, especially, the lack of data in tropical region, models must be prepared to provide the best possible estimates given the information currently available. The problem is to take the available statistical information and make statistical predictions of the occurrences of events that affect the availability of desired communication or remote sensing services.

The user communities have different needs for statistics. When a new service is proposed. It is often sufficient to present a catalog of worst-case events. As the service becomes more mature, the request is for a more complete statistical description with perhaps seasonal or worst-month features taken into account. At this juncture, for application to fixed or mobile communications services, the need is for a description of cumulative distribution of the occurrences of attenuation in the worst month and in an average year for any location where a system may be built for any frequency allocated to the service. Because, at frequencies above 10 GHz, it is not expected that a single propagation path will provide the availability needed for many services, additional statistical information on the joint occurrences of attenuation events on spatially separated paths is needed. Noting that the use of coding be considered as a way to change fade margin dynamically, statistical predictions are needed for the durations of fading events and of the time intervals between fades within a rain event. For each set of statistics,

seasonal information is also needed. As system designers become more sophisticated, information on the risk associated with a particular design will also become necessary [1].

1.2 Objectives and Confinement of Thesis

In this study, even though, observed rain and rain attenuation data are classed into short-term statistical data, they are directly observed from the physical experiment. Morita has suggested that a better prediction is made by using only the mean annual rainfall as the meteorological data depending on area [2]. Therefore, the mainly purpose of this study is to effectively manipulate with such limited available data.

Conditional distributions of rainfall rate and durations [3] of rainfall rate data observed at Klong Yai, Trad and KMITL, Bangkok are investigated. Then, fade duration characteristics could be well expressed by log normal function with mean and standard deviation, $\overline{\ln D}$ and $\sigma_{\ln D}$, respectively [3].

1-hour to 1-minute rainfall rate conversion has been proposed by Karasawa [4,5]. Specified empirical parameters for the experiment locations are required. Therefore, in this thesis the empirical parameters are proposed for the experiment locations by using some high-ranking of 1-hour rainfall rate data and 1-minute rainfall rate data for 0.01 and 0.1 %.

There are two performance measures for satellite channel performance, channel capacity and BER degradation, in the presence of rain attenuation [6,7]. Firstly, the characteristics of attenuation distribution are tested with log-normal function. Then, channel capacity and BER degradation on satellite-to-ground links are investigated.

Firstly, chapter 2 introduces wave propagation through atmosphere on the satellite-to-ground links. Rain and precipitation induce degradation on communication system. In final section, the development and evaluating process of rain attenuation models are given.

In chapter 3, the obtained experimental data are basically analyzed and characterized. Experiment systems are given at first. Annual, monthly, hourly distributions and also worst-month in typical year are characterized. Fade duration characteristics are classified as number of single exceedances of rainfall rate and signal attenuation. Last section illustrates comparisons of rain attenuation characteristics between observed data and ITU-R model.

Chapter 4 proposes at first the method to obtain the correlation between rainfall rate and rain attenuation on the path links based on their cumulative distributions. Conditional distribution of rainfall rates and durations are illustrated both time and number distribution. Consequently, the

number distributions are modeled by log-normal distribution. Finally, 1-hour to 1-minute rainfall rate conversion model is proposed.

Chapter 5 presents the satellite channel performance in the presence of rain attenuation in the experiment locations, Bangkok and Trad. Rain attenuation model, channel capacity and BER degradation on satellite links are respectively contained in this chapter.

Chapter 6 summarizes the materials that are obtain in the previous chapters and includes the discussion for further works.

CHAPTER 2

ATMOSPERIC EFFECTS ON THE PROPAGATION OF RADIOWAVE

The success of any communication depends on the influences of the propagation medium, especially, propagation in space since terrestrial to satellite-to-ground communication systems that atmospheric phenomena and terrain mainly effect on their mediums. The degree to which these influences affect propagation depends on the frequencies of the waves and, in some cases, also on the polarization. The effects of precipitation on the transmission path are of major concern in space communications, particularly for those systems operating at frequencies above 10 GHz. Precipitation can be many forms in the atmosphere. Hydrometeor is general term referring to the products of condensed water vapor in the atmosphere, observed as rain, clouds, fog, hail, ice, or snow. The presence of hydrometeors in the radio path, particularly rain, can produce major impairments to space communications. Raindrops absorb and scatter radiowave energy, resulting in signal attenuation, which can degrade the reliability and performance of the communications links.

2.1 Wave Propagation in the Atmosphere

The frequency range from 1 GHz to about 30 GHz is often referred to as the 'microwave' band (paralleling the notations 'long wave', 'medium wave' and 'short wave' most often used in relation to the broadcasting bands within LF, MF and HF, respectively).

Perhaps the most frequently encountered distinction of atmospheric influences is between those of the troposphere and those of the ionosphere (to be discussed later). The troposphere is the lowest region of the atmosphere, in which temperature generally decreases with height. Its upper height limit (the base of the tropopause, in which the temperature ceases to decrease with height, is about 17 km at the equator and 9 km at the poles. The height of the tropopause varies with the atmospheric conditions: for instance, at medium latitudes it is about 13 km in high-pressure zones (anticyclones), declining to less than 7 km in depressions. In clear air, the radio refractive index of the troposphere is slightly greater than unity (typically about 1.0003). The way in which the refractive index changes with height has much consequence for radiowave propagation at

frequencies greater than about 30 MHz, and, at frequencies greater than about 10 GHz, the absorption and scatter due to clouds, rain, snow etc. which occur in this region also have much effect. Fig. 2.1 illustrates some of these effects, separating the clear-air effects from those due to clouds and precipitation [8].

Table 2.1 Part of the electromagnetic spectrum

Frequency range	Wavelength	Descriptive designation	
Below 3 kHz	Above 100 km		ELF
30-300 kHz	10-100 km	Myriametric waves	VLF
30-300 kHz	1-10 km	Kilometric wave	LF
300-3000 kHz	100-1000 m	Hectometric waves	MF
3-30 MHz	10-100 m	Decametric waves	HF
30-300 MHz	1-10 m	Metric waves	VHF
300-3000 MHz	10-100 cm	Centimetric waves	UHF
30-300 GHz	1-10 mm	Milimetric waves	EHF
300-3000 GHz	0.1-1 mm	'Sub-milimetric waves'	
3-30 THz	10-100 μm	'Far-infrared waves'	
30-430 THz	0.7-10 μm	'Near-infrared waves'	
430-860 THz	0.35-0.7 μm	'Optical waves'	

Above 30 MHz the wavelength is comparable with the distance over which variations of atmospheric refractive index occur in the troposphere. These variations are due to changes of temperature, pressure and humidity. The refractive index of the troposphere generally decreases with height. This leads to a slight downward reflection of radio rays, which can be very important for communication at VHF, UHF and EHF. If the rate of refractive index decrease with height is sufficiently large and extends over a sufficient height interval and horizontal extent, it may give rise to atmospheric ducts that guide radio energy far beyond the normal horizon. Normal duct heights are such that complete trapping within them occurs only at centimetric wavelengths, but partial trapping (and very rarely total trapping) may also be found at the shorter metric wavelengths.

If, over a large horizontal area, the refractive index decreases with height abruptly, this may lead to partial reflection of radio energy. Both ducting and partial reflection mechanisms may cause multipath interference on line-of-sight or interpath interference on beyond horizon

links. Randomly distributed small-scale spatial fluctuations of refractive index about the local mean value cause weak signal levels always to be present at large distances beyond the horizon.

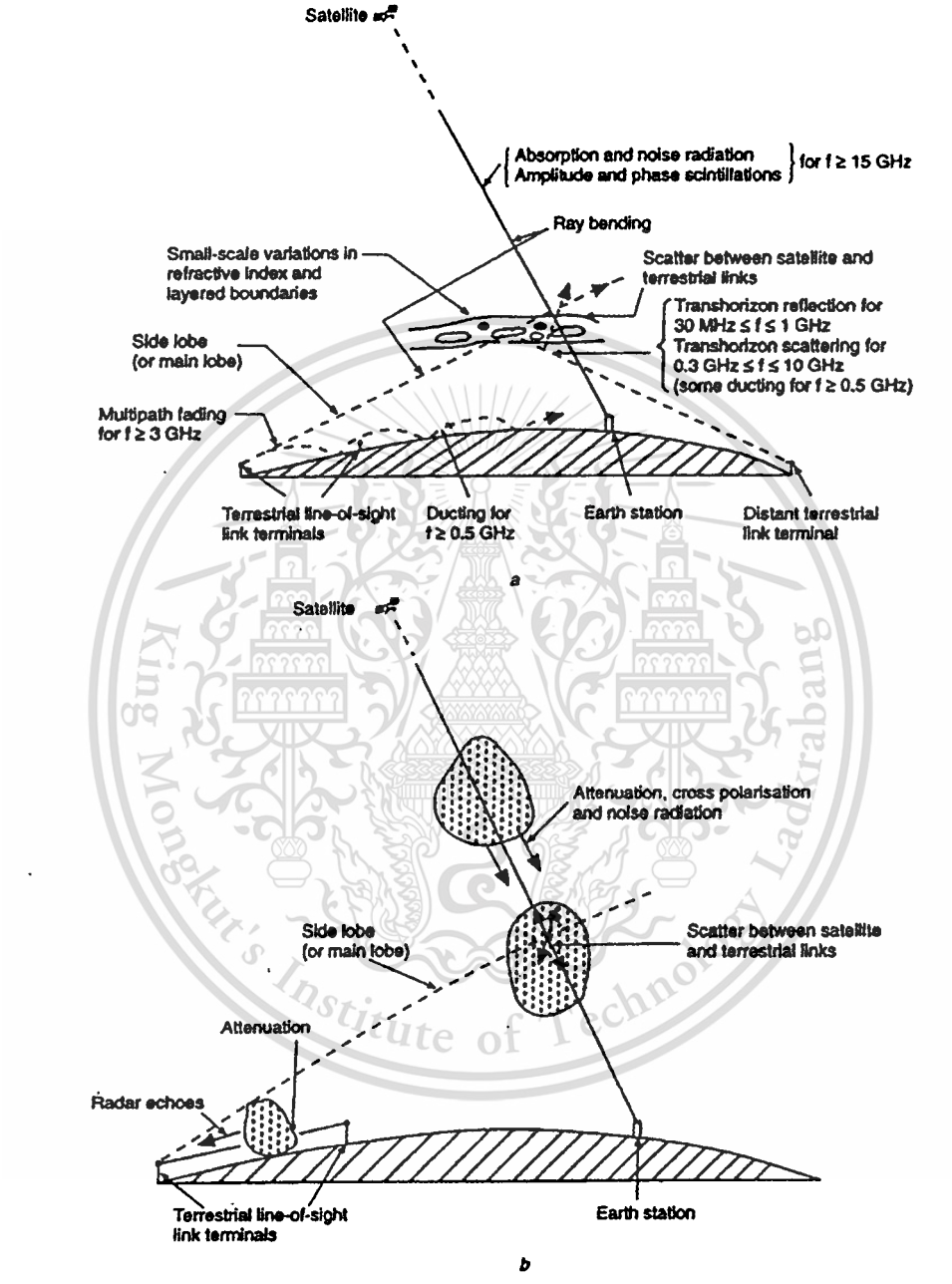

Fig 2.1 Some effects of the troposphere on radiowave propagation

(a) Effects of atmosphere gases (clear air) and associated refractive index changes

(b) Effects of could and precipitation (above 3 GHz)

This is due to tropospheric scattering from the irregularities, and such scattering may be used to provide radio communication over several hundred kilometres. On line-of-sight paths, these

refractive index fluctuations may cause significant scintillation (rapid fading), which is larger in magnitude for longer range or higher frequency.

For two terrestrial radio terminals within line-of-sight, there may often be a ground-reflected ray in addition to the direct ray. There may also be a reflected ray (or more than one) from layers of abrupt change of refractive index with height. According to their relative phase, the 'multipalh' contributions may give rise to slow signal enhancement or fading. For UHF, the abruptness of change with height must be greater than for VHF, but the reflecting surface area may be smaller. The latter means that relatively small terrain features may cause significant reflection at SHF.

The effect of obstacles such as hills, buildings or trees depends on the wavelength considered. Such obstacles cause reflection (and multipath), scatters, diffraction and absorption. In a built-up area this results in a wide variation in field strength. The losses caused by absorption and scattering increase with frequency, until, at frequencies above UHF, walls or masonry more than about 20cm thick may be regarded as opaque, together with buildings (except those of very light construction) and woods which are visually opaque.

If one (or both) of the terminals is mobile, or vehicles are moving nearby, the relative phases (and amplitudes) of multipath contributions cause a rapid fading, and there is also some Doppler shift of frequency. Such multipath propagation is more prevalent in city areas than rural areas.

At frequencies greater than 3 GHz. rain or cloud may give rise to significant absorption and scattering of radio energy. Such absorbing media also generate thermal noise that may be important in Earth-space systems. Scattering from cloud or precipitation (hydrometeors) may cause considerable interference between systems, but even in clear air the absorption by atmospheric gases alone, and the associated noise radiation, are important for frequencies greater than about 20GHz. (For the radio scientist, 'clear air' does not necessarily imply, high optical visibility, as 'hazy' conditions with high water vapour attenuation and scintillation are included whilst fog and other hydrometeor conditions are not.) Fig. 2.2 gives an indication of the relative importance of rain, fog and atmospheric gases in the centimetric wavelength to visible regions of the spectrum. The onset of these effects is quite rapid, but now, as a result of the continuing demand for radio frequency bandwidth, much effort is going into exploring the potential use of the 'windows' (and even the absorption peaks) in the millimetric- and submillimetric-wave range. Optical visibility in fog or cloud for 0.1 and 1 gm^{-3} (as shown in Fig. 2.2) is about 250 and 50 m,

respectively. The three levels of rainfall rate indicated correspond to light drizzle, moderate rain and very intense rain; there is very large variation in the different regions of the world for the time percentages for which such rainfall rates may be expected.

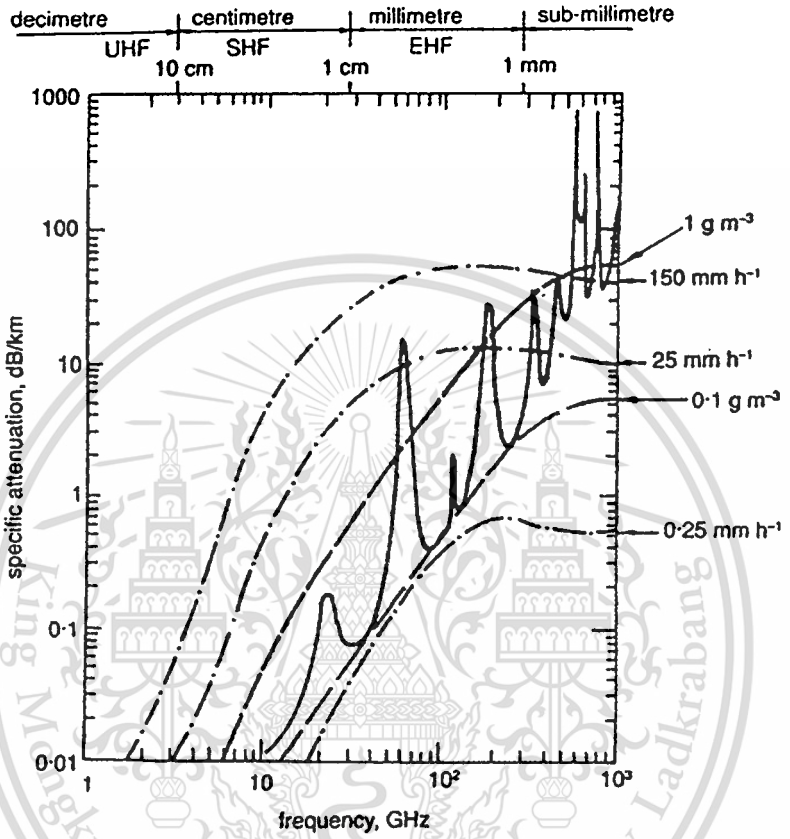

Fig. 2.2 Comparison of specific attenuation due to gaseous constituents, fog and precipitation near the Earth's surface

——— gaseous attenuation calculated assuming 1013 mb, 20 °C, 7.5 g/m^3

—·—·— rain attenuation for rate shown

– – – – fog attenuation for water content shown, at 20 °C

The ionosphere is the region of the atmosphere in which ionisation of gases (i.e. the concentration of free electrons) is particularly intense, and it extends from heights of approximately 60 km to 600 km. Fig. 2.3 shows regions of the atmosphere in terms of the temperature profile. It also shows the layers of the ionosphere. This region takes a major control on radiowaves at frequencies below about 30 MHz, and radio paths operating at frequencies up to a few hundred megahertz can occasionally encounter severe disruption from ionospheric effects.

The ionisation is caused by ultraviolet radiation from the sun acting in a height region where the molecular density is sufficiently low that recombination is not rapid. There are three main ionisation layers, designated by Sir Edward Appleton by the symbols D, E and F, in ascending height order. They vary in height and intensity according to the time of day, the time of year and the latitude. The typical diurnal variations of the E and F layers are indicated in Fig. 2.4. The D layer is not directly comparable since it does not display reflection at near-vertical incidence, and so its height (about 70 km by day and 90 km by night) cannot be expressed in terms of a 'virtual height', the height from which rays appear to be reflected, (i.e. if the velocity were the same as in free space).

In general at frequencies between about 3 kHz and 30 MHz, two types of propagation enter into consideration: ground wave propagation along the Earth's surface and indirect *sky wave* (or 'ionospheric wave'). The attenuation with distance of a ground-wave signal depends on the characteristics of the ground and the radio frequency. This attenuation is lower over surfaces with a high conductivity, such as the sea. At VLF, ground waves are propagated to large distances, whereas they can be used over only very short distances at HF. Some of the behaviour of sky waves at HF is indicated in Fig. 2.5. Below a certain 1 'penetration' frequency, and for a given launch angle, rays will be reflected back to Earth. Ionospheric refraction is less for higher frequencies and for higher elevation angles. As the elevation angle is increased, the height of reflection is increased, reaching a maximum for vertical incidence.

If, now, the frequency is increased, the height of reflection increases, and eventually, at the critical frequency, the ray will penetrate the ionospheric layer, this critical frequency being dependent on the maximum electron density of the layer. For frequencies somewhat below the critical frequency, rays transmitted with a zenith angle below a certain critical angle will be reflected back to ground. Some energy is scattered from the ground back along the tracks to the transmitter site, and some energy is scattered forward (or reflected forward). 'High rays' and 'low rays' may arrive together at distances beyond a skip distance within which no signals are received. In addition, some energy is scattered back from ionospheric irregularities, and some is absorbed.

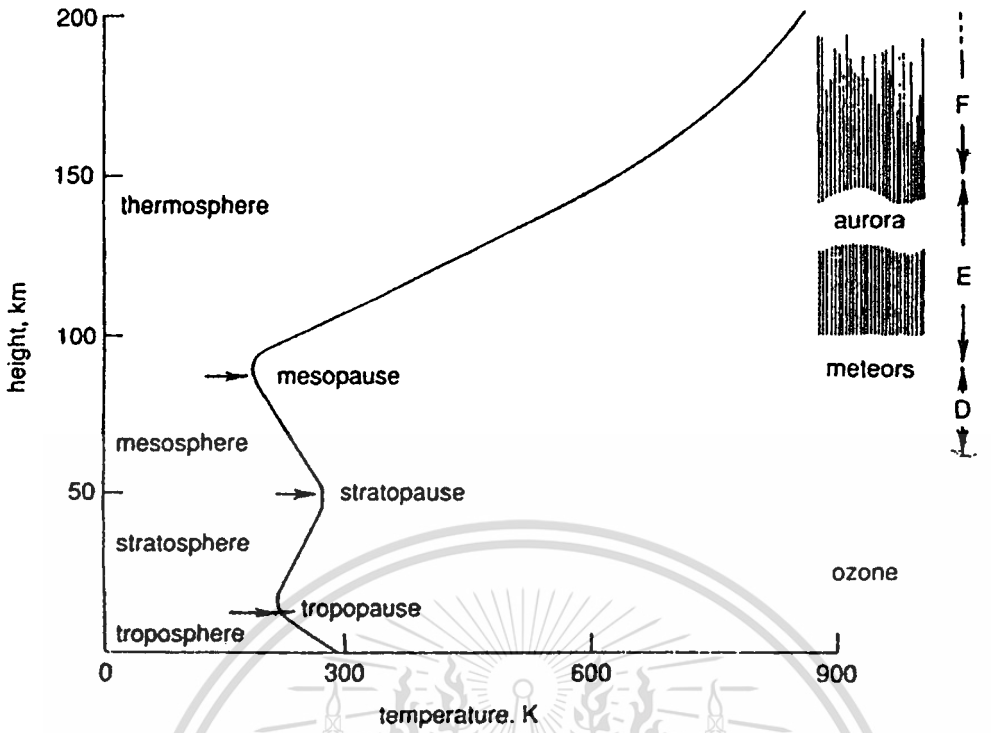

Fig. 2.3 Region of the Earth's atmosphere, showing the mean temperature profile, approximate heights of ionospheric region and other features.

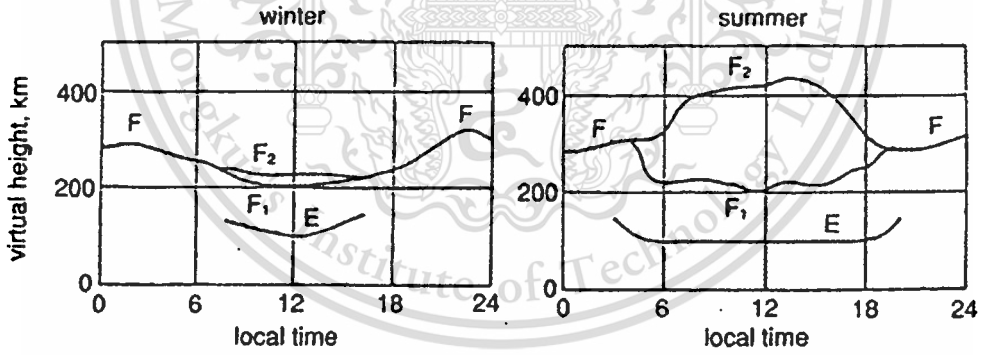

Fig 2.4 Typical diurnal variation of ionospheric layer

For transmission from one point on the Earth's surface to another, there will be a maximum usable frequency, less than the 'penetration frequency' and increasing with path distance. Because these characteristics depend on the ionisation density along the path in the ionosphere, which in turn depends on the amount of ultraviolet radiation received, they will also depend on the latitude, time of day, season of the year and point in the 11-year sunspot cycle. They will also be affected by bursts of radiation from solar surface eruptions, known as solar flares, and by bursts of streams of particles from the sun causing ionospheric storms.

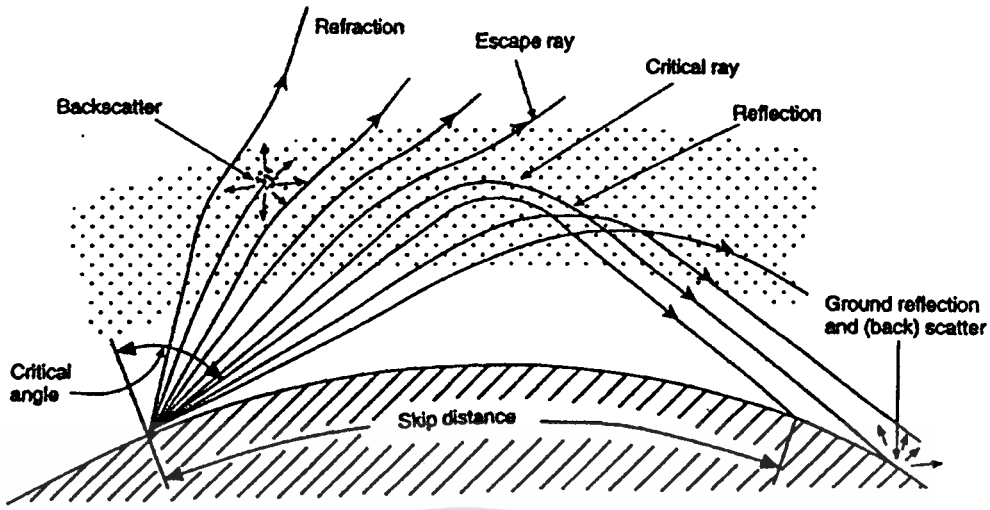

Fig. 2.5 Dependence of ionospheric rays at HF an angle of incidence

At HF and VHF it may be possible to distinguish the ground wave as having a Norton surface-wave component and a space-wave component. The surface wave travels close to the ground and is diffracted by it to follow the surface of the Earth. 'Close' here means in terms of the wavelength, so that the surface wave may occupy the space below the ionosphere at VLF. By contrast, the surface wave is very near the surface and highly attenuated at UHF (and above), and if the antennas are a wavelength or more above ground, as is normal at these frequencies, the surface wave may be neglected in comparison with the space wave. When considering VHF line-of-sight effects, it is mentioned that the space wave is made up from a direct wave and a ground-reflected wave. At MF it is not useful to separate the surface wave, direct wave and ground-reflected wave, but the ionospheric (sky) wave is distinct in leaving the transmitter in an upwards direction. A space wave is not distinguishable at low frequencies when the antenna height is low compared with the wavelength. The direct and ground-reflected waves then have equal magnitude and opposite phase and so give an almost zero resultant.

The amount of diffraction of the surface wave around the Earth depends on the ratio of the wavelength to the radius of the Earth, decreasing steadily as the wavelength is decreased. This wavebend is strengthened by the wavefront having a slight forward tilt due to a proportion of the radio energy propagating into, and being absorbed, by currents induced in the Earth. The rate of absorption, and so the rate of attenuation of the wave travelling above the Earth's surface, depends on the conductivity and permittivity of the ground. These characteristics differ considerably for different types of ground. At low frequencies the surface wave is mainly dependent on conductivity and is strongest for high conductivity. At higher frequencies a high permittivity is

the important factor in giving a strong surface wave. Thus for all frequencies surfacee-wave propagation is best over sea and worst over dry land.

Although (as mentioned above) the direct wave and ground-reflected wave almost cancel for an antenna low to the ground (compared with the wavelength), there is a pronounced phase delay to the reflected ray (relative to the direct ray) as the antenna is raised above the ground. The space components become increasingly important, and the resultant field must be calculated as the vector sum of the space and surface waves. Although there may be only a slight increase in signal at first, there comes a region at which the rate of signal increase with height is almost constant before it falls off again. The rate of signal increase with height is referred to as the height-gain factor. It is a function of the ground conductivity and permittivity, the polarisation and the frequency. It is larger over sea than over land, and larger at VHF than HF. In addition, relative phase changes of the direct and reflected rays produce a series of maxima and minima.

Above 30 MHz the ionosphere becomes increasingly permeable to the sky wave as the frequency rises, and, except for occasional sporadic E layer effects, it may be considered that the ionosphere ceases to act as a reflector. However, space-to-Earth paths do continue to experience some ionospheric-scintillation and Faraday-rotation effects.

2.2 Nature of Precipitation and Cloud

Water appears in the atmosphere in a variety of form, usually referred to by the term 'hydrometeor', which includes particles as diverse as cloud, rain drops, snowflakes, ice crystals, hail and graupel. Of these, rain, hail, graupel and snow are generally recognised as 'precipitation'. The effects that hydrometeors have on communications systems are dependent both on the system frequency and the type of particle present. At any given instant, of course, more than one type of particle will effect a given link. For example, an Earth-space link may often encounter rain over the lower part of its path, and snow at greater heights [8].

2.2.1 Riandrop-Size Distribution

In modelling the effects of rain on radio waves propagating through it, or scattered from it, the usual problem is to numerically relate two physically distinct quantities. For example, we might wish to relate a microwave specific attenuation to a rainfall rate or to a radar reflectivity, a rainfall rate to a reflectivity, or a differential attenuation between two polarisations to an absolute attenuation in one etc. All these quantities are obtained as integrals over the drop-size-distribution function $N(D)$, defined such that $N(D)dD$ is the number of drops per cubic metre with drop

diameters D between D and $D + dD$. (As all but the smallest drops are nonspherical, D is usually defined as that of an equivolumic sphere.) Nearly always the contributions to the two quantities to be related have a different D dependence, and some assumptions about the shape of the function $N(D)$ must be made.

Satisfactory results are generally obtained by using an ideal mathematical form for $N(D)$, described by a small number of free parameters. Large departures from the ideal forms undoubtedly occur in real rain, but the situation is eased by the fact that relationships between quantities are, in practice, often only required to hold on a mean statistical basis. Also fine structure in $N(D)$ tends to disappear in the integration.

Much modelling to date has used an exponential form for $N(D)$ of the form

$$N(D) = N_0 \exp(-\Lambda D) \tag{2.1}$$

Early work indicated that Λ tended to increase with rainfall rate R, and that these distributions could be reduced to a one-parameter family by treating the relation as deterministic, with

$$\Lambda = 4.1\, R^{-0.21} \qquad (\Lambda \text{ in mm}^{-1}, R \text{ in min}^{-1}) \tag{2.2}$$

Once Λ is determined from R, so is N_0 by the requirement that the integral of $N(D)D^3V(D)$, where V is the drop terminal velocity, actually gives R. Typical values of N_0 were found to be around 8000 $\text{mm}^{-1}\text{m}^{-3}$, with this form of distribution becoming known as the Marshall-Palmer distribution. The parameter A can be shown to be related to the median volume drop diameter of the distribution Do through the relation

$$\Lambda = 3.67 / D_0 \tag{2.3}$$

The Laws-Parsons distribution, which predates the Marshall-Palmer one and is also much used, is an empirically measured form for $N(D)$ which is tabulated numerically rather than expressed mathematically. It is similar to the Marshall-Palmer form except that it has slightly fewer small drops.

Subsequent work which followed the development of disdrometers (instrurnents capable of automatically recording the size distribution of drops), showed that N_0 could, in fact, vary quite

considerably, both from one event to another and even within a rain event. In addition, the shape of the distribution was also found to vary significantly, which led to a more general form of distribution, the gamma-type distribution, being proposed [9]. This takes the form

$$N(D) = N_0 D \exp\{-(3.67 + m)\, D / D_0\} \tag{2.4}$$

Positive values of m reduce the numbers of drops at both the large and small ends of the size spectrum, compared with the exponential distribution obtained when $m = 0$. In contrast, negative values of m increase the numbers of drops at each end of the spectrum. Fig. 2.6 shows this effect for three different distributions, all with the same rainfall rate (5 mm h^{-1}) and the same D_0 (1 mm).

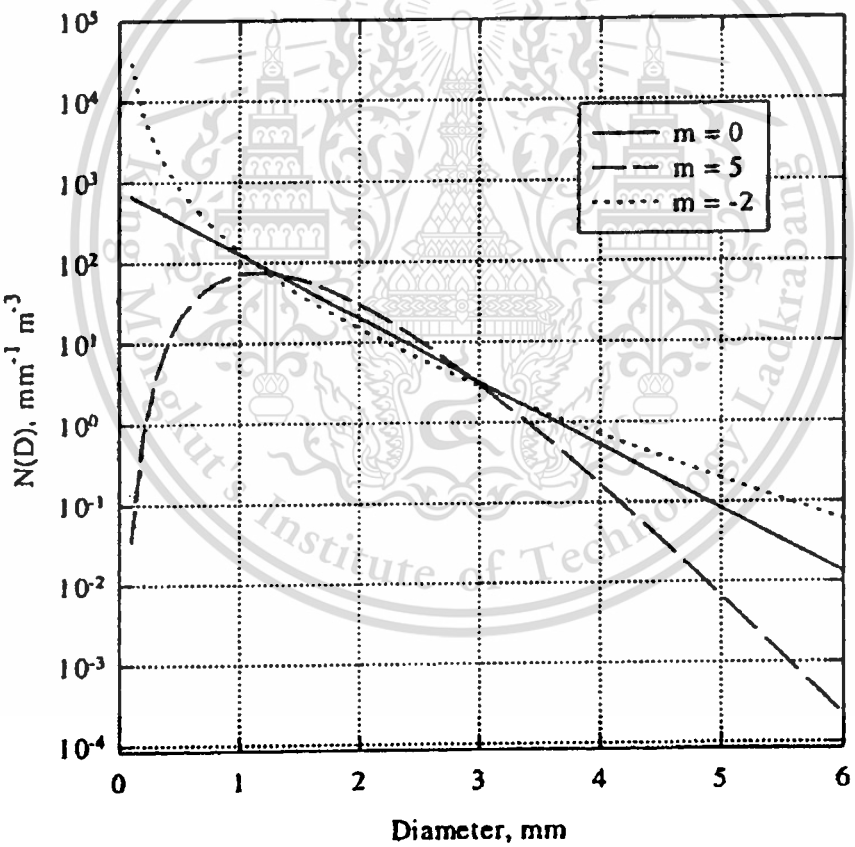

Fig. 2.6 Example of three different drop-size distributions, with a rainfall rate of 5 mm h^{-1}, and a D_0 value of 1 mm

Note from Fig. 2.6 that the three distributions have very different numbers of small and large drops, but the same integrated rainfall rate. The reason for this can be seen in Fig. 2.7,

which indicates the contribution from each drop size to the total rainfall rate. For example, drops between 1 and 2 mm. Diameter contribute 60% of the total rainfall rate of 5 mm h^{-1}.

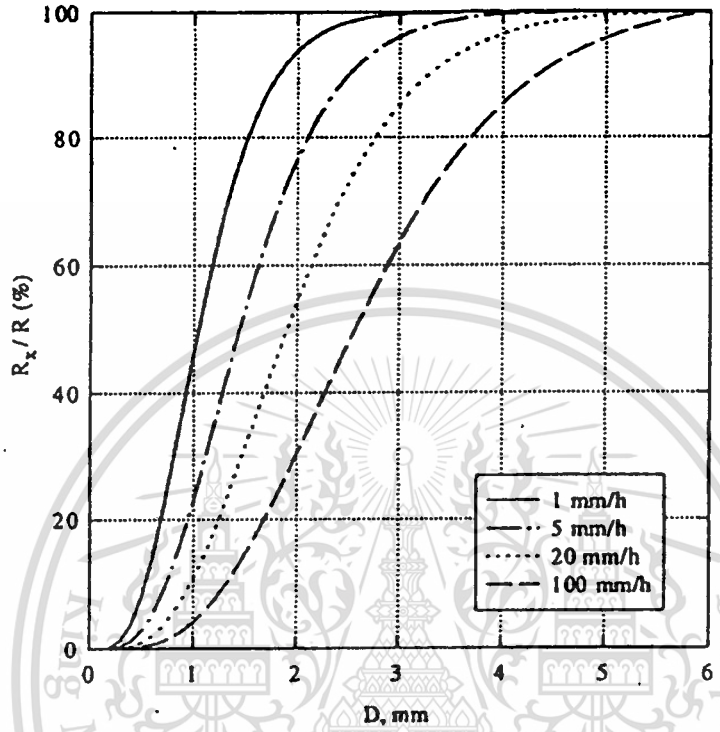

Fig. 2.7 Contribution of different drop size to integrated of rainfall rate, for various exponential drop-size distribution with N_0=8000 $mm^{-1} h^{-3}$

It must be stressed that there is at present no single model for drop-size distributions which is generally accepted as representing physical reality, even as a statistical mean over many rain events. Observations of quantities that are very sensitive to large drops, such as radar differential reflectivity, and certain crosspolarisation measurements, have tended to indicate the presence of fewer very large drops than in an exponential distribution. They have been well fitted using a gamma distribution with *m* between *3* and 5. This model, incidentally, reduces the assumed density of small drops (below 1 mm diameter) even though the experimental data may have little to say about them. Other measurements, particularly of attenuation at 30-300 GHz, are more sensitive to small drops and make no strong implication about the presumed large-drop cutoff, while work in the UK has suggested that a log-normal form of distribution would be appropriate for millimetric attenuation prediction [10]. Deductions about small drops have sometimes been contradictory [9, 10]

It has generally been found that the Marshall-Palmer distribution is satisfactory for statistical predictions of attenuation in the 10-30 GHz range, if not on an event-by-event basis, and probably remains a good guess for statistical work at slightly higher frequencies. Fortunately, for particular modelling purposes it is not essential that the assumed distribution represents physical truth at all drop sizes.

2.2.2 Liquid-Water Clouds and Fog

Nonprecipitating clouds containing only liquid water are not very significant for frequencies below about 100 GHz. The liquid-water content is too low to cause much absorption of energy; the droplets are too small to cause much scattering of energy and, being virtually spherical, do not cause measurable crosspolarisation. The most useful parameters to note here are:

(i) Liquid-water content

typical in small cumulus clouds: 0.5 gm^{-3}

stratiform clouds: 0.05-0.25 gm^{-3}

cumulus congestus and cumulonimbus: 0. 5-2.0 gm^{-3} (extreme);

(ii) Droplet size

small cumulus: may particles 3-10 μm radius, few above 35 μm; those in range 15-30 μm contribute about half the total volume

cumulus congetus and cumulonimbus: large number of particles in the range 10-20 μm, with few above 80 μm. Particles in the range 20-45 μm contribute about half the total volume.

The liquid-water content typically peaks about 2 km above the cloud base and then decreases towards the top of the cloud which may be several kilometers higher.

Fog can be considered to have similar physical properties to cloud, except that it occurs nearer than the ground.

2.2.3 Ice Hydrometeor

There is an enormous variety of forms of atmospheric ice particles, and the physics of their formation is extremely complex. However, some simple classifications may be made for radio purposes. Harden et al. [10] give a much more detailed discussion.

2.2.3.1 Ice Crystals

From the radio-propagation point of view, single crystals at high altitudes appear to be the most important form of atmospheric ice, as they give rise to crosspolarisation effects. *A* very crude picture, which nevertheless appears adequate to interpret radio effects (particularly crosspolarisation), is to divide them broadly into 'plate' and 'prism' (or needle) forms. The first group includes simple hexagonal plates with typical diameters up to 0.5 mm and thicknesses perhaps one-tenth of the diameter, and the classical dendritic form with complex hexagonal symmetry. The latter may reach 5 mm. in diameter, with a thickness probably less than 0.05 mm. The second group includes a variety of long thin shapes including both needles and hexagonal prisms; typical lengths are around 0.5 nun, and the ratio of length to breadth ranges from one to five. For modelling radio scatter when the crystals are small compared with the wavelength, treating them as either very oblate or very prolate spheroids can make a start.

The type of crystal depends in a complex way on the temperature at which it formed, and hence on the height. In the range -8 to -270 °C, plate types are typical, with dendrites dominant in the subrange -14 to -17 °C. Below -27 °C prisms are formed. Both classes can form in the 0 to -8 °C range, but they are probably less important for propagation, except where differential phase effects are of concern.

2.2.3.2 Snow

This consists of aggregated ice crystals, with large flakes forming only at temperatures just below freezing, when the crystal surfaces become particularly 'sticky'. In stratiform rain most of the ice is present as large flakes down to a few hundred metres above the melting level, while at greater heights single crystals are mainly present. Dry snow does not appear to be very important for propagation of radio waves, at least below 30 GHz. This is partly because of its low-density structure (generally around 0.1 gm^{-3}), giving it a permittivity close to unity, and (for polarisation effects) partly because the flakes tend to tumble without a preferred orientation.

2.2.3.3 Hail and Graupel

These particles are mainly formed by the accretion of supercooled cloud droplets in convective storms. Hail particles have densities close to water, and are often of roughly spherical shape, although a wide variety of shapes have been recorded. Graupel has a density intermediate between hail and snow and is usually of conical shape. Although of a higher apparent permittivity than snow, dry hail and graupel are only weakly attenuating below 30 GHz and do not appear to

be very important for wave-propagation effects. However, when they begin to melt, they scatter like very large raindrops. Noticeable polarisation effects might be expected but these seem to be of little significance on a statistical basis, at least in a climate such as that of the UK.

2.2.3.4 Melting Layer

In stratiform rain, partially melted snowflakes exist within a height interval of about 500 m around the 0 °C isotherm. The melting particles combine a large size with a large apparent permittivity, and have a high spatial density because of their relatively small fall velocity. The melting layer thus produces intense radio-scattering effects. An example of this is shown in Fig. 2.8, where the 3 GHz backscattered-radar reflectivity is shown as a function of height during a typical stratiform rain event.

Also shown in the Fig. 2.8 is the difference in scattered power between horizontal and vertical polarisation, where it can be seen that the large melting snowflakes scatter the horizontal polarisation much more strongly than the vertical, because of their much larger horizontal dimensions.

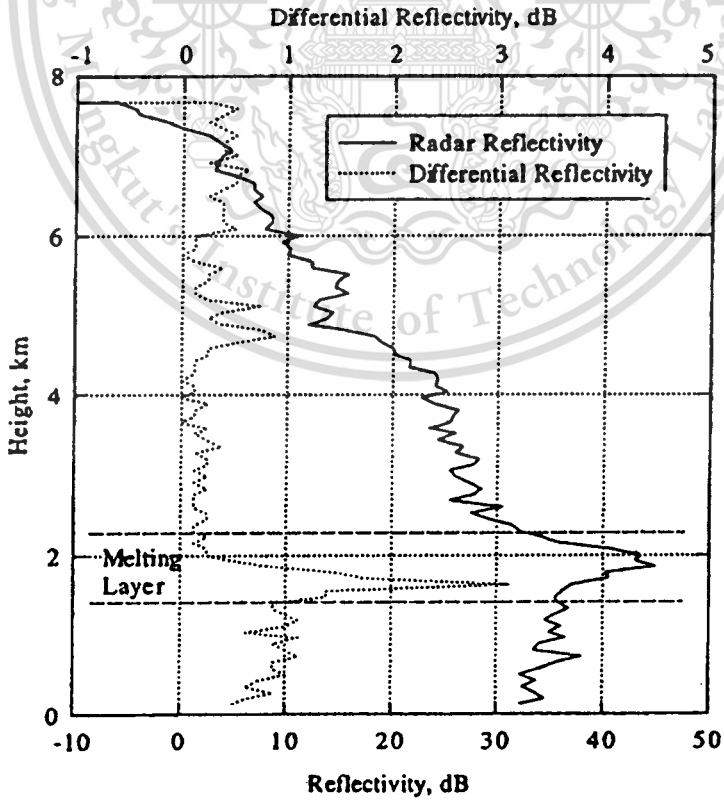

Fig. 2.8 Radar reflectivity and differential reflectivity (as function of height) obtained with the Chilbone radar

Although effects of the melting layer on most Earth-space paths are small because of the limited length of path within the layer, in climates such as the UK it is likely that terrestrial-link paths frequently traverse large lengths of melting layer and could be subject to more attenuation than expected from the rain fall rate seen at the ground.

Above the melting layer, the lower permittivity of snow reduces the magnitude of differential scatter to close to zero, except where, as near 5 km. height, there are significant quantities of highly asymmetrical ice plates. Below the melting layer, oblate raindrops produce significant differential scatter, in this case of the order of 1 dB. In this example, the changes in reflectivity and differential reflectivity with respect to height within the rain are due to wind-shear effects, rather than, for example, evaporation.

2.2.4 Hydrometeor Scattering Theory

2.2.4.1 General

The far field scattered from a particle is commonly described by a dimensionless function S of the scattering angles [11], and is defined by

$$E_{scat} = E_{inc} S\left\{\frac{(\theta,\varphi)}{jkr}\right\}\exp(-jkr + j\omega t) \qquad (k=2\pi/\lambda) \qquad (2.6)$$

where r id the radial distance from the particle. For forward scatter, S is written in $S(0)$. The total extinction cross-section of the particle is given by

$$C_{ext} = \lambda^2 / \pi \qquad (2.7)$$

A plane wave propagation through a medium containing N randomly distributed particles per unit volume experiences an attenuation of $NC/2$ nepers per unit distance (1 neper is a voltage ratio of e, a power ratio of e^2, or 8.7 dB)

$$\alpha = 8.7\left(\frac{N\lambda^2}{2\pi}\right)\mathrm{Re}[S(0)] \qquad (2.8)$$

The corresponding specific phase shift is

$$\beta = \left(\frac{N\lambda^2}{2\pi} \right) \mathrm{Im}[S(0)] \tag{2.9}$$

For rain with a distribution of drop size, the term *NS* can be written as an integral over *D* and *N(D)S(0,D)*

2.2.4.2 Rayleigh-Scattering Region

A scattering particle of radius *a* and refractive-index *n* is in the Rayleigh-scattering region when it is both electrically small ($2\pi a/\lambda << 1$) and phase shifts across it are small ($2\pi a/\lambda << 1$). In this condition Rayleigh's approximation can be used, which assumes that:

(a) the scattered field is that of a dipole; and

(b) the dipole moment induced in the particle is related to the incident electric field in the same way as for electrostatic fields.

At frequencies, the approximation is especially useful for cloud droplets and atmospheric ice crystals, and it gives partial insight into rain scatter.

If *P* is the induced dipole moment per unit incident field, *S(0)* is given by

$$S(0) = jP\varpi^3 \mu_0 / 4\pi c \tag{2.10}$$

Then *P* can be written as

$$P = \varepsilon_0(\varepsilon_r - 1)\,\xi v = \varepsilon_0 U v \tag{2.11}$$

when v is the particle's volume and ξ is the ratio of the internal to the external field. This ratio is given by $\xi = 3/(\varepsilon_r + 2)$ for a sphere. For a vary oblate spheroid ('flat plate'), ξ is 1 when the field is applied along the longest axis, and is $1/\varepsilon_r$ when the field is applied along the shortest axis. For a vey prolate spheroid ('thin needle') it is 1 when the field is parallel to the long axis, and is $2/(\varepsilon+1)$ when at right angles to it. Values of *U* for water and ice spheres and ice needles and plates are shown in Table 2.2. imaginary parts are not shown as they are very small for ice.

Table 2.2 Values of U for different hydrometeors

	Water Sphere	Ice Sphere	Ice Needle	Ice Plate
$U_{parallel}$	3z	1.26	2.32	2.32
$U_{perpendicular}$	3z	1.26	1.04	0.68

Specific attenuation and phase shift in a cloud of the particles are given by

$$\alpha=(\pi V/\lambda)\mathrm{Im}(U) \qquad \text{neper per unit distance} \qquad (2.12)$$

$$\beta=(\pi V/\lambda)\mathrm{Re}(U) \qquad \text{radians per unit distance} \qquad (2.13)$$

Here $V=Nv$ is the fractional volume of space occupied by the particles. Important features of these two expressions are their direct proportionality to frequency (if n frequency-incident) and to total particle volume, regardless of how distributed between sizes. The first equation includes only extinction due to absortion, and the Rayleigh approximation can be proved by adding to C_{ext} a scatter cross-section equal to the total power radiated by induced dipole, which is $P^2/3\varepsilon_0{}^2\lambda^4$. This term varies as D^6f^4 and becomes noticeable for raindrops at electrical size which are approaching breakdown of the Rayleigh approximation.

2.2.4.3 Optical- and Resonance-Scattering Regions

The optical-scattering region is that in which the incident wavelength is much less than the diameter of the scattering particle. The larger raindrops are approaching this condition at 100 GHz and above. The scattering may be described by a ray model. Provided that the rays which enter the particle are well attenuated within the diameter, which is true in the high radio range but not of course at truly optical frequencies, the extinction cross-section approaches a value of twice the scatterer's geometric area. The factor of *2* is known as the 'extinction paradox', see [11].

Between the Rayleigh and optical regions lies the resonance region in which no simple approximation for the scattered fields is available. Mie's theory gives exact results for a sphere but requires considerable computation. Several numerical methods have been developed for nonspherical particles, for example [12]. Fig. 2.9 shows extinction cross-sections for raindrops as functions of drop size and frequency, and several features of the three scattering regions can be observed.

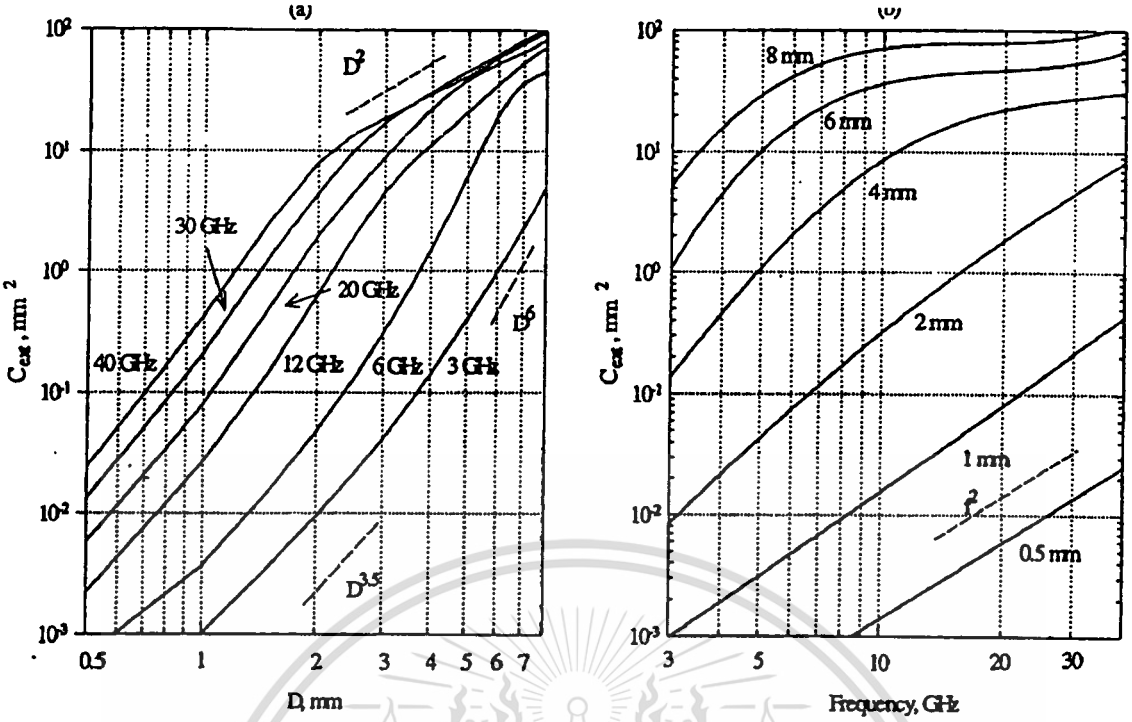

Fig. 2.9 Extinction cross-section against drop diameter and frequency

(a) Diameter

(b) Frequency

Taking Fig. 2.9*a* and *b* together, we can see cross-sections increasing roughly as D^3f^2 in the Rayleigh region. (2.8) predicts this kind of dependence, with absorption increasing in proportion to particle volume and to *f*Im(z), and it was already noted that Im(z) increases roughly as f over most of the frequency range. In Fig. 2.9*a*, a transition to D^2 behaviour can be seen for large drops, the transition occurring at a smaller size as the frequency is raised. Both graphs show fine structure due to resonance. In Fig. 2.9*a*, it is seen that the resonances become increasingly damped at the higher frequencies; at the lower frequencies, as D is increased towards the first strong resonance, the dependence becomes a good deal steeper than D^3. This is particularly clear at 6 GHz. Similarly, Fig. 2.9*b* shows a much steeper dependence than f^2 at intermediate sizes and lower frequencies and the relative independence of frequency for larger particles at the higher frequencies is also clear.

2.3 Classical Development for Rain Attenuation

The classical development for the determination of radiowave attenuation due to rain began with studies by early investigators in the years immediately following the Word War II.

The development has proceeded from those early studies to the present, with further enhancements and improvements. Most recently with the addition of slant paths to allow for space communications links. The classical development of rain attenuation is based on three assumptions describing the nature if radiowave propagation and precipitation [13].

1. The intensity of the wave decays exponentially as it propagates through the volume of rain.
2. The rain drops are assumed to be spherical water drops, which both scatter and absorb energy from the incident radiowave.
3. The contributions of each drop are additive and are independent of other drops. This implies a "single scattering" of energy; however the empirical results of the classical development do allow for some "multiple scattering" effects.

The determination of rain attenuation for a radiowave path proceeds from application of these assumptions.

The attenuation of a radiowave propagating in a volume of rain of extent L in the direction of wave propagation can be expressed as

$$A = \int_0^L \alpha dx \tag{2.14}$$

where α is the specific attenuation of the rain volume, expressed in dB/km, and the integration is taken along the extent of the propagation path, from x=0 to x=L.

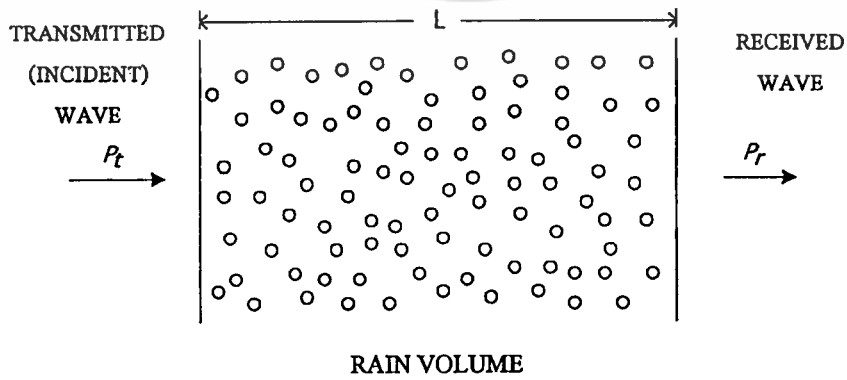

Fig. 2.10 Radiowave incident on a volume of spherical, uniformly distributed water drops

Consider a plane wave of transmitted power P_t incident on a volume of uniformly distributed spherical water drops, all of radius r, extending over a length L, as shown in Fig. 2.10. The received power P_r will be

$$P_r = P_t e^{-kL} \tag{2.15}$$

where k is the attenuation coefficient for the rain volume, expressed in units of reciprocal length.

The attenuation of the wave, usually expressed as a positive decibel (dB) value, is given by

$$A(dB) = 10 \log_{10} \frac{P_t}{P_r} \tag{2.16}$$

Converting the logarithm to the base e and employing equation (2.15)

$$A(dB) = 4.343kL \tag{2.17}$$

The attenuation coefficient k is expressed as

$$k = \rho Q_t \tag{2.18}$$

where ρ is the drop density, i.e., the number of drops per unit volume, and Q_t is the attenuation cross section of the drop, expressed in the units of area. Q_t is the sum scattering cross section Q_s and an absorption cross section Q_a. The attenuation cross section is function of drop radius, r, wavelength of the radiowave, λ, and complex refractive index of the water drop, m. That is

$$Q_t = Q_s + Q_t = Q_t(r, \lambda, m) \tag{2.19}$$

The concept of cross section, developed in early radar studies, describes the physical profile that an object to a radiowave. It is defined as the ratio of the total power extracted from the wave (in watts) to the total incident power density (in watts per square meter); hence the unit of area, square meter.

The drops in a real rain are not all of uniform radius, and the attenuation coefficient must be determined by integrating over all of the drop sizes, i.e.,

$$k = \int Q_t(r,\lambda,m)n(r)dr \tag{2.20}$$

when $n(r)$ is the drop size distribution, $n(r)dr$ can be interpreted as the number of drops per unit volume with radii between r and $r+dr$.

The specific attenuation, in dB/km, is found from the above result for k and equation (2.17) , with L=1 km,

$$\alpha\left(\frac{dB}{km}\right) = 4.343\int Q_t(r,\lambda,m)n(r)dr \tag{2.21}$$

The above result demonstrates the dependence of rain attenuation on drop size, drop size distribution, rainfall rate, and attenuation cross section. The first three parameters are characteristics of the rain structure only. It is through the attenuation cross section that the frequency and temperature dependence of rain attenuation is determined. All of the parameter exhibit time and spatial variabilities which are not deterministic or directly predictable, hence most analyses of the rain attenuation must rely on the statistical analyses to quantitatively evaluate the impact of the rain on communications systems.

The solution of equation (2.21) requires Q_t and $n(r)$ as a function of the drop size. Q_t is found by employing the classical scattering theory for a plane wave radiating an absorbing sphere. The resulting series expansion solution for Q_t is found as follows

$$Q_t = \frac{\lambda^2}{2\pi}\sum_{n=1}^{\infty}(2n+1)\,\mathrm{Re}(a_n + b_n) \tag{2.22}$$

where a_n and b_n are the Mie scattering coefficients, which are complex functions of r, λ and m. Re indicates "the real part of."

Equation (2.22), known as the Mie scattering cross section. Is difficult to calculate; however, it can be simplified under the conditions where $2\pi r << \lambda$, that is, where the size of the rain drop is much less than the wavelength of the radiowave. This condition, known as the

Rayleigh approximation, is valid up to frequencies of 40-80 GHz. Under this condition, the attenuation cross section reduces to

$$Q_t = \frac{8\pi^2}{\lambda} r^3 \operatorname{Im}\left[\frac{m^2 - 1}{m^2 + 1}\right] \tag{2.23}$$

where Im indicates "the imaginary part of." Equation (2.23) is referred to as the Rayleigh scattering cross section.

Several investigators have studies the distribution of rain drop size as a function of rainfall rate and type of storm activity, and the drop size distributions were found to well represented by an exponential of the form

$$n(r) = N_0 e^{-\Lambda r} = N_0 e^{-\left|cR^{-d}\right| r} \tag{2.24}$$

where R is the rainfall rate, in mm/hr, and r is the drop radius, in mm. N_0, Λ, c and d are empirical constants determined from the measured distributions.

Table 2.3 Drop size distribution used for rain attenuation calculations

Drop Size distribution	Empirical Constant	
	$N_0, \left(\frac{1}{m^2}\frac{1}{mm}\right)$	$\Lambda, \frac{1}{mm}$
Marshall-Palmer	8×10^3	$8.2R^{-0.21}$
Joss :		
drizzle	30×10^3	$11.4R^{-0.21}$
widespread rain	7×10^3	$8.2R^{-0.21}$
thunderstorm	1.2×10^3	$6R^{-0.21}$

The Marshall-Plalmer and Joss distributions were obtained from radar measurements and the empirical constants of equation (2.24) for those distributions are listed in the Table 2.3. The Laws and Parsons distribution was measured directly and presented in tabular form for specific rainfall rate values from 0.25 mm/hr to 150 mm/hr.

The specific rain attenuation as given in equation (2.21) can be now expressed as

$$\alpha\left(\frac{dB}{km}\right) = 4.343 N_0 \int Q_t(r,\lambda,m) e^{\Lambda r} dr \tag{2.25}$$

where Q_t is obtained from equation (2.22) or (2.24). The above integral equation can be solved numerically for specified values of refractive index, frequency, and drop size distribution

The total rain attenuation for a given path is then obtained integrating the specific attenuation over the total path length L.

$$A(dB) = 4.343 \int_0^L \left[N_0 \int Q_t e^{-\Lambda r} dr \right] dx \tag{2.26}$$

where the integration over x is taken the extent of the rain volume in the direction of propagation. In general both Q_t and the drop size distribution will vary along the path and these variabilities must be included in the integration process. A determination of the variations along the propagation path is very difficult to obtain, particularly for slant paths to an orbiting satellite. We shall see later that these variations must be approximated or treated statistically for the development of useful attenuation prediction models.

2.4 Rain Attenuation Prediction Models

The evaluation of the effects of rain on a satellite system design requires a detail knowledge of the attenuation statistics for each ground terminal location at the specific frequency of interest. Direct long-term measurements of rain attenuation for all of the ground terminal locations are not practical, therefore modeling and prediction methods must be used to make a best estimate of the expected attenuation for each location. Over the past several years extensive efforts have been undertaken to develop reliable techniques for the prediction of path rain attenuation for a given location and frequency, and the availability of satellite beacon measurements has provided a data base for the validation and refinement of the prediction models. This section reviews several of the more promising rain attenuation prediction techniques [13].

2.4.1 Rice-Holmberg Rain Model

A global surface rain rate developed from extensive long term rain rate statistics from over 150 locations throughout the world was developed by Rice and Holmberg [14]. The Rice-Holmberg model constructs a rain rate distribution by assuming that the rain structure can be divided into two types, or modes, "thunderstorm rain" and "all other rain." Each mode is modeled by exponential functions and the sum of the two modes produces the total distribution. the percent of an average year for which the rain rate exceeds R mm/hr at a medium location is given by,

$$P(R)\% = \frac{M}{87.6}\left\{0.03\beta e^{-0.03R} + 0.2(1-\beta)\left[e^{-0.258R} + 1.86e^{-1.63R}\right]\right. \tag{2-27}$$

where M is the average annual rainfall accumulation (in mm), M_1 is the average annual accumulation of thunderstorm rain (in mm), $\beta = M_1/M$, and R is the clock minute rain rate, in mm/hr.

Global maps for M, M_1, and β are provided in the model, or directly measured data can be used when available. The Rice-Holmberg model, one of the first developed for radiowave propagation studies, has been shown to provide very good agreement with measured data for locations in the United States where long term rain rate data has been measured directly.

2.4.2 Dutton-Dougherty Attenuation Prediction

The global rain rate model of Rice-Holmberg described above dose not provide a prediction of rain attenuation on a radiowave path. The Rice-Helmberg model, however, was later extended by Dutton and Dougherty to include an attenuation prediction [15]. The Dutton-Dougherty (DD) Model is based on meteorological considerations of the propagation path. It begins by expressing the clock minute rain rate distribution for an average year in three segments,

$$P(R) = \begin{cases} 0.0114(T_{11} + T_{12})e^{-R/R_1'}, & R < 5 \quad mm/hr \\ 0.0114T_{21}\exp(-\sqrt[4]{R/R_{21}}), & 5 \le R \le 30 \quad mm/hr \\ 0.0114T_{11}e^{-R/\overline{R_{11}}}, & R > 30 \quad mm/hr \end{cases} \tag{2.28}$$

where T_{11}, T_{12}, R'_1, and $\overline{R_{11}}$ are linear combinations of M, β and D=24+3M, determined from the regression equations

$$T_{21} = b_{11}M + b_{21} \pm S_2$$

$$R_1' = b_{31}M + b_{41}\beta + b_{61} \pm S_3 \tag{2.29}$$

$$\bar{R}_{11} = \frac{\beta M}{T_{11}} = a_{11}M + a_{21}\beta + a_{31}D + a_{41} \pm S_1$$

The DD attenuation distribution prediction is then determined from the rain rate distribution through the following assumptions:

1. A Marshell-Palmer deopsize distribution
2. A storm height distribution of Granthan and Kantor.
3. Vertical dependence of liquid water content from Dutton
4. The specific attenuation coefficients $a(f)$ and $b(f)$ of Crane.

2.4.3 Lin Rain Attenuation Model

An empirical method for estimating rain induced outage probabilities on radiowave path was developed at Bell Laboratory by Lin [16]. The Lin model is based on a 5-minute point rainfall rate than one minute or less rain gage integration times of other prediction techniques. Two arguments are presented to justify the use of the 5-minute averaging time. First, the available long term rain rate data in the United States by National Weather Service have a minimum integration times of five minutes, and attempts to estimate shorter times from the original strip chart data produce significant errors. Second, the five-minute averaging time effectively produces a path average rain rate distribution from a point rain rate distribution, that is, the spatial average of the rain rate along a single point on the path.

The relationship between path attenuation and five minute rain rate was determined empirically from measurement on nine 11 GHZ terrestrial paths, 5-43 km in length, at five location in the United States. The resulting relationship for path attenuation was

$$A_L = aR_5^b L \left[\frac{1}{1 + \frac{L}{\bar{L}(R_5)}} \right] \tag{2.30}$$

where R_5 is the 5-minute point rain rate, L is the terrestrial path length, and a and b are frequency dependent constants described in ITU-R (Specific rain attenuation). The term in brackets is called a path length correction factor by Lin, Chosen to represent the empirical ratio between the five-minute point rain rate and the radiowave path average rain rate at the same probability level.

The function $\bar{L}(R_5)$ was determined from the terrestrial path measurements as

$$\bar{L}(R_5) \cong \frac{2636}{R_5 - 6.2} \tag{2.31}$$

Lin extended the terrestrial path to a slant path at elevation angle θ by geometric considerations to obtain

$$L = \frac{H - G}{\sin\theta} \tag{2.32}$$

where H is the long term average 0° isotherm height, assumed by Lin to be 4 km for Eastern United States locations, and G is the ground terminal elevation (height) above sea level.

The resulting prediction equation for slant path rain attenuation is then

$$A_\theta(dB) = aR_5^b \left[\frac{2636}{R_5 - 6.2 + \frac{2636\sin\theta}{4 - G}} \right] \tag{2.33}$$

The term in brackets corresponds to the effective to path length parameter for the Lin model.

2.4.4 ITU Recommendation Rain Attenuation Model

ITU-R rain attenuation model has been widely used to predict and estimate the affects of rain on the satellite communication links. Moreover, the models of ITU-R have been often updated and improved. The prediction models of rain attenuation of ITU-R are expressed and, simultaneously, used to estimate the results of the experiment in this study in section 4.1.

2.5 Conclusions

This chapter gives an introduction of radiowave propagation in the atmosphere. All effects on the communications path are briefly introduced. On the communication systems at frequencies above 10 GHz, precipitation in the atmosphere causes serious degradation. All forms of the precipitation in atmosphere, troposphere, are physically classified. Especially, affects of rain on communication links at the frequencies above 10 GHz are considered as critical degradation.

Therefore, classical development of rain attenuation is briefly introduced since the early studies to the present. Finally, some of rain attenuation models proposed by the former research are given. The widely used model of ITU-R will be discussed in detail in the next chapter.

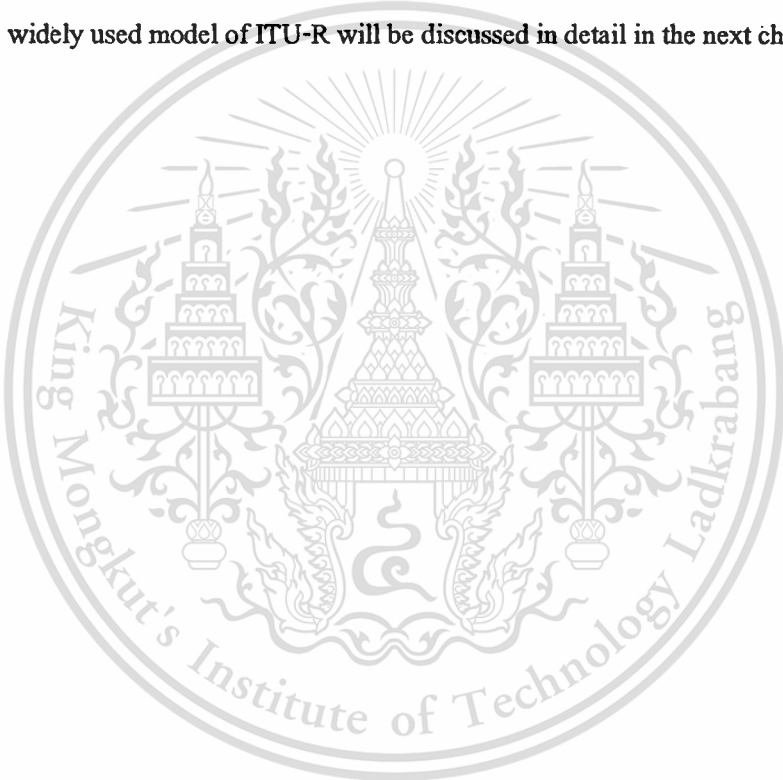

CHAPTER 3

OBSERVED RAINFALL RATE AND RAIN ATTENUATION DATA

In order to obtaining rainfall rate and rain attenuation characteristics of each experiment sites, obtained experimental data are analyzed. In this chapter, we deal with general concepts of analyses separated to be in three parts. Firstly, experiment site information and also apparatus are briefly introduced. Secondly, observed experimental data are manipulated and, then, presented in general characteristics of rainfall rate and rain attenuation in each site. Cumulative distributions, local time in a day of raining, worst month characteristics, etc. are characterized. Fading duration and rain fading time characteristics indicate the number of rain and attenuation exceeding thresholds against their duration. Finally, the obtained general characteristics are compared with the other published prediction models.

3.1 Systematic Information

In this study, instrument measurements have been installed in two experiment sites, meteorology station at Klong Yai, Tard since August 1999 and Satellite Communication Laboratory, KMITL, Bangkok since 1999.

Owing to obtain the good resource of rainfall rate data, Klong Yai, one of the highest rainfall regions of Thailand, is chosen as one of experiment location. Beacon measurement has been hold by observing the variation in signal level from Thaicom3 satellite and, simultaneously, rainfall rate has been observed. Klong Yai is an ampor in Trad province in the eastern part of Thailand next to the bolder of Cambodia-Thailand, about 380 km from Bangkok. The Landscape of terminal location is the narrow planar area between mountain range and seashore.

Referring to Post-PARTNERS Project, variation in signal level from JCSAT and 1-minute rainfall rate have been observed as one of activities in Satellite Communication Laboratory, Research Center for Communication and Information Technology, KMITL, Bangkok since 1999. Beacon measurement of Thaicom3, another experiment system, had been observed in 1999 at KMITL, Bangkok. The following Table gives some information of instrument and experiment locations.

Due to the recorder of variation in observed satellite signal on Thaicom3-Trad and Thaicom3-Bangkok links are paper type recorders, therefore, recording papers are read with 1 minute sampling interval by calibrated scale. Saturated levels of attenuation of Thaicom3-Trad and Thaicom3-Bangkok are set to be 7.5 and 8 dB, respectively, corresponding to the dynamics range of recorders the small receiving antennas and other conditions of observing sytems. After reading and collecting rainfall rate and signal attenuation, obtained data are primarily manipulated in Microsoft excel by artificial Macros.

Table. 3.1 Satellite and receiving terminal information

	Thaicom3-Tard	JCSAT-Bangkok	Thaicom3-Bangkok
Frequency	12.292 GHz	12.747 GHz	12.292 GHz
Terminal location	102°53′ E, 11°46′ N 10 m asl ITU-R Zone N	100°48′ E, 13°45′ N 45 m asl ITU-R Zone N/P	100°48′ E, 13°45′ N 45 m asl ITU-R Zone N/P
Receiving antenna	0.45 m diameter	1.8 m diameter	0.45 m diameter
Elevation angle	58.7°	32°	59.6°
Signal recorder	Paper receiving type	Data logger 1-minute interval	Paper receiving type
Polarization tilt angle	Horizontal linear polarization	Vertical linear polarization (15°)	Horizontal linear polarization
Satellite and position	Thaicom3, 78.5°E	JCSAT-1B, 150° E	Thaicom3, 78.5°E
Rain gauge type	0.5 mm tipping bucket	0.5 mm tipping bucket	-
Availability of observed data - Satellite signal - Rainfall rate	 1 year, 2000 2 years 2000-2001	 2 years, 2000-2001 2 years, 2000-2001	 1 year, 1999

In addition, 10-second rainfall rate data at Bangkok are available 4 months, May-August 1999 from COMMETS project that had been installed at KMITL. The rain gauge is raindrop type. Even though, they are short-term observed data, they give a good resource of high rainfall rate that is additionally analyzed in some condition.

3.2 Measurement Results

By using the measurement and instrument as mentioned in Table 3.1, the signal reception level and point rainfall rates have been measured and, then, recorded. Satellite signal (beacon) reception level from Thaicom3 satellite have been recorded at Klong Yai, Trad from September 1999 to November 2000, and at KMITL, Bangkok from January 1999 to December 1999. Satellite signal reception level from JCSAT has been recorded since August 1999. Correspondingly, he point rainfall rate data have been obtained. In this section, the observed results are shown in detail.

3.2.1 Cumulative Distributions

Observed rainfall rate and signal attenuation data from each experiment site are generally characterized into average annual cumulative distributions. The rain and rain attenuation cumulative distributions provide the probability of exceeding in percentage of time in a typical year. These propagation data are required for the design of broadcasting-satellite systems. Especially, for the future demands of personal satellite communications [17], the rain margin of each location is needed differently at the same percentage of availability. Thus, propagation data of narrow area covered by narrow beam of satellite support the high efficient satellite system design in the near future.

The percent time that given attenuation or rainfall rate are equaled or exceeded on the ordinary and the attenuation and also rainfall rate are on the abscissa. The percentage of time represents the outage time for a given link budget and the exceeding rainfall rate for a given threshold. Fig. 3.1 and Fig. 3.2 show the average annual cumulative distributions of rainfall rate and attenuation, respectively.

Table 3.2 Rain intensity of exceeded (mm/hr)

Percentage of time (%)	N	KMITL, Bangkok	Klong Yai, Tard	P
1	5	-	22	12
0.3	15	14	64	34
0.1	35	48	95	65
0.03	65	90	120	105
0.01	95	120	144	145
0.003	140	157	167	200
0.001	180	176	180	250

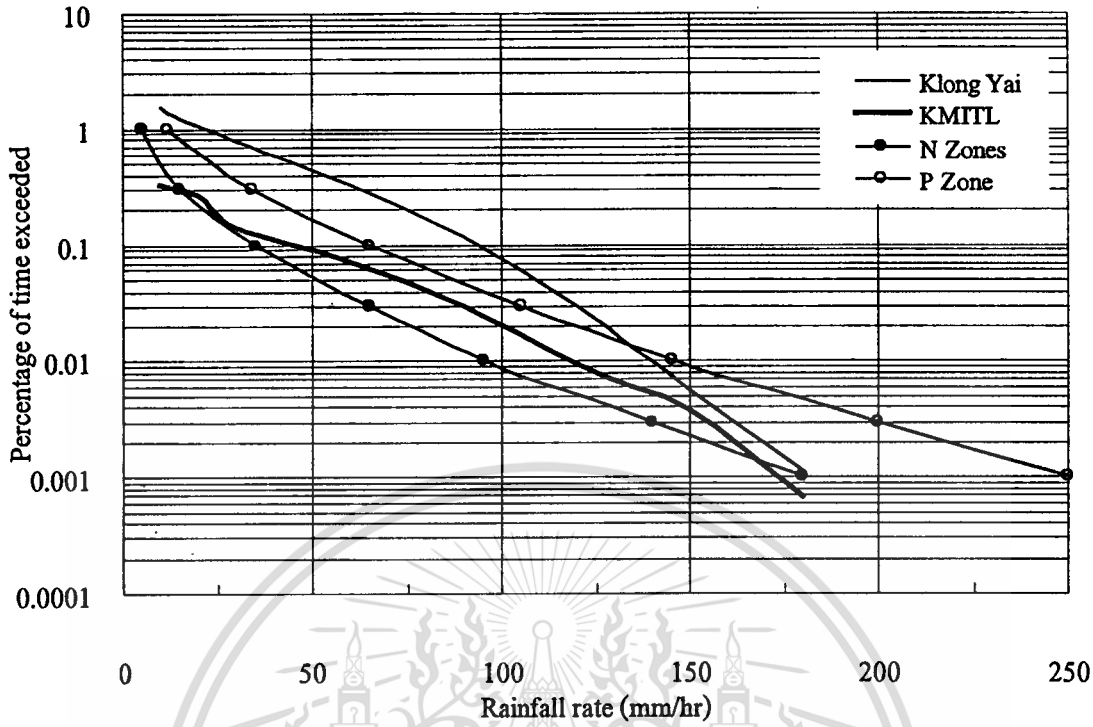

Fig. 3.1 Average annual cumulative distribution of point rainfall rate at Klong Yai, Trad and KMITL, Bangkok (from January 2000 to December 2001)

Fig. 3.1 shows not only the observed results of rainfall rate at KMITL, Bangkok and Klong Yai, Trad but also the rainfall rate distribution of world rain climate zones P and N. According to the world rain climate zones in Appendix A, Trad are located in N zone and Bangkok is located on the contour line between N and P zones. The comparative rainfall rates at percentage of time are also listed in Table. 3.2.

Owing to the saturated of satellite receiving set both at Klong Yai and KMITL, 0.45-m diameter parabolic antennas, the saturated attenuation levels are limited to 7.5 dB and 8 dB at Klong Yai and KMITL, respectively. As shown in Fig. 3.2, the percentage of time of the attenuation exceeded 7.5 dB at Klong Yai is 0.11475 % or 10 hours 3 minutes in 1 year and the percentage of time of the attenuation exceeded 8 dB at KMITL is 0.150589% or 13 hours 12 minutes in 1 year. With a 1.8-m diameter antenna, the satellite attenuation from JCSAT is saturated at 23 dB, then the percentage of unavailable time of satellite signal is 0.038763 % or 3 hours 23 minutes. In addition, the comparison of the observed cumulative distribution with estimated distribution would be discussed in section 3.3.4.

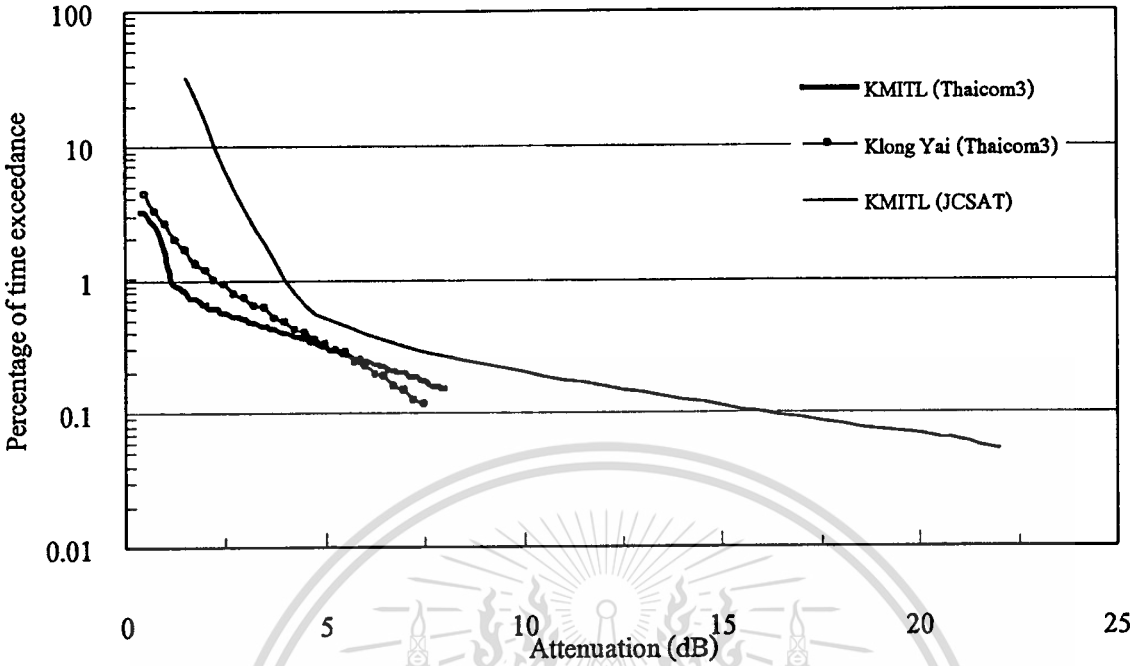

Fig. 3.2 Average annual cumulative distribution of satellite signal attenuation on Thaicom3-Bangkok 1999,Thaicom3-Trad 2000 and JCSAT-Bangkok 2000-2001

3.2.2 Hourly and Monthly-Hourly Distributions

Provided that the data bank is available, it will be very useful to discriminate the yearly intensity outage on the hour of the day inclusive (if possible) of the calendar month. This will permit to resolve which periods of the year contribute most to the small outage in other words, we wish to find out the periods whose rain rate exceeds about 60 mm/hr. This value compare to compared to the 50 mm/hr quoted in [18] which other authors would class as a limit for convective precipitate rate. The one reason that we consider at 60 mm/hr is due to the experiment sites being classed in tropical region. This may be of particular importance to secure high density communications irrespective of the social or unsocial hours of the troughs of probability for those season (months) when heavy shower may occur.

The hourly revolution of probability of outage was investigated looking at periods in the day of 2 GMT hours, and then counting the duration of exceedance of the given thresholds. For the first type of investigation, we consider at the exceeding rainfall rates throughout an average day as threshold for each outage. As shown in the following figures, the percentage of outage

time are indicated as a function of time of day at the rainfall rate exceeded, for example, 30, 60 and 120 mm/hr, respectively

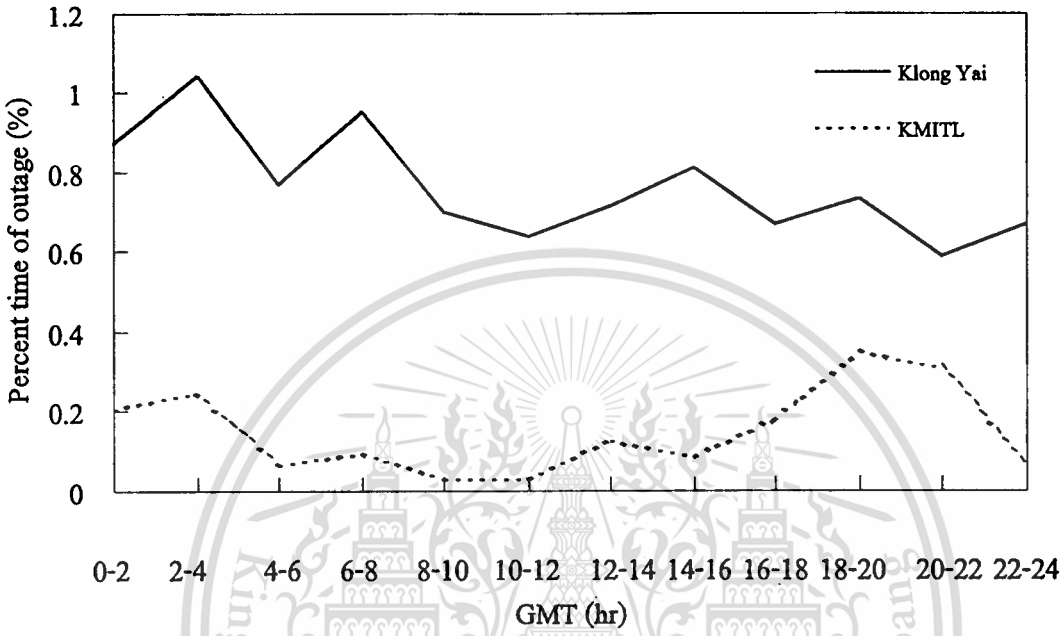

Fig. 3.3 The percent time of outage at 30 mm/hr

At KMITL site, the rainfall rate exceeding 30 mm/hr rather considerably occurs on evening and night more than on daytime, either do the rainfall rate exceeding 60 and 120 mm/hr. For example, the maximum percentage of time of the rainfall rate exceeding 60 mm/hr, in Fig. 3.4, is 0.35% or 2 hours and 33 minutes occurring at 18:00-20:00 for average annual. For the Klong Yai data, the percentages of outage of the rainfall rats exceeding 30 and 60 mm/hr rather gradually decrease from the midnight. For the rainfall rate exceeding 120 mm/hr, the highest of percentage of outage occurs at the midnight but the percentage of outage rather fluctuate. However, the percentages of outage of all rainfall rates exceeding at Klong Yai are obviously higher than those of at KMITL, Bangkok.

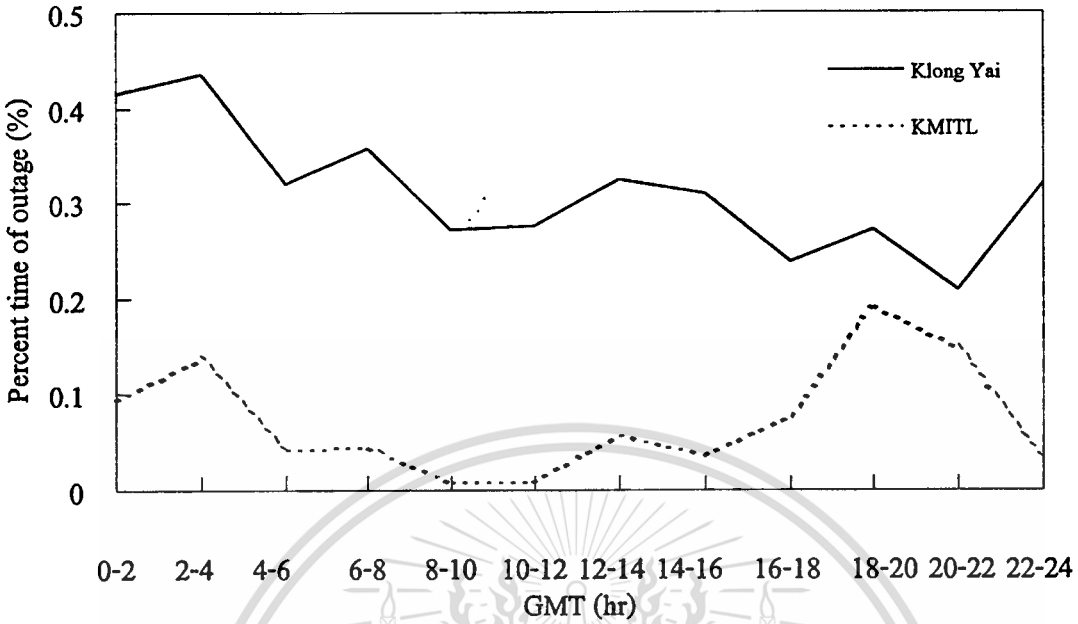

Fig. 3.4 The percent time of outage 60 mm/hr

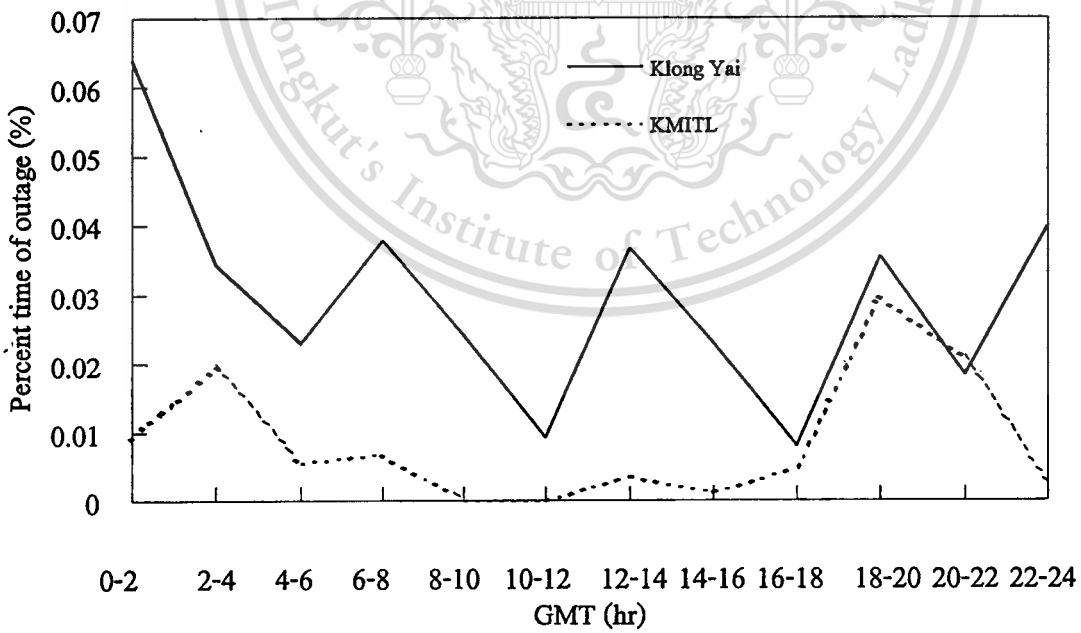

Fig. 3.5 The percent time of outage 120 mm/hr

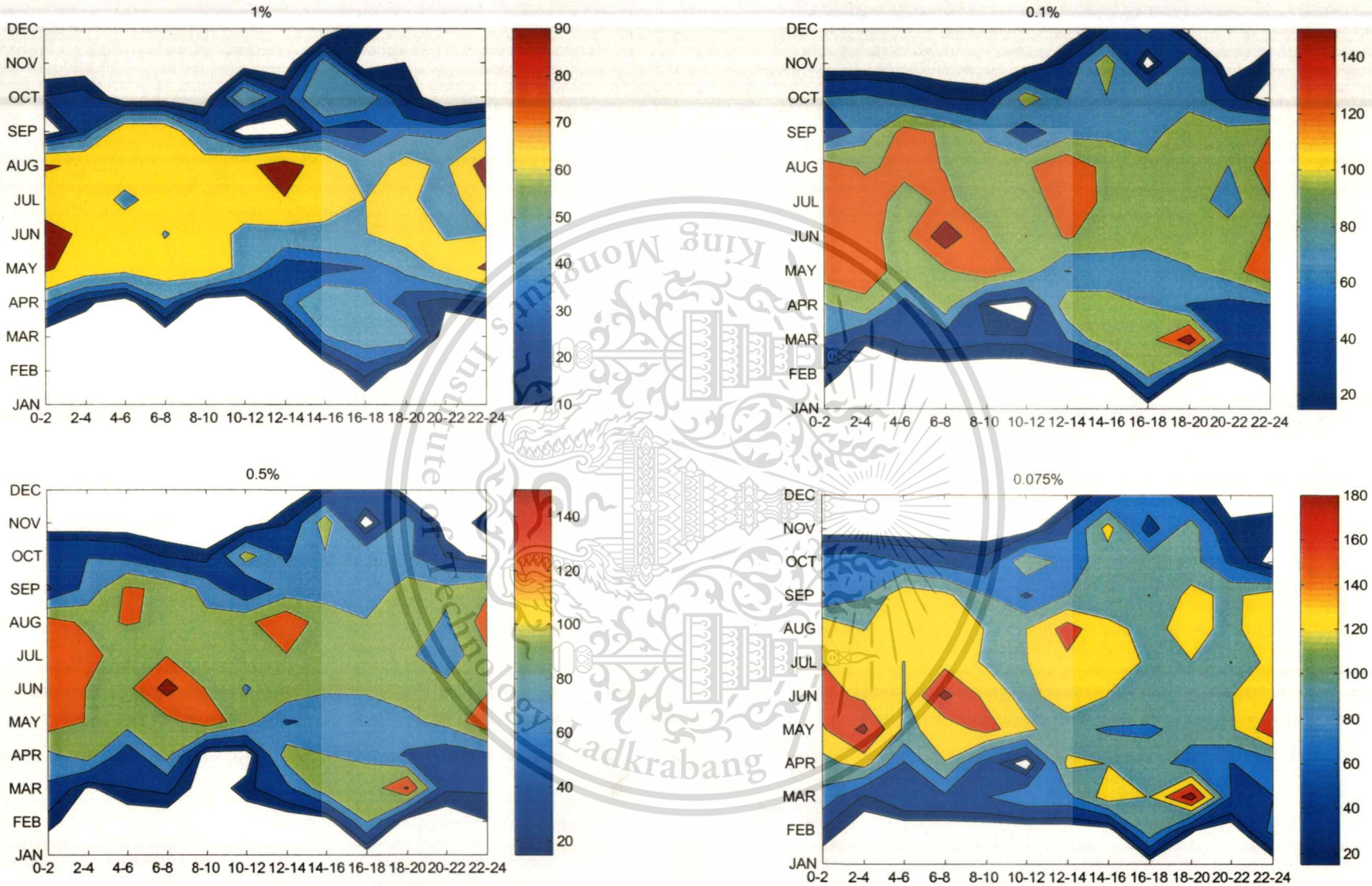

Fig. 3.6 Values of the rain intensity responsible for the indicated percent outage as a function of time of day and month at Klong Yai

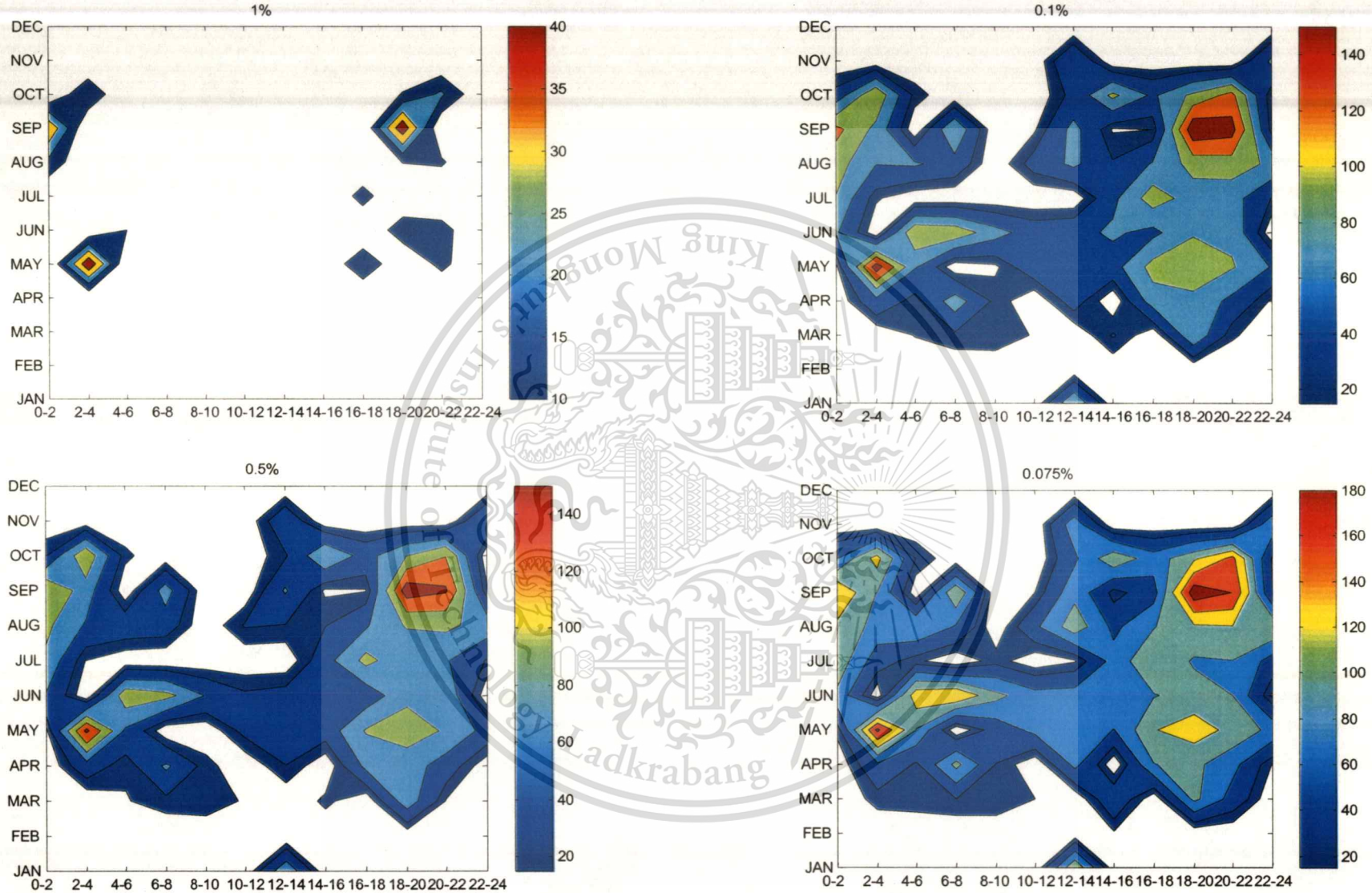

Fig. 3.7 Values of the rain intensity responsible for the indicated percent outage as a function of time of day and month at KMITL

Consequently, the above study leads naturally to resolve the hourly evolution of the probability in the terms of the month as will be called Monthly-hourly distribution. There are considerably 4 variables existing, therefore rainfall rates are indicated in terms of the percentage of outage time as a function of time of day and month. Contour surface plots are suitably considered to indicate the discussed evolution as shown in Fig. 3.6 and 3.7 of Klong Yai and KMITL, respectively.

3.2.3 Worst-Month Characteristics

The annual worst month for rainfall rate and attenuation by rain are those months within a year that have the largest fraction of time during which the rainfall rate and attenuation on a propagation path exceed some threshold of interests. The worst-month statistic of interest is the expected fraction of the time in the worst month that path attenuation and rainfall rate exceed specified threshold values or, as often be applied, the expected interests for a specified probability threshold. The worst month is not a specific calendar month but the month that produces the most outage for a specified fading margin. The worst month in any calendar year may vary from one month to another as the attenuation threshold is changed. In climate regions with definite rainy seasons the months that may possibly be a worst month may be confined to the rainy season.

The CCIR considered the reference of performance criteria for radio communication system often referring to any month. For the design of such system it is necessary to have statistics of propagation effects that are relevant to the period of reference of the performance criteria. Therefore, there is a need for unambiguous definition for the period of reference. The fraction of time during which a preselected threshold is exceeded in the worst month of a year is referred to as the annual worst-month time fraction of excess. The statistics relevant for the performance criteria referring to any month is the average of the annual worst-month time fraction of excess. The worst month of a year for a preselected threshold for any performance degrading mechanism, is that month in a period of twelve consecutive calendar months, during which the threshold is exceeded for the longest time. The worst month is not necessarily the same month for all threshold levels.

In Fig. 3.8, we can considerably group monthly cumulative distribution of Klong Yai data based on the percentage of outage into 3 groups of 4 months. First group, highest percentage, consists of May, June, July and August. Second and third groups contain (March, April, September and October) and (January, February, November and December), respectively. In

addition, the highest of percentage of time of exceeding rainfall rate selected as threshold is indicated as MW lines shown in the above figures. The selection on a monthly basis of this highest percentage or probability leads to synthetic distribution, which is an envelope of the monthly distribution.

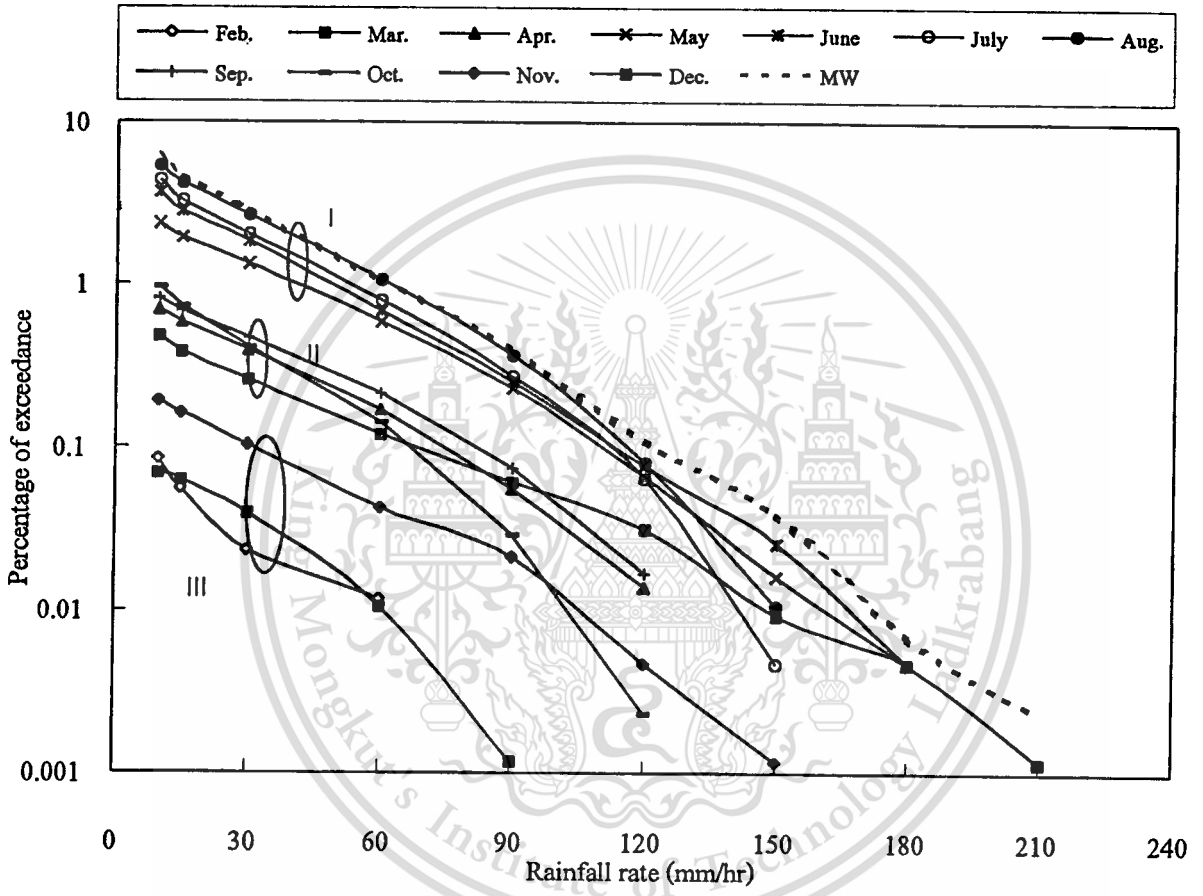

Fig. 3.8 Monthly cumulative distribution at KlongYai, Tard

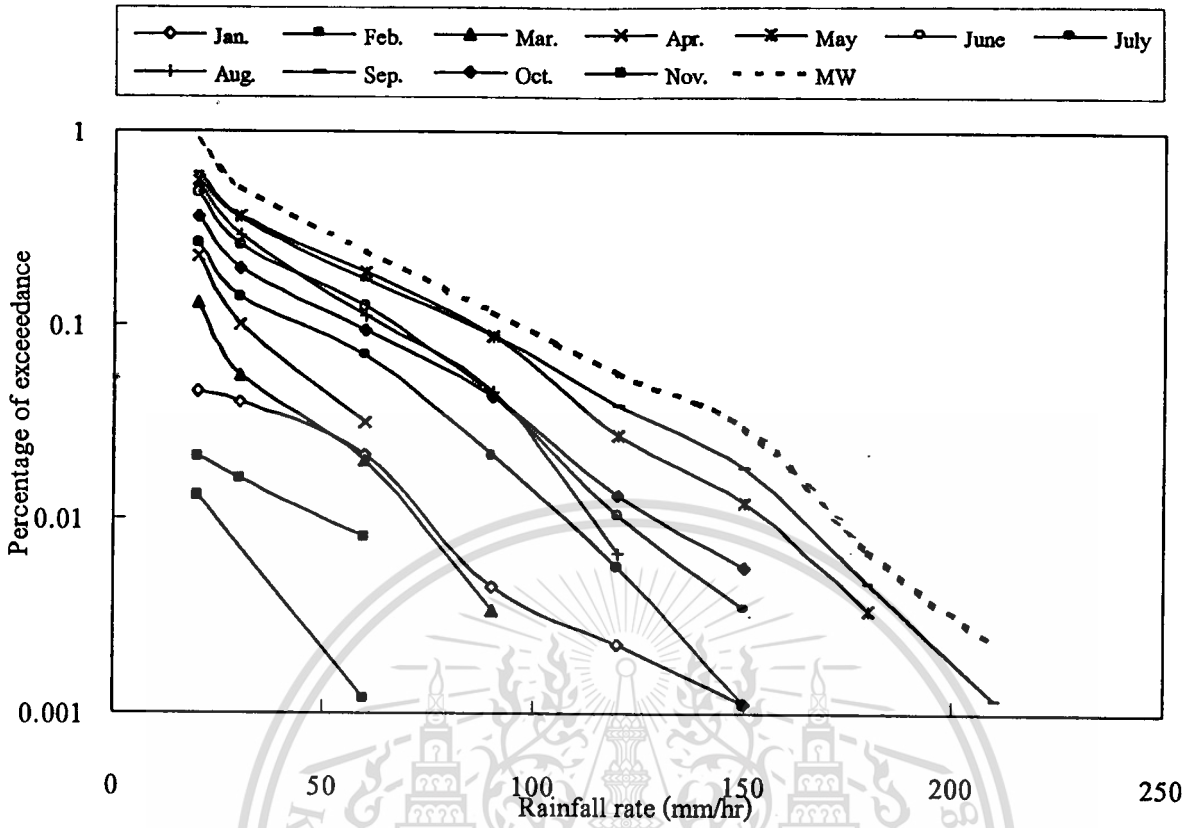

Fig. 3.9 Monthly cumulative distribution at KMITL, Bangkok

Alternatively, we can consider in detail at the evolution in the values of rainfall rate throughout the months of an average year, which is corresponding to a specified percentage of outage (percentage of month that indicated rainfall rate is equaled or exceeded). The particular results observed data from both experiment sites are shown in Fig. 3.10 and 3.11. Therefore, we can consider the worst calendar months for discussion the most availability month later.

Due to the rather high percentage of outage at Klong Yai for all over one year as shown in Fig. 3.10, the worst-month can be classed into 2 types, extremely high rainfall rate but low cumulative rain and high both rainfall rate and cumulative rain, for example, March and June, respectively. December, January and February are considered to be high availability month for radio links. For KMITL as shown in Fig. 3.11, the worst calendar months can be clearly considered as May and September.

Worst month characteristics will be additionally discussed again in section 3.4 later.

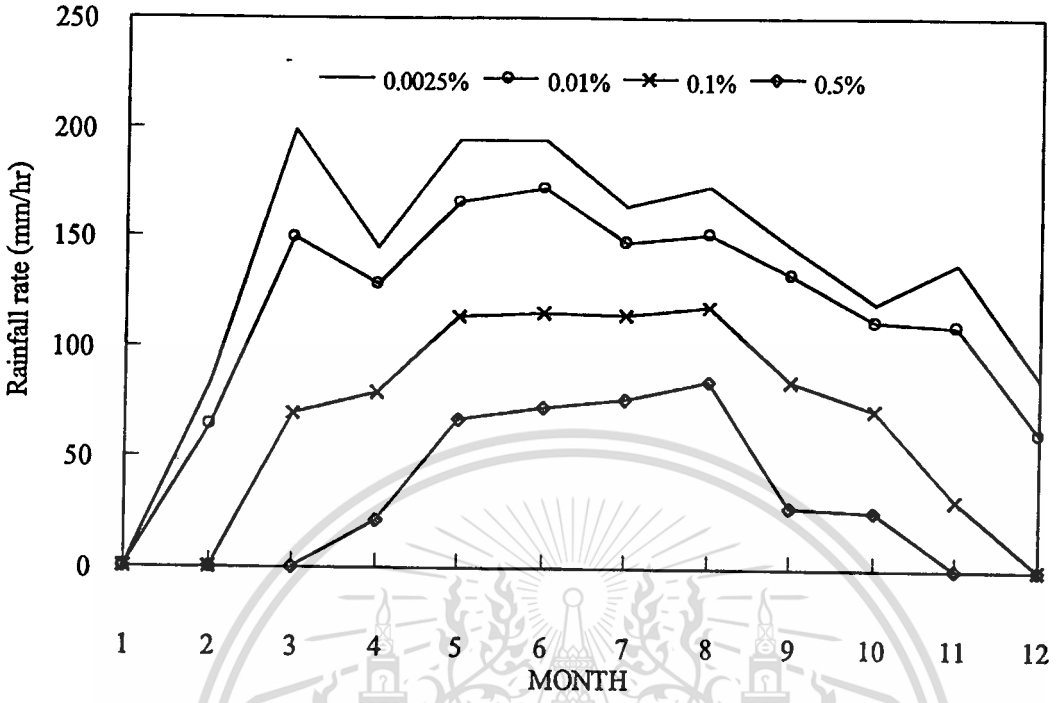

Fig. 10 Evolution of rain intensity throughout an average year for the indicated outage at Klong Yai site

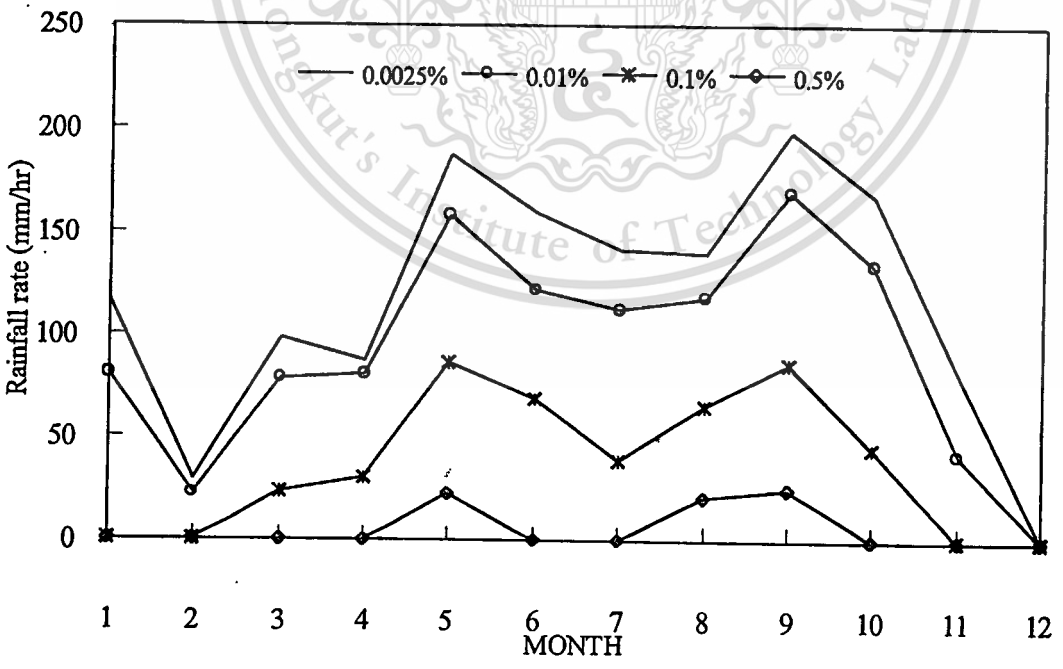

Fig. 3.11 Evolution of rain intensity throughout an average year for the indicated outage at KMITL site

3.3 Fading Time Duration

In the centimeter and millimeter regions, rain is well known as the main contributor to fading and often determines the propagation dependence of the carrier-to-noise spectral density ratio required for the design of microwave communication systems. Strategies to combat fading and accommodate bursts in traffic demand are being considered world-wide, and involve combinations of transmitter power control and adaptive data rates and coding [3].

From above considerations, it emerges that not only the characteristics of magnitude and probability of occurrence of fading as in former sections are important (whether annual or worst month) but also, in this section, the duration is important, too. To put it simply, if it is known how long a certain level of fading is likely to last on average, then a decision can be made to take action or wait for the signal to recover.

3.3.1 Number of Single Exceedances of Rainfall Rate

The time series of both rainfall rate and attenuation data are considered as, for example, the following Fig. 3.12. We shall call a rain event a continuous record of rain. In the figure, we have certain 3 maxima. We further notice that within an event, any threshold that equals or less than the maximum of the event will be exceeded at least one. This leads to important concept of single exceedance of the threshold R which is the occurrence of rain continuously exceeding (or equaling) the rainfall rate R. Therefore, the third event of Fig. 3.12 displays one single exceedance of level $R1$, two of level $R2$, and one of level $R3$. Each exceedance has an associated duration $D(R)$ and they are also illustrated. There are more than one single exceeding in one event of rain that depend one the selected rainfall rate thresholds. The above explanation processes are used to run over all time series of observed rainfall rate and signal attenuation data of both experiment sites.

Owing to the 1-minute interval observed data of our experiments, the minimum time duration of rain and signal fading is set as 1 minute. Cumulative average numbers of single exceedances per year are counted for all events of rains and signal attenuation by computational methods. Even though the maximum observed the rainfall rate is 210 mm/hr, the optimum rainfall rates using as the selected threshold are in the range 10-150 mm/hr. The selected thresholds (10, 15, 30, 60, 90, 120, and 150 mm/hr) are confined by the specification of the 0.5 mm tipping bucket rain gauges that have been used in both experiment fields. Consequently, the single exceeding 10 and 15 mm/hr for the duration less than 3 and 2 min, respectively, can not be

directly obtained by 0.5 mm tipping bucket rain gauge with the interval 1 min. Because it can measure rainfall rate at least 30 mm/hr. However 10 and 15 mm/hr can be determined by average estimation. Therefore duration less than 3 and 2 min of single exceeding 10 and 15 mm/hr, are neglected to be indicated in as shown in Fig. 3.13 and Fig. 3.14. Reasonably, the higher thresholds of outage, the smaller duration and the less number, respectively, of single exceedances are. Considering from the obtained data, the maximum time duration of the maximum observed rainfall rate, 210 mm/hr, is only 1 minute at Klong Yai. On the other hand, the maximum time duration of 10 mm/hr rainfall rate is 171 minutes and 55 minutes at Klong Yai and KMITL, respectively. Comparing to each other sites, at the same threshold of rainfall rate, the number of single exeedances and the duration at Klong Yai site are obviously greater and larger than those of KMITL site.

The computed average rainfall time per year can be determined by summing the multiplication of average number of single exceedances and time duration. The number of single exceedances of each rainfall rate are indicated in Fig. 3.13 and Fig. 3.14. of Klong Yai and KMITL, respectively. We would not consider at the single exceeding 10 and 15 mm/hr due to the above conditions. The average time per year of single exceedances above 30, 60, 90, 120 and 150 mm/hr are (4128, 1681, 605, 156 and 29 min) and (757, 366, 146, 34 and 12 min) of Klong Yai and KMITL, respectively.

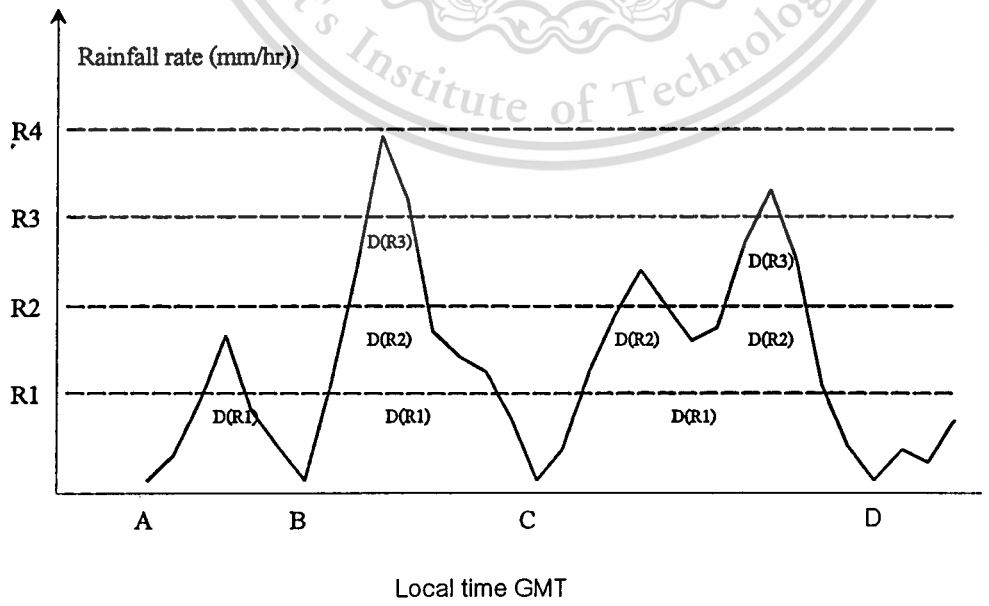

Fig. 3.12 Example of duration of single exceedances D(R)

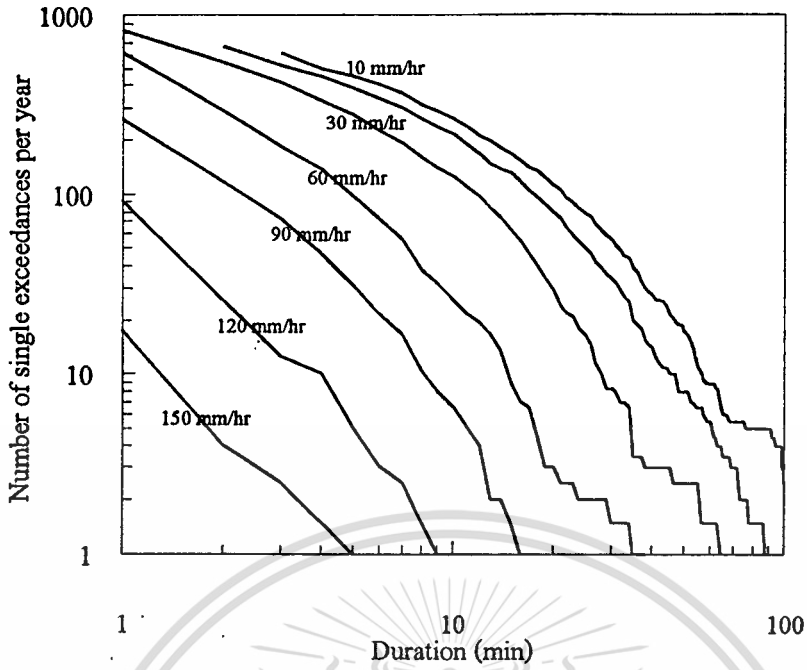

Fig. 3.13 Average number of single exceedances per year above the specified threshold with durations equal or greater than the specified value at Klong Yai, Tard

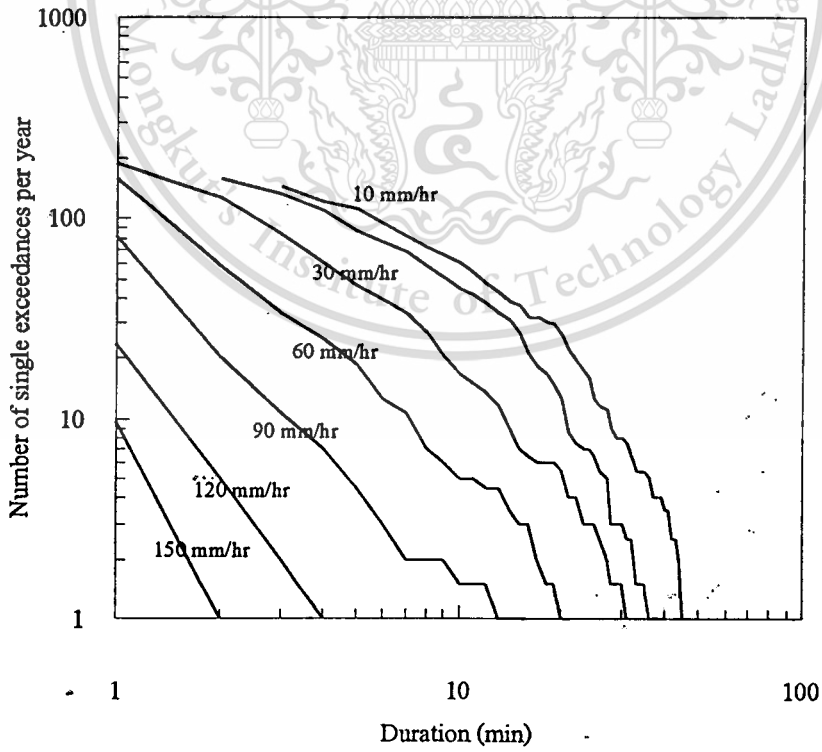

Fig. 3.14 Average number of single exceedances per year above the specified threshold with durations equal or greater than the specified value at KMITL, Bangkok

3.3.2 Number of Single Exceedances of Signal Attenuation

In addition, the same procedures to determine the single exceedances of rain, in section 3.2.1, can be processed on satellite signal attenuation data for obtaining the number of single exceedances of signal attenuation [19] as shown in the following figures. Fig. 3.15 to 3.17 indicate the number of single exceedances of observed signal attenuation on JCSAT-KMITL link, 12.7475 GHz, Thaicom3-Klong Yai link, 12.292 GHz and Thaicom3-KMITL link, 12.292 GHz.

For entire attenuation threshold, the numbers of single exceeding at smaller duration are more occurred than the larger ones conformed to the number of single exceedances of rainfall rate. For example, at threshold 13.5 dB in Fig. 3.15, the number of occurrence for single exceeding 13.5 dB for the duration exceeding 5 and 15 min are 40 and 11 times, respectively.

Characteristics of fading duration are further discussed in section 4.3.

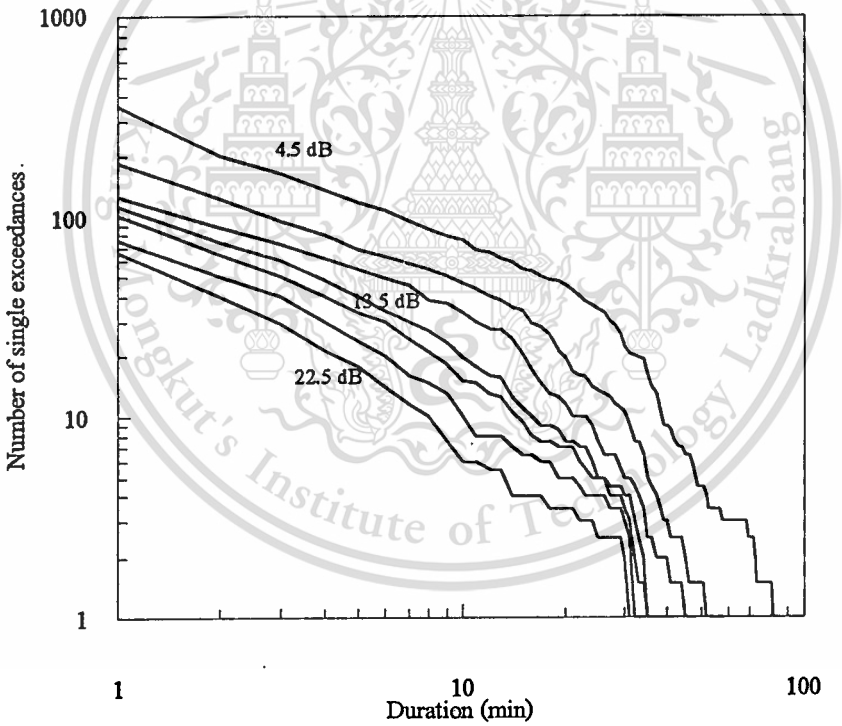

Fig. 3.15 Average number of single exceedances per year for satellite signal attenuation receiving beacon of JCSAT (12.7475 GHz) at KMITL Bangkok, 2000-2001

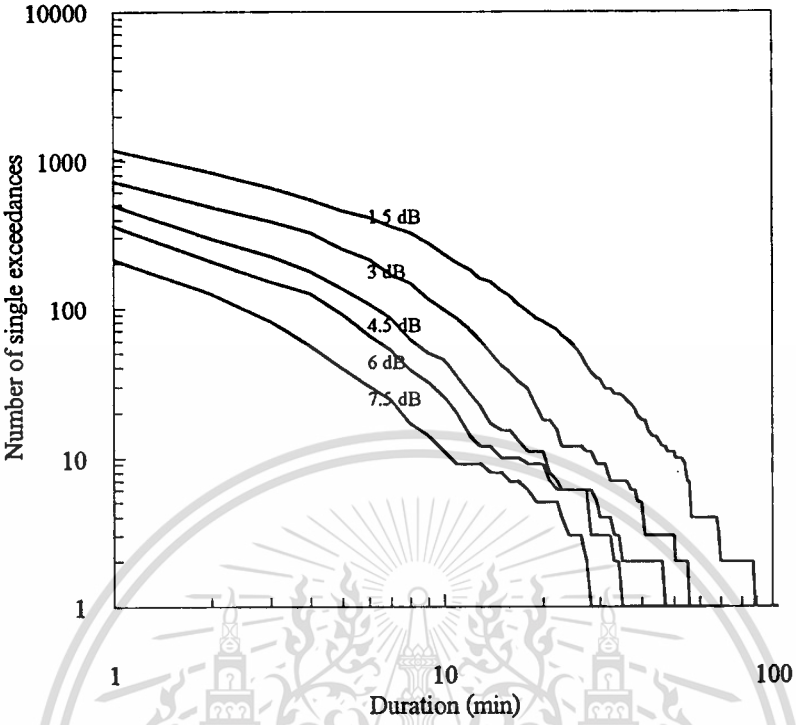

Fig. 3.16 Number of single exceedeances for Thaicom3 satellite signal (12.292 GHz) attenuation at Klong Yai, Trad, 2000

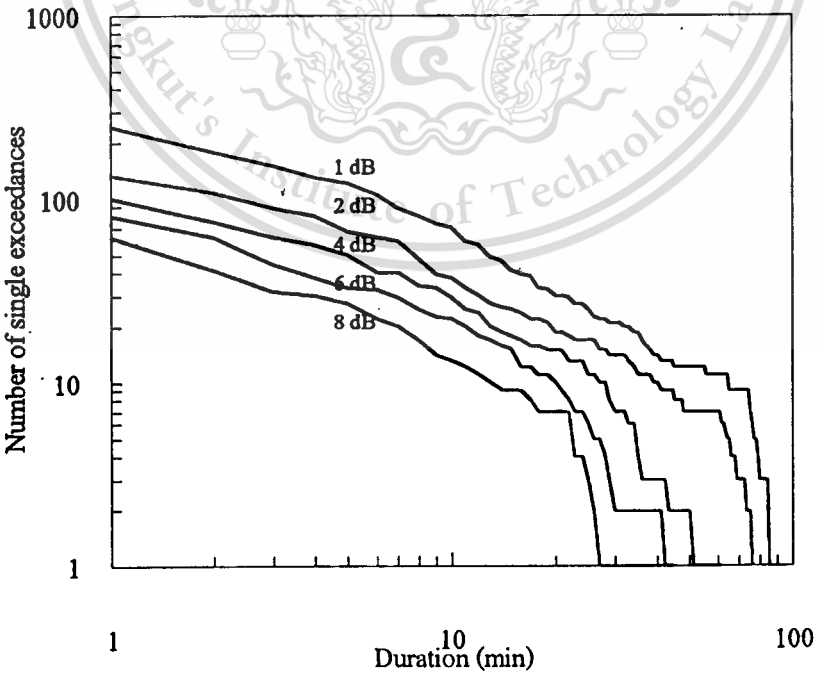

Fig. 3.17 Number of single exceedeances for Thaicom3 satellite signal (12.292 GHz) attenuation at KMITL, 1999

3.4 Estimated and Obtained Rain and Rain Attenuation Characteristics

Owing to knowledge of the natural variability of propagation phenomena is required for using in telecommunication system design, even though the long-term experimental data are lacking, there are some estimated models providing estimated data. The general method to predict attenuation due to precipitation and clouds along a slant propagation path is presented in 3.4.1. Then, 3.4.2 presents the conversion of annual statistics to worst-month statistics.

3.4.1 Calculation of Rain Attenuation Statistics from Point Rainfall Rate

The following procedure provides estimation of the long-term statistics of the rain attenuation on slant-path at a given location for frequencies up to 55 GHz. The following parameters are required [20]:

$R_{0.01}$: rainfall rate for the location for 0.01% of an average year (mm/hr)

h_S: height above mean sea level of the earth station (km)

θ: elevation angle (degrees)

φ: latitude of the earth station (degrees)

f: frequency (GHz)

R_e: effective radius of the Earth (8500 km)

- Calculate the rain height, h'_R, which is equivalent to h_0 as given in Recommendation The effective rain height is the height of the 0 ° C isotherm during rainy conditions. The following model is used for the global estimation of h_r (mean 0 ° C isotherm height) [21].

$$h_0 = \begin{cases} 3.0 + 0.0028\varphi & 0^\circ < \varphi < 36^\circ \\ 4.0\text{-}0.075(\varphi\text{-}36^\circ) & \varphi \geq 36^\circ \end{cases} \quad \text{km} \qquad (3.1)$$

where φ is the latitude of the station.

- For elevation angle $\theta \geq 5^\circ$ compute the slant-path length, L_S, below the rain height from:

$$L_s = \frac{(h'_R - h_s)}{\sin\theta} \quad \text{km} \tag{3.2}$$

where h_s is the height from the sea level of installed out door unit.

For $\theta<5^\circ$, the following formula is used:

$$L_s = \frac{2(h'_R - h_s)\beta}{\left(\sin^2\theta + \frac{2(h'_R - h_s)}{R_e}\right)^{1/2} + \sin\theta} \quad \text{km} \tag{3.3}$$

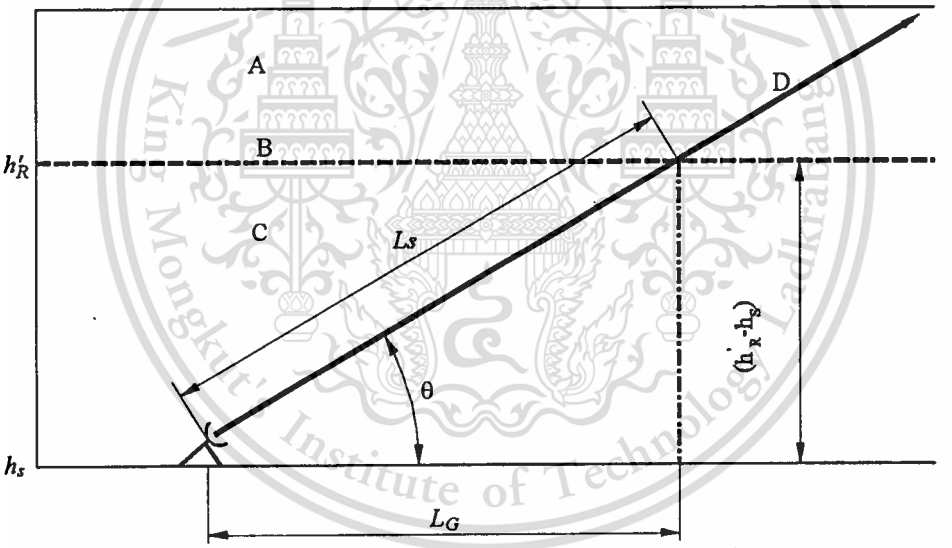

A: frozen precipitation
B: rain height
C: liquid precipitation
D: Earth-space path

Fig. 3.18 Schematic presentation of an Earth-space path giving the parameters to be input into the attenuation prediction process

- Obtain the rainfall rate, $R_{0.01}$, exceeded for 0.01% of an average year (with an integration time of 1 min) directly obtained from the cumulative distribution. If this

long-term statistic cannot be obtained from local data sources, an estimate can be obtained from the maps of rainfall rate given in Appendix A [22].

- Calculate the horizontal projection, L_G, of the slat-path length from:

$$L_G = L_S \cos\theta \qquad \text{km} \tag{3.4}$$

- Obtain the specific attenuation, γ_R, using the frequency-dependent coefficients, k and α, given and logarithm interpolation in Appendix B [23] and the rainfall rate, $R_{0.01}$, by using:

$$\gamma_R = k\left(R_{0.01}\right)^{\alpha} \qquad \text{dB/km} \tag{3.5}$$

- Calculate the horizontal reduction factor, $r_{0.01}$, for the 0.03% of time:

$$r_{0.01} = \frac{1}{1 + 0.78\sqrt{\frac{L_G \gamma_R}{f}} - 0.38\left(1 - e^{-2L_G}\right)} \tag{3.6}$$

- Calculate the vertical adjustment factor, $v_{0.01}$, for 0.01% of the time:

$$\zeta = \tan^{-1}\left(\frac{h'_R - h_S}{L_G r_{0.01}}\right) \qquad \text{degrees} \tag{3.7}$$

For $\zeta > \theta$, $L_R = \dfrac{L_G r_{0.01}}{\cos\theta}$ km

Else, $L_R = \dfrac{\left(h'_R - h_S\right)}{\sin\theta}$ km

If $|\varphi| < 36^{\circ}$, $\chi = 36 - |\varphi|$ degrees

Else, $\chi = \theta$ degrees

$$v_{0.01} = \frac{1}{1+\sqrt{\sin\theta}\left(31\left(1-e^{-(\theta/(1+\chi))}\right)\frac{\sqrt{L_R\gamma_R}}{f^2}-45\right)} \tag{3.8}$$

- The effective path length is:

$$L_E = L_R v_{0.01} \quad \text{km} \tag{3.8}$$

- The predicted attenuation exceeded for 0.01% of an average year is obtained from:

$$A_{0.01} = \gamma_R L_E \quad \text{dB} \tag{3.9}$$

- The estimated attenuation to be exceeded for other percentages of an average year, in the range 0.001% to 5%, is determined from the attenuation to be exceeded for 0.01% for an average year.

If $p \geq 1\%$ or $|\varphi| \geq 36^\circ$: $\beta = 0$

If $p < 1\%$ and $|\varphi| < 36^\circ$ and $\theta \geq 25^\circ$: $\beta = -0.005(|\varphi| - 36)$

Otherwise : $\beta = -0.005(|\varphi| - 36) + 1.8 - 4.25\sin\theta$

$$A_p = A_{0.01}\left(\frac{p}{0.01}\right)^{-\left(0.655+0.033\ln(p)-0.045\ln(A_{0.01})-\beta(1-p)\sin\theta\right)} \quad \text{dB} \tag{3.10}$$

As mention in the above methods, $R_{0.01}$ can be obtained from average annual distribution and from the maps of rainfall rate given in Appendix A. Therefore, we consider $R_{0.01}$ for both cases indicated as R0.01, rainfall rate 0.01% of obtained annual distribution, and $R_{0.01}$ of N and P zones. Fig. 3.19 to 3.21 illustrate observed experimental data and estimated of cumulative distribution of rain attenuation.

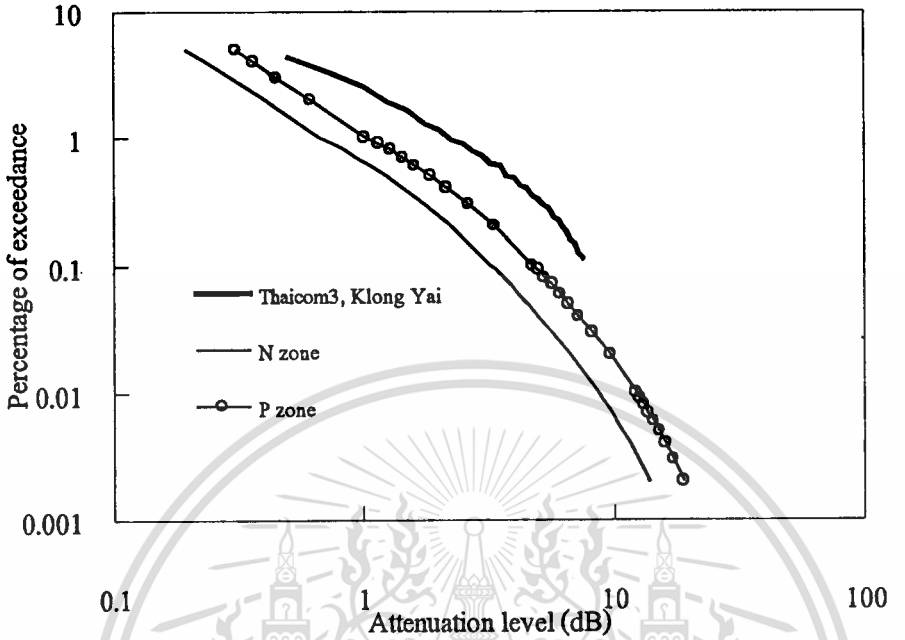

Fig. 3.19 Estimation of cumulative distribution of attenuation and observed data on Thaicom3-Trad link, September 1999 - August 2000

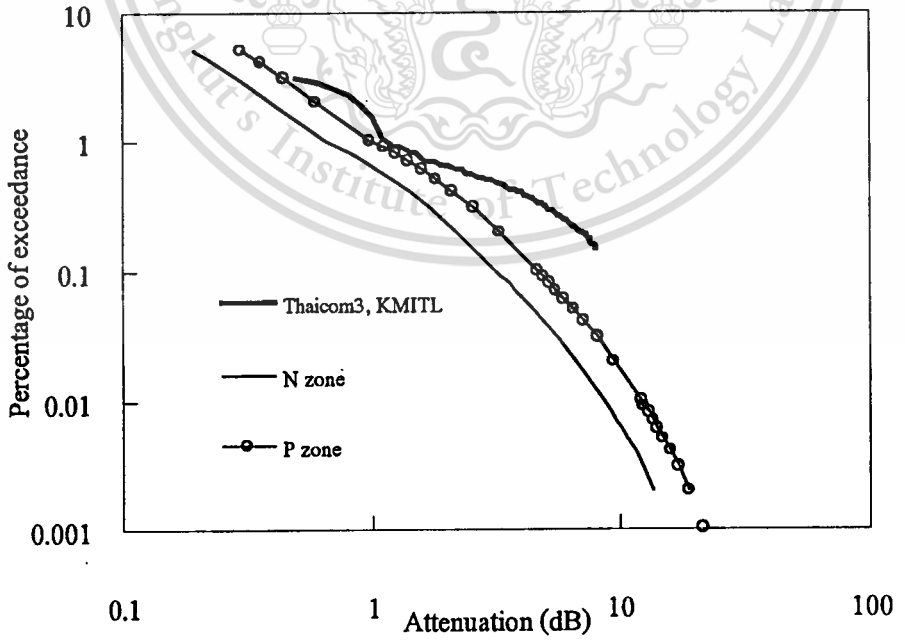

Fig. 3.20 Estimation of cumulative distribution of attenuation and observed data on Thaicom3-Bangkok link, 1999

In Fig. 3.19, observed data at Klong Yai are greater than all cases of estimation. As former mention that, even though, Klong Yai, is located in N climate zone, rainfall rate distribution are greater than those of the proposed model and estimation method as till now indication. Besides, in Fig. 20 and Fig. 21, the estimation results in the case of $R_{0.01}$ of observed annual distribution is located between the estimation results in the cases of given $R_{0.01}$ of N and P climate zone. The observed annual distributions of attenuation at Bangkok are rather greater than the all cases of estimation. Considerably, the estimation result of $R_{0.01}$ selected as 0.01% of predicted distribution in P zone agrees with the observed data at not exceeded 1% on JCSAT-Bangkok link.

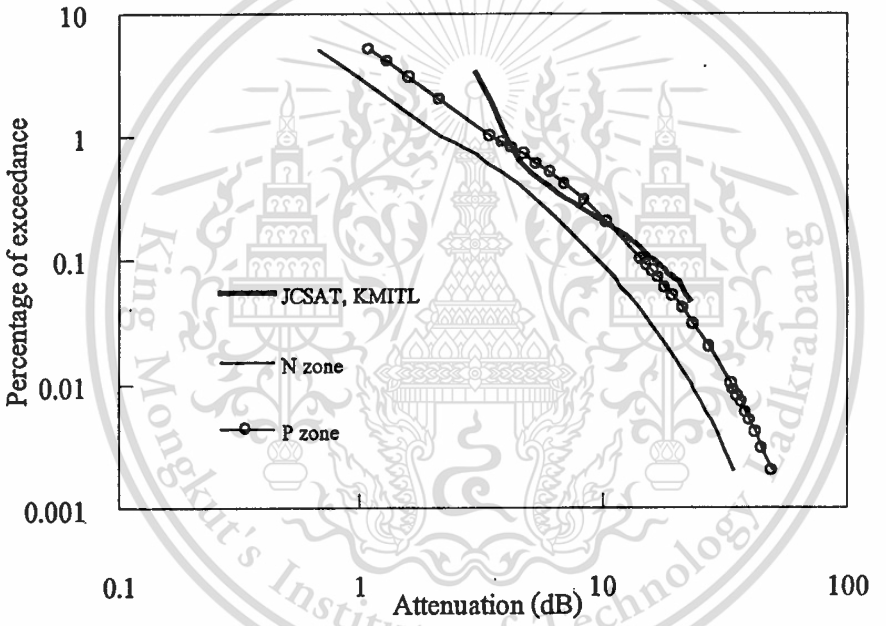

Fig. 3.21 Estimation of cumulative distribution of attenuation and observed data on JCSAT-Bangkok link, 2000-2001

3.4.2 Conversion of Annual Statistics to Worst-Month Statistics

Worst-month statistics is one of required statistics for design of radio communication systems. Normally, the reference statistics for many radio meteorological data and propagation prediction methods is the long-term average annual distribution. Consequently, the conversion model of the annual to the worst-month statistics is needed. The following procedure is used for conversion of the average annual time percentage of excess to the average annual worst-month time percentage of excess [24].

- The average annual worst-month time percentage of excess, p_W, is calculated from the average annual time percentage of excess, p, by multiplied with conversion factor Q as following expression:

$$p_W = Qp \tag{3.11}$$

where $1<Q<12$, and both p_W and p refer to the same threshold level.

- Q is defined by two parameters (Q_1, β) function of p (%).

$$Q(p) = \begin{cases} 12 & \text{for} \quad p < \left(\frac{Q_1}{12}\right)^{\frac{1}{\beta}} \\ Q_1 p^{-\beta} & \text{for} \quad \left(\frac{Q_1}{12}\right)^{\frac{1}{\beta}} < p < 3\% \\ Q_1 3^{-\beta} & \text{for} \quad 3\% < p < 30\% \\ Q_1 3^{-\beta}\left(\frac{p}{30}\right)^{\frac{\log\left(Q_1 3^{-\beta}\right)}{\log(0.3)}} & \text{for} \quad 30\% < p \end{cases} \tag{3.12}$$

- On the other hand, the calculation of the average annual time percentage of excess from the given value of average annual worst-month time percentage of excess is done through the inverse relationship.

$$p = p_W / Q \tag{3.13}$$

and the dependence of Q and p_W can be easily derived from the above given dependence of Q and p the resulting relationship for $12p<p_W(\%)<Q_1 3^{(1-\beta)}$ is ($p_0 = (Q_1/12)^{1/\beta}$):

$$Q = Q_1^{1/(1-\beta)} p_W^{-\beta/(1-\beta)} \tag{3.14}$$

- For global planning purposes the following values for the parameters Q_1 and β

$$Q_1 = 2.85 \quad \text{and} \quad \beta = 0.13 \tag{3.15}$$

- For more precision the values of Q_1 and β for the different climatic regions and various propagation effects given in Appendix C should be used where appropriate. Therefore, for the above estimation, we alternatively try the factors of Indonesia because Indonesia is located in the same tropical region as the experiment sites.

$$Q_1 = 1.7 \quad \text{and} \quad \beta = 0.22 \tag{3.16}$$

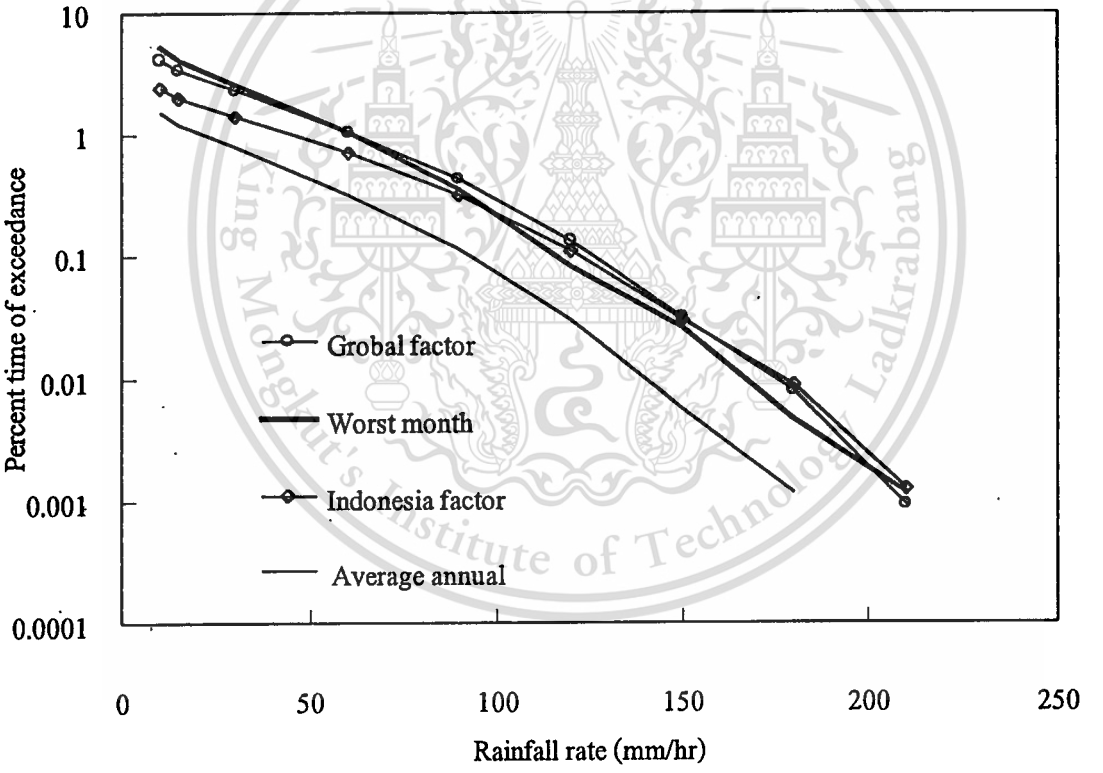

Fig. 3.22 Worst month conversion of rainfall rate at Klong Yai, Tard

Fig. 3.22 and Fig. 3.23 show the result of the above worst month conversion of rainfall rte cumulative distribution in Klong Yai, Trad and KMITL, Bangkok, respectively. In Fig 3.21, we consider that with using the global factor ($Q_1 = 2.85$ and $\beta = 0.13$) totally gives a good fit with worst month at Klong Yai site. On the other hand, for KMITL site, with the factor ($Q_1 = 1.7$

and $\beta = 0.22$) of Indonesia gives a good fit with the average annual worst month. However, both cases can be considered to satisfy the worst month conversion.

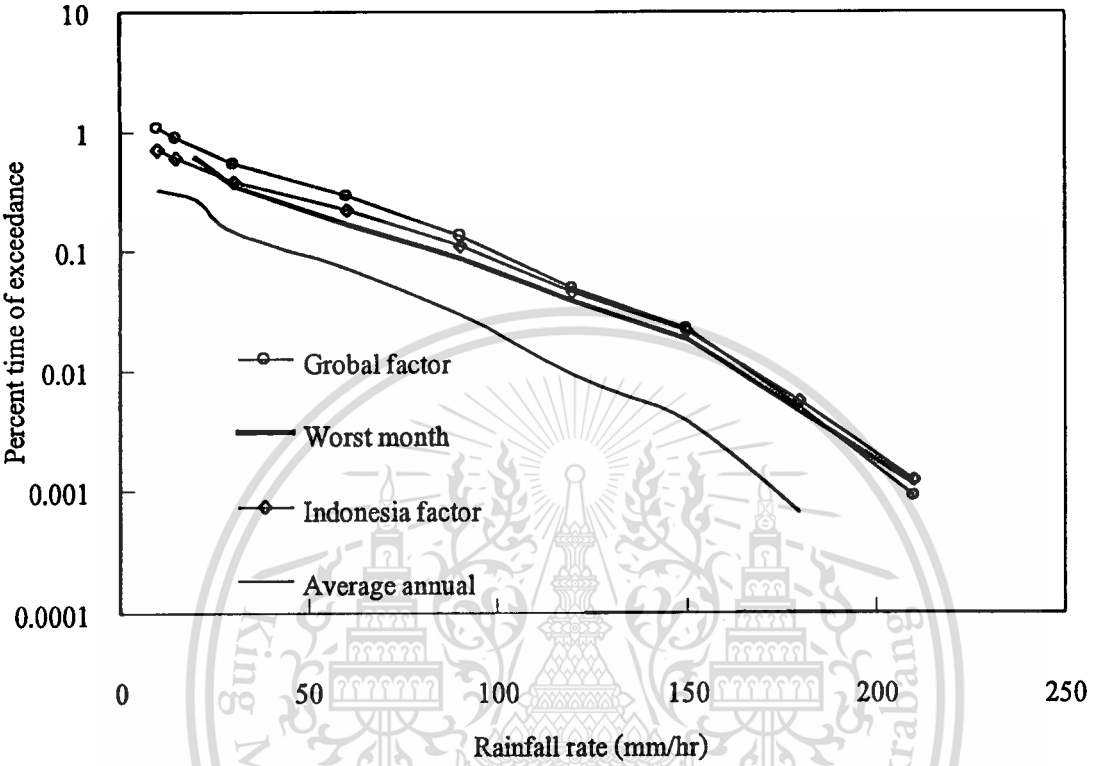

Fig. 3.23 Worst month conversion of rainfall rate at KMITL, Bangkok

3.5 Conclusions

From 2-year observation of the rainfall rate data of Klong Yai, Trad and KMITL, Bangkok, cumulative distribution are firstly analyzed and presented. Percentages of time of rainfall rate exceeded are illustrated versus those rainfall rates. Klong Yai located in N zone on ITU-R rain climate zone give percentage of exceedance over those of N and P zones in the range of rainfall rate less than 130 mm/hr. KMITL located on the contour line between N and P zones give the results agreed with the prediction proposed be ITU-R rain climate model. On the other hand, in the range of rainfall rates exceeded about 170 mm/hr percentage of excedances of both data give the percentage lower than those of N zone. Hourly and monthly-hourly distributions represent the probability of occurrence of rainfall rate based on local time in a day and also based on moth.

Number of single exceedances of both rainfall rate and signal attenuation represents the number of times that the rainfall rate and attenuation exceed the threshold while time duration exceed the threshold in the period of typical year.

Finally, average year cumulative distribution of signal attenuation are comparatively plotted on with the model of rain attenuation of ITU-R. The observed result of Klong Yai site exceeds those estimated by ITU-R model. At the KMITL site, rainfall rate at 0.01% of cumulative distribution of observed data gives the better fit than those estimated by N and P climate zones. Moreover, the worst-month statistics can be obtained from conversion of annual statistics to worst-month statistics proposed ITU-R. By using parameters of both locations, global and Indonesia (even though, they are parameters for rain effecting on terrestrial), gives acceptable results rather fitting with the observed worst-month.

CHAPTER 4

CHARACTERISTICS OF RAINFALL RATE ATTENUATION

Since in chapter 3 has presented some general characteristics of rainfall rate and rain attenuation of data obtained from each experiment sites, this chapter deals with further useful analysis methodology. Firstly, the problem of un-correlation between rainfall rate and signal attenuation based on GMT of obtained data is solved with proposed method, alternatively, based on the cumulative distributions of rainfall rate and signal attenuation data. Secondly, conditional distributions of rain fading duration and rainfall rate exceedance are presented. In the following section, fading duration distribution characteristics are discussed as statistical distribution form. Finally, 1-hour rainfall rate to 1-minute rainfall rate conversion is presented.

4.1 Correlation Between Rainfall Rate and Rain Attenuation

Rain is main effect that causes serious degradation of radio signals at frequencies above 10 GHz. Some researchers have tried to define the correlation between rainfall rate and signal attenuation. The correlation can be obtained directly from observed experimental data. Both rainfall rate and signal attenuation data are measured and recorded simultaneously. ITU-R P.838 [23], Specific attenuation model for rain for use in prediction methods, provides calculating process to predict the correlation for each location. Due to unreasonable correlation obtained directly from experimental data, based on recording local time, we also propose an idea to obtain more appropriate correlation.

4.1.1 ITU-R Rain Attenuation Prediction Model

The ITU Radio communication assembly, considering that there is a need to calculate the attenuation due to rain from a knowledge of rain rates, recommends that the following procedure be used.

Firstly, specific attenuation model for use in prediction methods [23], Specific attenuation γ_R (dB/km) is obtained from the rain rate R (mm/hr) using the power-law relationship:

$$\gamma_R = kR^{\alpha} \tag{4.1}$$

The frequency-dependent coefficients k and α are given in Appendix B for linear polarizations (horizontal: H, vertical: V) and horizontal paths. Values of k and α at frequencies other than those in Appendix B can be obtained by interpolation using a logarithmic scale for frequency, a logarithmic scale for k and a linear scale for α. Moreover, k and α can also calculated as following methods [25].

$$k_H = \begin{cases} 4.0848\times10^{-5} f^{(1.4550+0.3925\ln f)} & for \quad 1 \le f < 15 \quad GHz \\ 2.8790\times10^{-7} f^{(5.7988-0.5431\ln f)} & for \; 15 \le f < 400 \quad GHz \end{cases} \tag{4.2}$$

$$a_H = \begin{cases} 0.8424 + \dfrac{0.3151}{(\ln f - 2.0462)^2 + 0.6394} & for \quad 1 \le f < 15 \quad GHz \\ 0.6789 + 0.7005\exp(-0.02600 f) & for \; 15 \le f < 400 \quad GHz \end{cases} \tag{4.3}$$

$$k_V = \begin{cases} 3.7332\times10^{-5} f^{(1.4169+0.467\ln f)} & for \quad 1 \le f < 15 \quad GHz \\ 2.9220\times10^{-7} f^{(5.1898-0.5297\ln f)} & for \; 15 \le f < 400 \quad GHz \end{cases} \tag{4.4}$$

$$a_V = \begin{cases} 0.81558 + \dfrac{0.2850}{(\ln f - 2.0775)^2 + 0.5694} & for \quad 1 \le f < 15 \quad GHz \\ 0.6887 + 0.6371\exp(-0.02493 f) & for \; 15 \le f < 400 \quad GHz \end{cases} \tag{4.5}$$

For linear and circular polarization, and for all path geometrics, the coefficients k and α can be calculated by the following equations:

$$k = \left[k_H + k_V + (k_H - k_V)\cos^2\theta\cos 2\tau\right]/2 \tag{4.6}$$

$$a = \left[k_H a_H + k_V a_V + (k_H a_H - k_V a_V)\cos^2\theta\cos 2\tau\right]/2k \tag{4.7}$$

where θ is the path elevation angle and τ is the polarization tilt angle relative to the horizontal (τ=45° for circular polarization).

Obtained specific attenuation, then, provides signal attenuation on slant path by being multiplied with the length of the slant path. The slant path length can be found as following methods:

- Calculate the rain height, h'_R, which is equivalent to h_0 as given in Recommendation The effective rain height is the height of the 0 ° C isotherm during rainy conditions. The following model is used for the global estimation of h_r (mean 0 ° C isotherm height).

$$h_0 = \begin{cases} 3.0 + 0.0028\varphi & 0^\circ < \varphi < 36^\circ \\ 4.0\text{-}0.075(\varphi\text{-}36^\circ) & \varphi \geq 36^\circ \end{cases} \quad \text{km} \qquad (4.8)$$

where φ is the latitude of the station.

- For elevation angle $\theta \geq 5^\circ$ compute the slant-path length, L_S, below the rain height from:

$$L_s = \frac{\left(h'_R - h_s\right)}{\sin\theta} \quad \text{km} \qquad (4.9)$$

where h_s is the height from the sea level of installed out door unit.

For $\theta < 5^\circ$, the following formula is used:

$$L_s = \frac{2(h'_R - h_s)}{\left(\sin^2\theta + \frac{2(h'_R - h_s)}{R_e}\right)^{1/2} + \sin\theta} \quad \text{km} \qquad (4.10)$$

From the specific attenuation, therefore, the predicted correlation can be expressed as:

$$\begin{aligned} A &= \gamma_R \cdot L_s \\ &= kR^{\alpha} L_s \quad \text{dB} \end{aligned} \qquad (4.11)$$

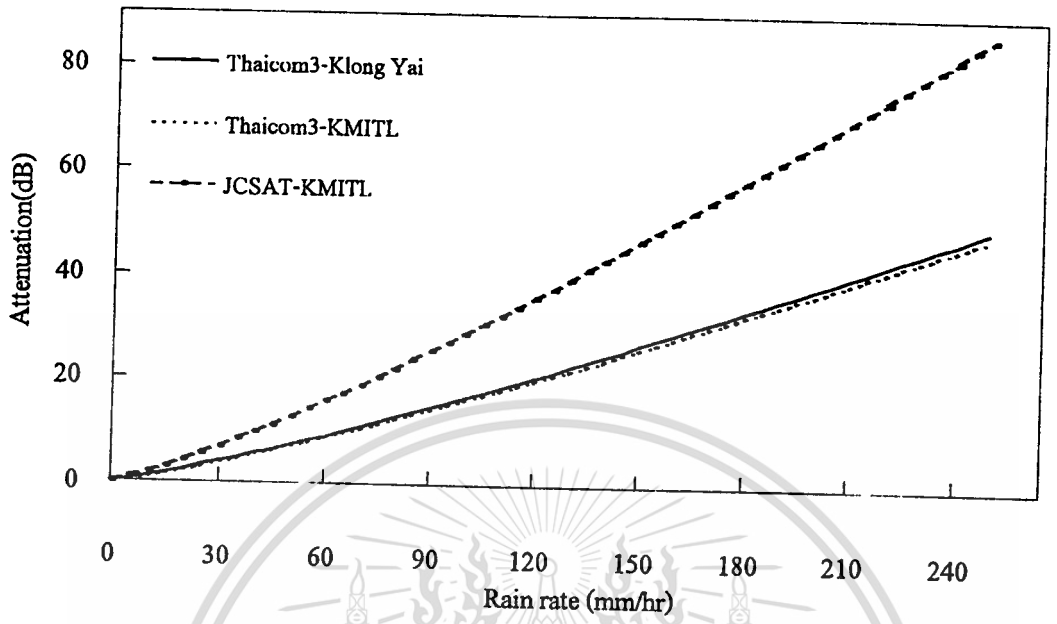

Fig. 4.1 The relation between rain and rain attenuation by ITU-R model at each experiment sites

The results of predicted model of the relation of rain attenuation and rainfall rate are indicated in the Fig. 4.1. We consider that the predicted results on the slant path of Thaicom3 at KMITL and Klong Yai sites are obviously the same because all parameters for both predicted methods are nearly the same. For example, at the rainfall rate about 60 mm/hr, satellite from Thaicom3 satellite signal is attenuated on the slant-path about 8.9 dB and 8.7 dB at Klong Yai, Trad and KMITL Bangkok, respectively. For satellite signal from JCSAT satellite, signal is attenuated about 15.8 dB at KMITL site.

4.1.2 The Correlation of Rainfall Rate and Attenuation Based on Percentage of Exceeding

From observed experimental data of each sites, Klong Yai, Trad and KMITL, Bangkok, the correlation of rain and signal attenuation can be normally obtained based directly on recorded local time of rainfall rate and signal attenuation data. Thus, the obtained correlations are considerably unreasonable. Even though the obtained data have been measured and recorded simultaneously. The mentioned unreasonable conditions may be caused by, for example, asynchronous time of equipment, rain in the slant-path, electric power shut down, etc. They seem to be complex problems to mention here. Therefore, they should be neglected to avoid complexity. The simple procedure is briefly explained as the following paragraph.

We consider the cumulative distributions of rainfall rate and signal attenuation from 3.2. In addition, to obtain more reliable average data, not only average annual cumulative distributions but also cumulative distributions per month are employed. At the same percentage of exceeding of rainfall rate and signal attenuation distributions, the coordinate of rainfall rate and attenuation data are obtained by appropriate interpolation methods. Then the obtained coordinates are used to perform the reasonable correlation indicated as following [19].

In addition, the predicted data are comparatively indicated for each experiment sites. The correlation data obtained by manipulating experimental data with the above proposed procedures rather agree with the estimated correlation referred to the above mentioned. Fig. 4.2 illustrates the correlation between rainfall rate and satellite signal attenuation along the slant path about 5.7 km from ETS V satellite at KMITL site. Fig. 4.3 and Fig. 4.4 illustrate satellite signal 12.292 GHz from Thaicom 3 satellite attenuated along slant path correlating with rainfall rate at Klong Yai, Trad and KMITL, Bangkok, respectively.

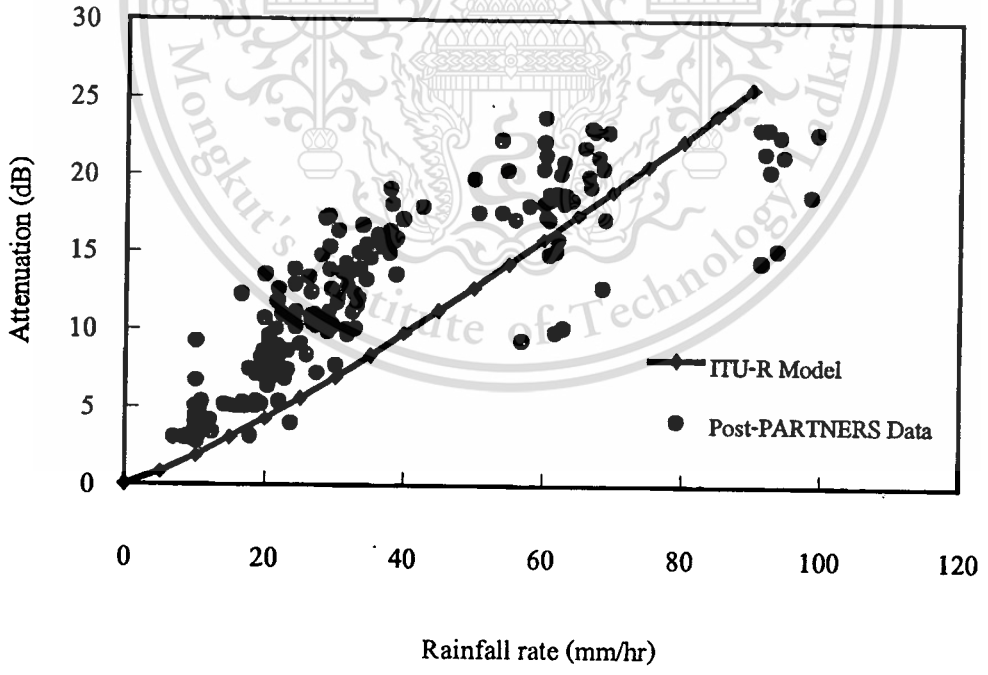

Fig. 4.2 The correlation between rainfall rate and satellite signal attenuation at KMITL Bangkok

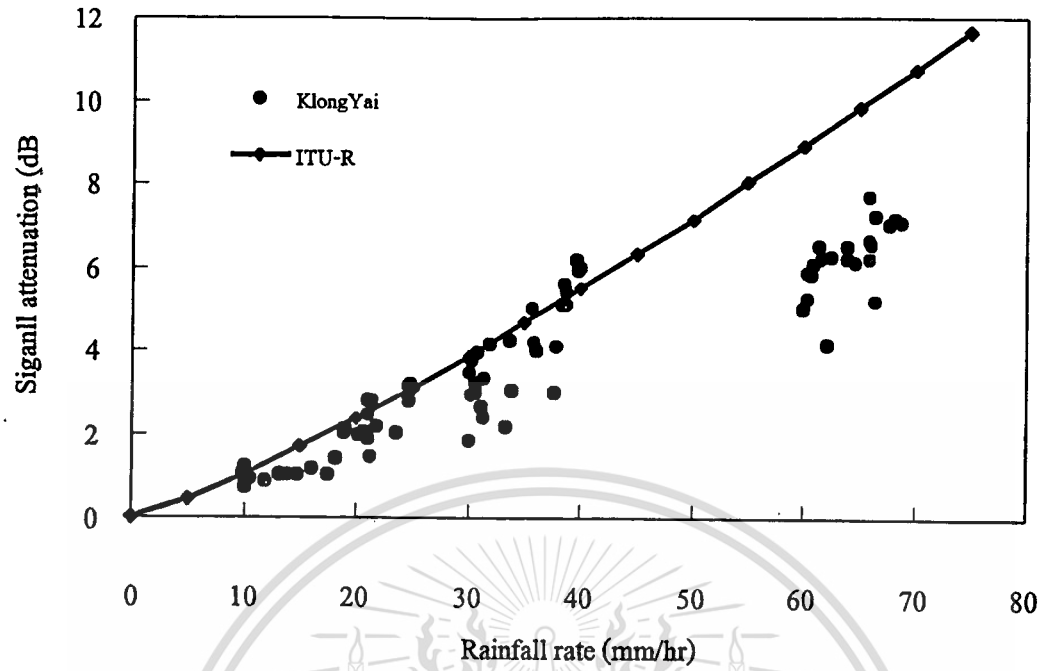

Fig. 4.3 The correlation between rainfall rate and satellite signal attenuation at Klong Yai, Trad

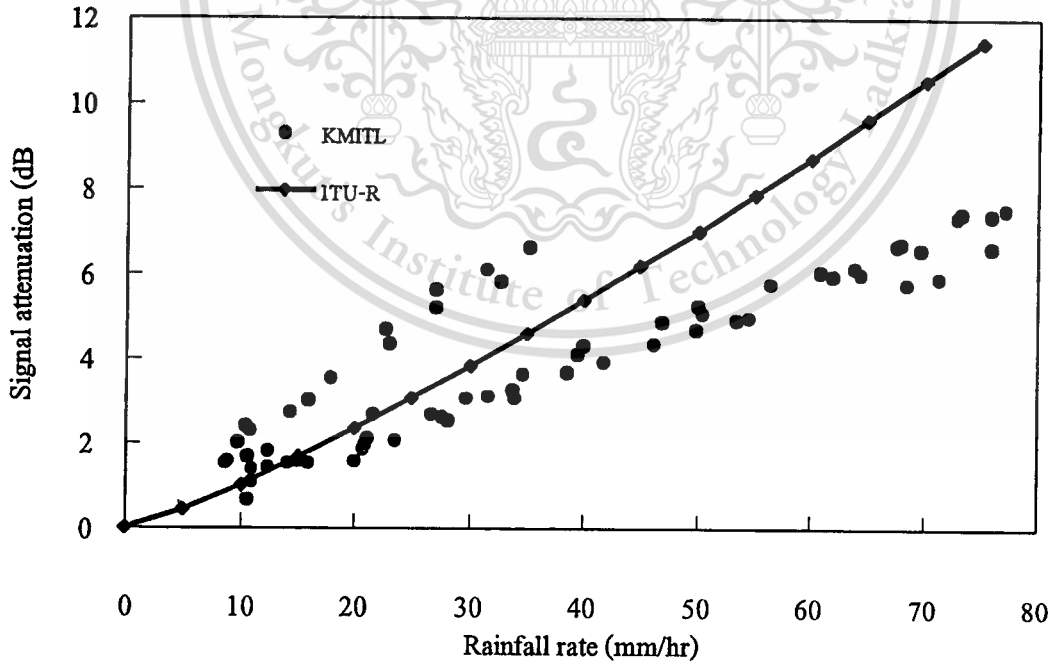

Fig. 4.4 The correlation between rainfall rate and satellite signal attenuation at KMITL, Bangkok

There are advantages of the above-proposed methods to find the correlation of rainfall rate and satellite signal attenuation along the slant path. We can neglect the local time of the data that is the problem for such the paper-recorded data observed from satellite signal recorder. Satellite signals from Thaicom3 satellite are recorded by paper recorder at both Klong Yai , Trad and KMITL, Bangkok. It is unreasonable to obtain the correlation between rainfall rate and signal attenuation based normally on the recorded local time. In addition, the cumulative distributions of both rainfall rate and signal attenuation are generally available. Therefore, it is not complex to estimate the correlation based on them.

4.2 Conditional Distributions

In section 3.3, fading duration concept and definite were introduced. They dealt with 2 variables, rain fading dept and fading duration (continuous time of outage). In this section, we further discuss about these two variables. Conditional probabilities dealing with 2 variables called "conditional distribution" are characterized as "number" distribution and "time" distribution [3]. The conditional distribution of rainfall rate fading and time duration is one of the most useful presents for being use to advantage in the system designing.

The conditional distribution presents the probability of number and time of event of the single exceeding time duration (fading duration), threshold, assume that rainfall rate exceed the threshold. Therefore, the conditional distributions are considered as $\text{Prob}(D' \geq D \,/\, R' \geq R)$ where D and D' are threshold and fading duration on obtained data and R and R' are threshold rate and rainfall rate on the obtained data. Owing to the number and time of an event of single exceedance, there are two types of conditional distribution being discussed: the "number" distributions that are defined as

$$P_n(D/R) = \frac{\text{Number of cases } (D' \geq D | R' \geq R)}{\text{Number of cases } (D' \geq 0 | R' \geq R)} \tag{4.12}$$

and the "time" distributions, defined as

$$P_t(D/R) = \frac{\text{Total minutes } (D' \geq D | R' \geq R)}{\text{Total minutes } (D' \geq 0 | R' \geq R)} \tag{4.13}$$

equation (4.3) gives the probability of exceeding D once R has been exceeded, whereas equation (4.12) indicates how frequently this takes place. P_t will give the conditional probability of duration D, which if exceeded will require corrective action in the communication system. On the other hand, P_n will give an indication of how often the minimum duration D will present once R was exceeded. Both can be used to advantage in system designing.

The parametric study is illustrated in Fig. 4.5 and Fig. 4.6 for P_n and in Fig. 4.7 and Fig. 4.8 for P_t. As mentioned about the limitation of the instrument and measurement in the experiment, the D step is set to be 1 minute. In addition, the minimum of duration also set as 1 minute, therefore, we can not observe the rainfall rate duration less than 1 minute. The first step of the duration for determining the conditional distribution is 2 minute.

In Fig. 4.5, for example, total number of all single events that fading durations are greater or equal 10 minutes while rainfall rates are greater than or equal 90 mm/hr is 3 % of all rain events (fading duration greater than or equal 1 minute, for above condition) which rainfall rates exceed 90 mm/hr. In the same condition, in Fig. 4.6, the percentage is 2.5 %.

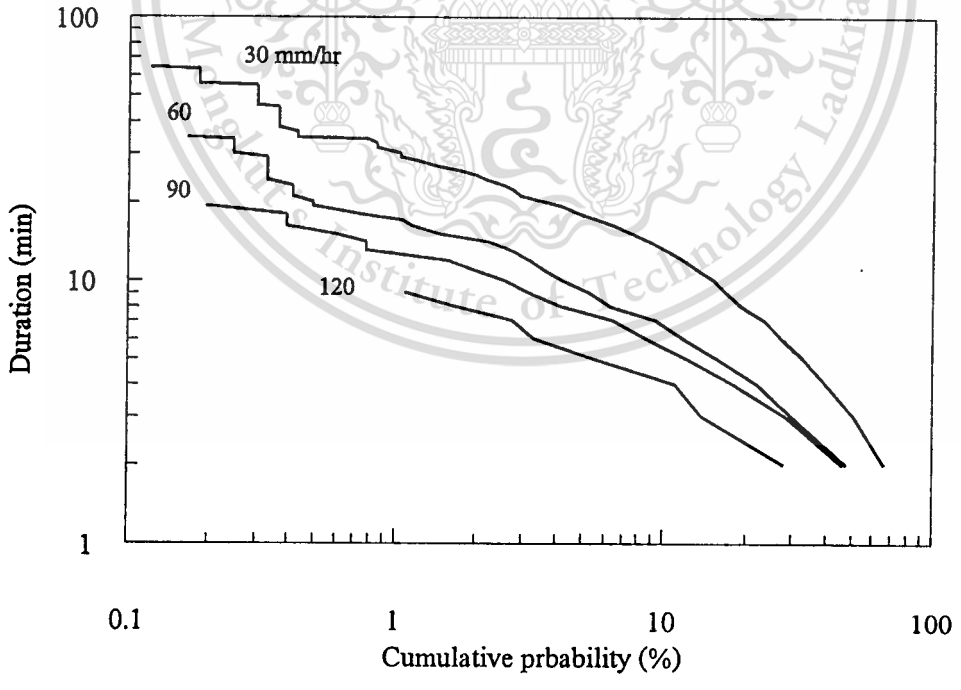

Fig. 4.5 Example of the number distribution $P_n(D/R)$ in log-normal coordinate of observed data at Klong Yai, Trad

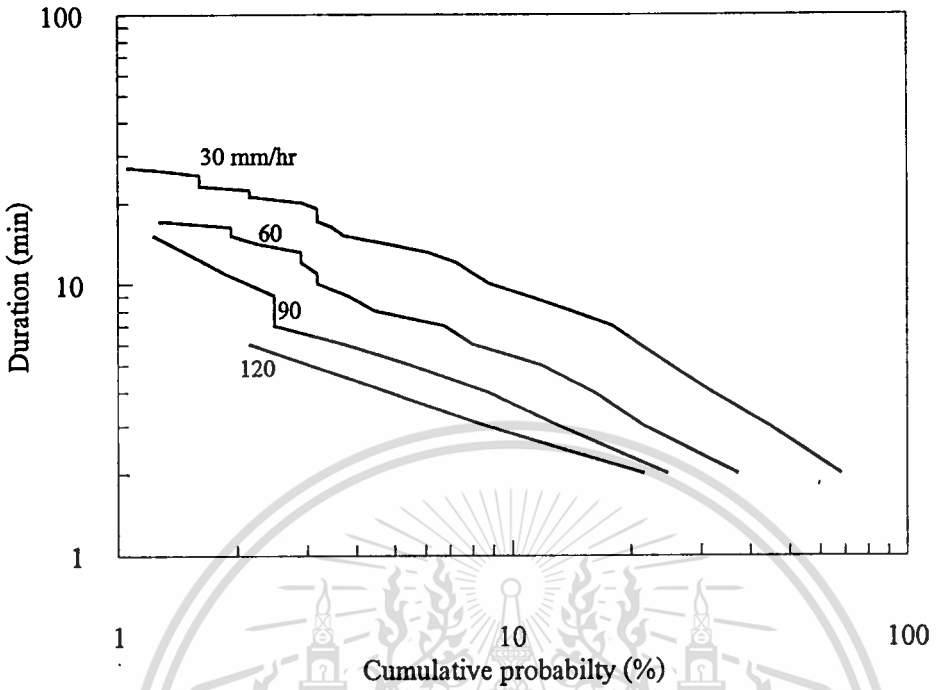

Fig. 4.6 Example of the number distribution $P_n(D/R)$ in log-normal coordinate of observed data at KMITL, Bangkok

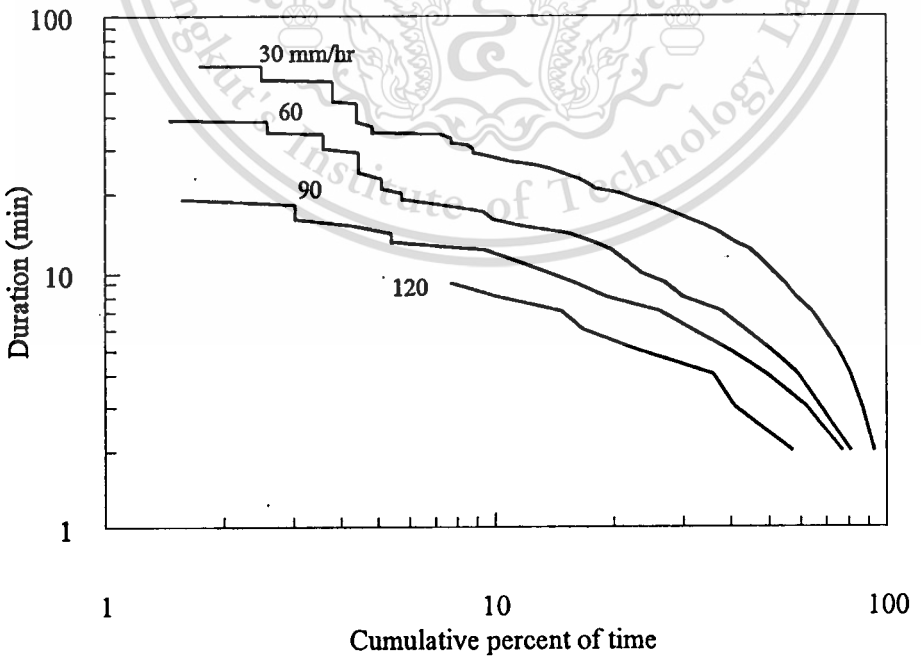

Fig. 4.7 Example of the time distribution $P_t(D/R)$ in log-normal coordinate of observed data at Klong Yai, Trad

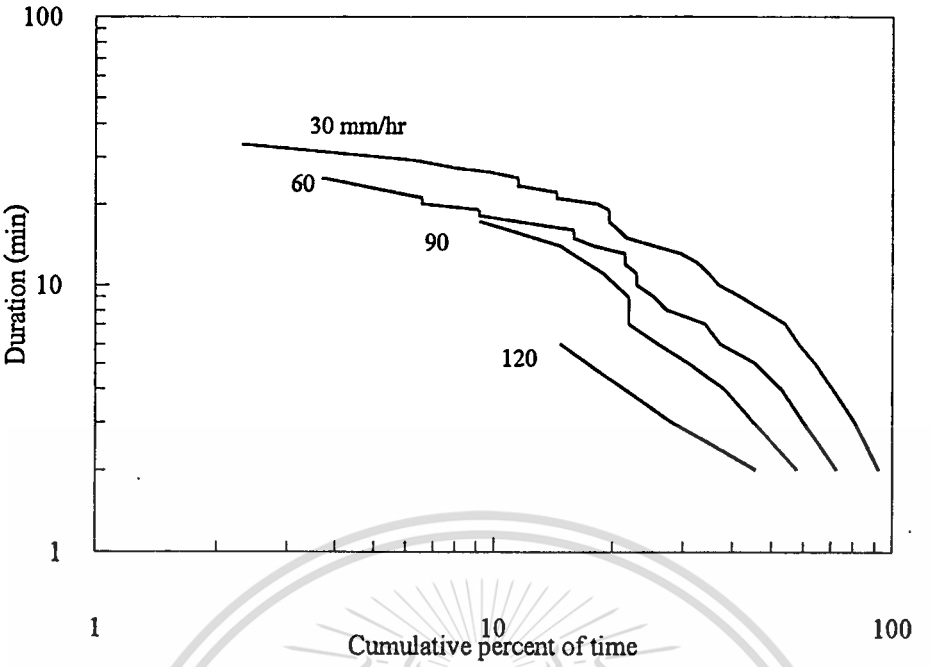

Fig. 4.8 Example of the time distribution $P_t(D/R)$ in log-normal coordinate of observed data at KMITL, Bangkok

In Fig. 4.7 and 4.8, consequently, cumulative percentages on the x-axis indicate the percentage total time of considered exceedance of threshold. For example, at the threshold 60 mm/hr and 10 minutes the percentages of exceedance are about 15% and 25% in both Fig. 4.7 and 4.8, respectively.

The higher cumulative probabilities for P_n and higher percentage of time for P_t can not be indicated due to the insufficient sampling interval 1-minute to obtain higher rainfall rate. It might considerably be one of the affects on the observed data.

Considerably, in Fig. 4.5 to Fig. 4.8 are selected plots on log-normal probability coordinate. These features would be considered further as log-normal distribution in the following section that former researchers have reached this conclusion of log-normality.

4.3 Fading Duration Characteristics

4.3.1 Analysis of the Average Number and Duration of Single Exceedances

It seems intuitive that as R increases, the number N of single exceedances of that threshold should diminish. The same applies to durations D of the exceedance of R. Enric vilar

[3,26] proposed that of 49 year rain data in Barcelona, Spain, for the range 20-250 mm/hr the annual average of N, $\overline{N}$, was found to be well modeled by

$$\log_{10}\overline{N} = -8.966\times10^{-2}R + 2.012 \tag{4.14}$$

From the obtained 2 years rain data of Klong Yai and KMITL, for the range 20-180 mm/hr the annual average of N, $\overline{N}$, was found to be linearly fit by the following equations (4.15) and (4.16) respectively

$$\log_{10}\overline{N} = -1.6\times10^{-2}R + 3.633 \tag{4.15}$$

$$\log_{10}\overline{N} = -1.4\times10^{-2}R + 2.951 \tag{4.16}$$

The dependence of $\overline{N}(D)$ for each threshold R exceeded and therefore gives the conditional distribution as previous section. For the above equations we can conclude here that at the same rainfall rate the number of exceeded occurrences at Klong Yai are greater than KMITL and at both site in Thailand are greater than in Barcelona, Spain.

Table 4.1 Average Number of times per year $\overline{N}(R)$

R (mm/hr)	20	30	40	60	70	90	120	140	150	160	CCIR Zone and Remarks
Klong Yai	-	823	-	611	-	255.5	91.5	-	17.5	-	Zone N 2 years
KMITL	-	188	-	156.5	-	81	23	-	9	-	Zone N/P 2 years
Barcelona (Spain)	60	40.4	21.8	16.8	12.9	6.2	3.9	2.4	-	1.5	Zone L, Jardi 49 years
Slough (UK)	17	6.5	3.5	-	1.8	-	-	-	-	-	Zone E, Enric 5 years
Ile-Ife (Nigeria)	100	-	-	40	-	9.5	4	1.3	-	0.4	Zone M/N, Enric 26 months

Table 4.1 also gives the comparison between the results obtained data from both sites and those of Enric et al [3] Barcelona, Spain, and Harden et al. [27] in Slough, England, and Ajayi et

al. [28] in Ile-Ife, Nigeria. The choice of 1 min base for D facilitates possible coparison to results from the other locations. We see the dependence upon the climate zone.

Similar analysis was carried out for the mean $\overline{D}$ and standard deviation σ_D, of the durations of exceedances of R over the 2 years. It found that they could be fit by (4.17) and (4.18) for Kolng Yai and KMTIL, respectively.

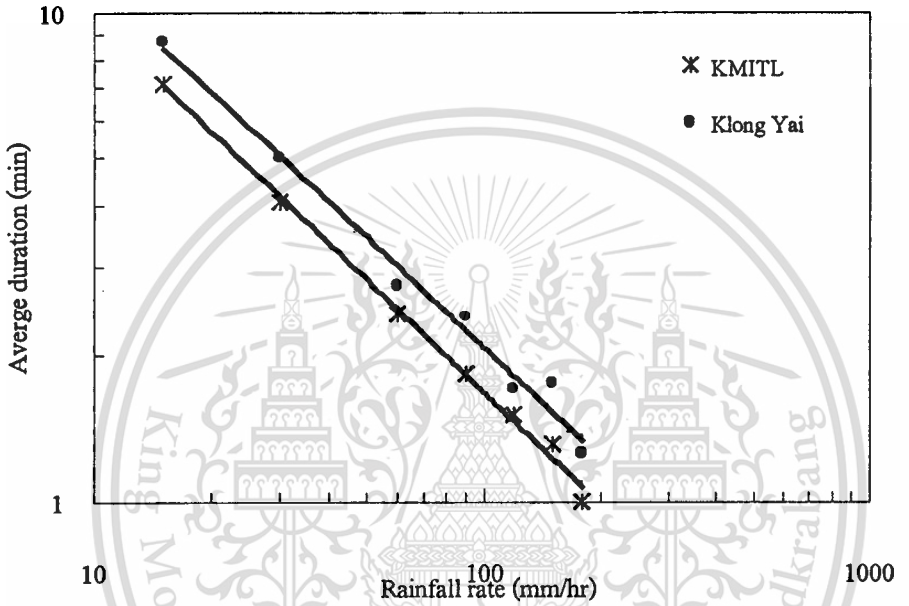

Fig. 4.9 Average duration of single exceedances and fit

$$\overline{D}(R) = 62.83R^{-0.75} \quad \text{min} \tag{4.17}$$

$$\overline{D}(R) = 54.46R^{-0.75} \quad \text{min} \tag{4.18}$$

with good fit, according to a least square criterion.

Some preliminary calculations illustrate the use of these results. For example, an estimate of total average exceedance per year of level R can be obtained by multiplying $\overline{N}(R)$ and $\overline{D}(R)$. This value divided by the number of minutes of an average year (525,600) should give an estimate of the conventional outage probability $P(R)$ that the level R is equal or exceeded.

4.3.2 Fading Duration Distribution

Since fading duration has been analyzed as conditional distribution and then plotted on log-normal paper in the section 4.2, the characteristics of those conditional distribution are considered. All range of rainfall rate, the conditional probability $P_n(R)$ and $P_t(R)$ can be modeled by log-normal distribution [3,29]. Moreover, this conclusion has also been reached by Yamada et al. [30], in Japan, and Fedi [31], in Italy, and agrees with the modeling of the distribution of single duration of propagation fading and depolarization.

Fig. 4.10 and 4.11 show conditional probability of number of occurrences, $P_n(D/R)$, at rainfall rate 10, 15 and 30 mm/hr, and log-normal distribution with mean and standard deviation of those experiment data of Klong Yai and KMITL, 2000, respectively. Log-normal distribution estimated lines give a good fit with obtained data. Parameters of the log-normal function, mean (μ) and standard deviation (σ), can be determined directly from observed data by using Mathcad accessory in Appendix D. Means and standard deviations of $P_n(ln\ D)$ are illustrated in Table 4.2.The estimated lines then are obtained by cumulative log-normal distribution. The test of fit values of estimated lines with obtained data are increased as the rainfall rates increase.

Table 4.2 Means and standard deviations of $P_n(ln\ D)$

	Klong Yai, Trad			KMITL, Bangkok		
Rain rate (mm/hr)	10	15	30	10	15	30
Mean ($\overline{\ln D}$) μ	1.947	1.602	1.048	1.982	1.656	0.939
Standard deviation $\sigma_{\ln D}$	0.998	1.021	0.994	0.913	0.949	0.85

For example, from the Table 4.2, we can determine probability density $P(D)$ and cumulative density $P(D' > D)$ as the following expressions, respectively,

$$P(D) = \frac{1}{\sqrt{2\pi} D \sigma_{\ln D}} \exp\left[-\frac{1}{2}\left(\frac{\ln D - \overline{\ln D}}{\sigma_{\ln D}} \right)^2 \right] \tag{4.19}$$

$$P(D' > D) = \int_D^{\infty} P(D')dD' \qquad R>0 \tag{4.20}$$

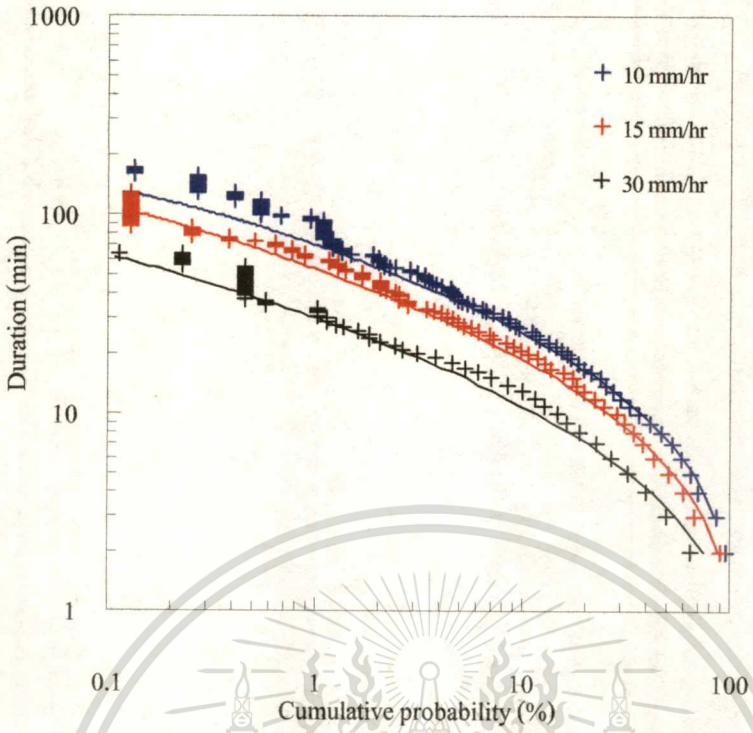

Fig. 4.10 Examples of the cumulative number distribution $P_n(D/R)$,(+), and cumulative distribution of estimated log-normal function, (solid lines), at Klong Yai

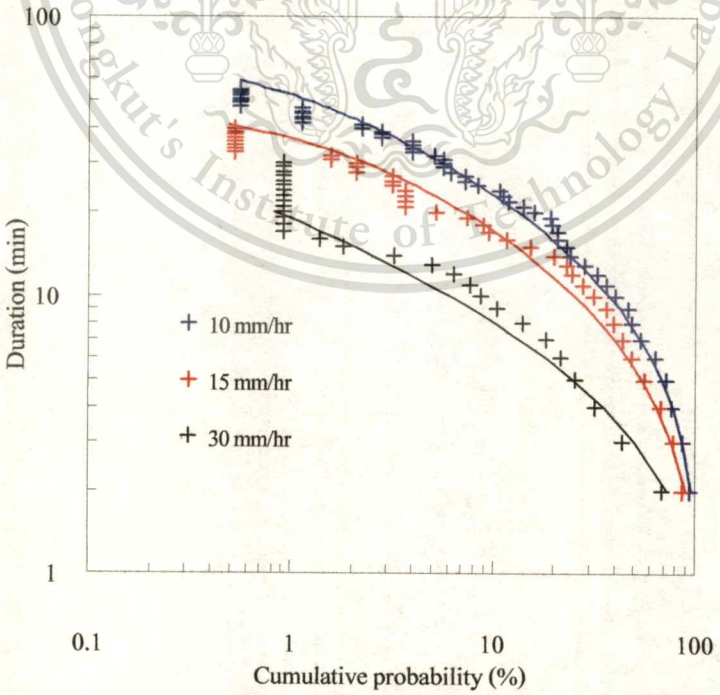

Fig. 4.11 Examples of the cumulative number distribution $P_n(D/R)$, (+), and cumulative distribution of estimated log-normal function, (solid lines), at KMITL

The probabilities corresponding to duration in the range less than 1 minute are not shown in Fig. 4.10 and 4.11. They do not conform to the line approximation probably as a result of the underestimate in the number of exceedances of that class caused by the limit response time of instrument. The time interval of observation, 1 minute, might be insufficient for observing high rainfall rate data. And the results fitting test of log-normal distribution as in Appendix D are not acceptable. Therefore, at rainfall rates above 30 mm/hr, the estimated lines also do not agree with the experimental data.

In addition, in 1999, the COMETS project was installed equipment to observe Ka-band satellite communication. Unfortunately, 10-second rainfall rate data are available 4 months, May-August 1999. Fading duration characteristics are analyzed and tested the same as the above mention procedures. Even though, the data are available only 4 months, they provide a rather better agreement with log-normal function than 1-minnute rainfall rate data as shown in Fig. 4.12.

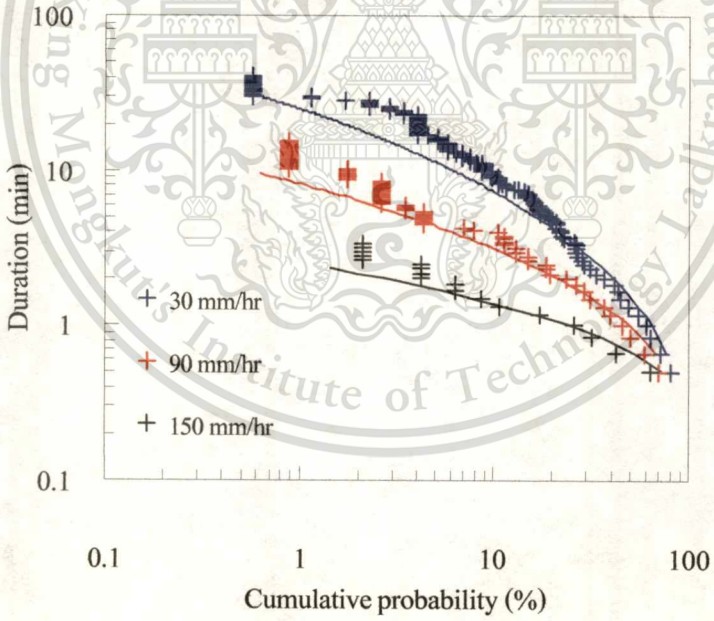

Fig. 4.12 Examples of the cumulative number distribution $P_n(D/R)$, (+), and cumulative distribution of estimated log-normal function, (solid lines) of 10 second rainfall rate data at KMITL

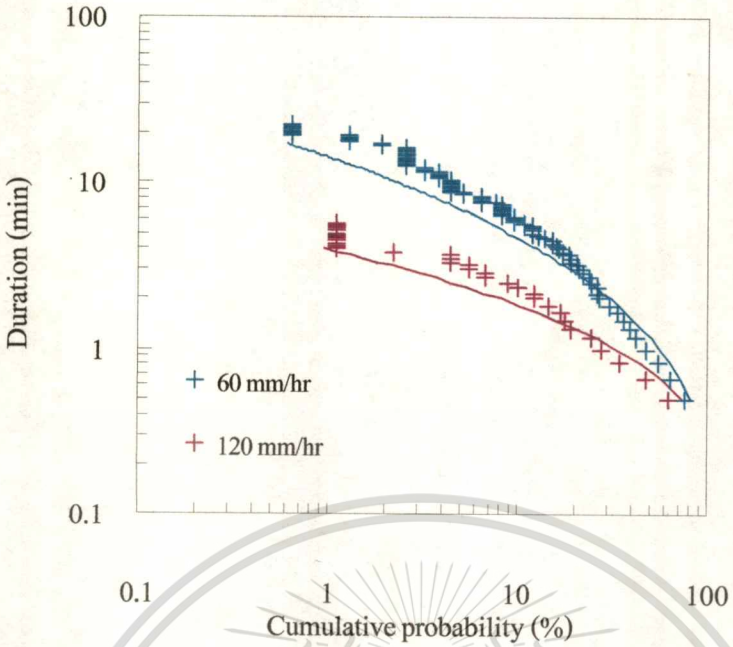

Fig. 4.12 (continued)

However, the following important point should be noted. The probability of exceeding a given value D from a population of durations can be considered either as a fractional number of exceedances or as a fractional time of exceedances. Thus, if during a given period of observation T, one notes n exceedances of D, the cumulated time due to the class D will be nD. Because of this property if the probability $P_n(D)$ is log-normal, so that $P_n(\ln D)$ is normal with some mean μ and variance σ^2, then $P_t(D)$ becomes the first order moment distribution of P_n and it is also log-normal. The mean and variance of $P_t(\ln D)$ are $\mu+\sigma^2$ and σ^2, respectively, [3,29]. Therefore, theoretically the variance $\sigma^2_{\ln x}$ should have been equal in both case, and difference is likely to be due to truncation and lack of long durations. The implications of the above property are that if the distribution P_n is known, then P_t can be calculated and conversely.

4.4 One-Hour Rainfall Rate to One-Minute Rainfall Rate Conversion

Almost all rain attenuation prediction methods, including that of CCIR (International Radio Consultative Committee) and ITU-R, require 1-min rainfall rate data as meteorological data of the place concerned. However, there very few areas where the 1-min rain rate data are available. 1-hour rain rate data, on the other hand, are usually collected by meteorological observation. Although the data collected by meteorological observation of The

Hydrometeorology Department of Thailand are 1-hour rainfall rate, it can be expected to have invaluable information concerning spatial and temporal rainfall rate statistics. Methods of predicting 1-min rainfall rate distribution from 1-hour rainfall rate data are very useful.

In this section conversion methods of 1-hour rainfall rate to 1-minute rainfall rate are firstly discussed. Finally, results of the conversion methods are compared to the observed about 2 years 1-min rainfall rate data.

Referring to the specific Moupfama distribution, Professor Yoshio Karasawa [5] adopted it to specify the distribution as (f : PDF ; F : cumulative distribution) :

$$f(R;r,u)=\frac{r}{R}\left(\frac{1}{R}+u\right)\exp(-uR) \tag{4.21}$$

$$F(R;r,u)=\int_{R}^{\infty} f(R;r,u)\,dR$$
$$=\frac{r}{R}\exp(-uR) \tag{4.22}$$

p=F×100%; p : percentage of time

In these above expression, r and u are parameters of the distribution and R is a rainfall rate. The region in, which above expressions is valid, is $I<1$. Since our primary interest lies in F <0.01 (1%), the limitation range is not matter of concerning in practical cases. The above expressions approximate a gamma distribution for a percentage of time less than 0.01% and a log-normal distribution above 0.01%.

The conversion using some high-ranking 1-hour rainfall rate data methods was firstly proposed by Karasawa [4,5]. It is characterized by: 1) a simply calculation scheme and 2) good accuracy for both short-term and long-term prediction. The calculation expressions are given by

$$u_m=\frac{1}{aR_{1-5h}-bR_{1-10h}}\ln\left(\frac{10bR_{1-10h}}{aR1-5h}\right) \tag{4.23}$$

$$r_m=10^{-4}aR_{1-5h}\exp(au_mR_{1-5h}) \tag{4.24}$$

where $R_{1\text{-}Nh}$ (N=5 and 10) is the mean value of the top N values of 1-hour rainfall rates for a year (i.e., from the largest one to the Nth one in the annual ranking). In the references document, Karasawa and Maekawa [5] proposed the parameters, a and b as 2.3 and 0.96, respectively, based on an examination using their various measured data. After testing with the data obtained from our experiment sites, Klong Yai, Trad and KMITL, Bangkok, the parameters a=2.3 and b=0.96 provide unsatisfied results. In addition, Karasawa also proposed that 1-minute rainfall rates for 0.01% and 0.1% of the time are simply determined in their observed data by

$$R_m(p=0.01\%)=2.3R_{1-5h} \tag{4.25}$$

$$R_m(p=0.1\%)=0.96R_{1-10h} \tag{4.26}$$

Owing to the above explanation, we consider that 2.3 and 0.96 are values of a and b, respectively. Therefore, we can rewrite (above equations) as

$$R_m(p=0.01\%)=aR_{1-5h} \tag{4.27}$$

$$R_m(p=0.1\%)=bR_{1-10h} \tag{4.28}$$

The parameters a and b can be determined from 0.01% of time of 1-minute rainfall rate data and top-five mean value of 1-hour rainfall rate data and at 0.1% of time of 1-minute rainfall rate data and top-ten mean value of 1-hour rainfall rate data, respectively.

From 2-year observed data of experiment sites, Table 4.3 shows the empirically calculated parameters. For determining the parameters, each year and average year obtained data give the coincident parameters.

Parameters u_m and r_m can be used into the Moupfama distribution (CDF) to provide estimated 1-minute rainfall rate cumulative distribution of each experiment sites as illustrate in the following Fig. 4.13.and 4.14.

Table 4.2 Parameters for 1-hour to 1-minute rainfall rate cumulative distribution

Experiment site	R_m (p=0.01%) (mm/hr)	R_m (p=0.1%) (mm/hr)	$R_{1\text{-}5h}$ (mm/hr)	$R_{1\text{-}10h}$ (mm/hr)	a	i	u_m	r_m
Klong Yai Trad	144	95	53.64	47.82	2.6846	1.9868	0.039	3.88
KMITL Bangkok	120	48	35.23	31.07	3.0649	1.5449	0.025	0.158

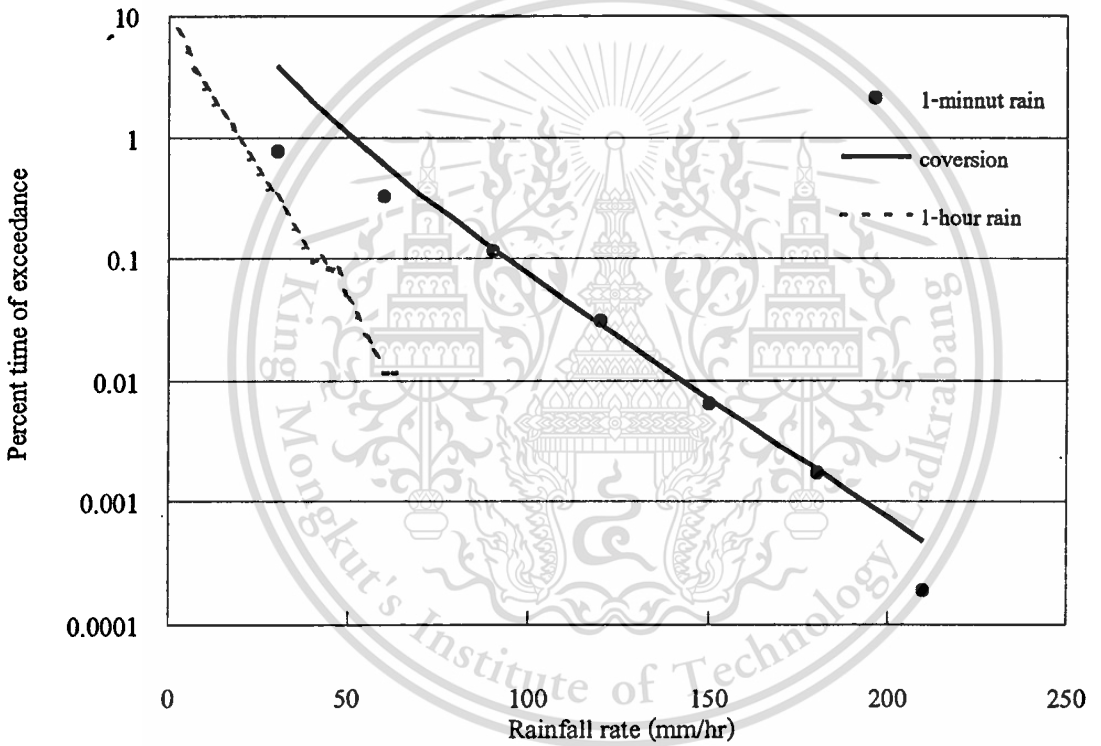

Fig. 4.13 Conversion of 1-hour to 1-min rainfall rate of average 2 years data at Klong Yai

Fig. 4.13 and Fig. 4.14 give a good fitting with average 2 year obtained data in the range about 0.3-0.00075% of exceeding time. In addition, we can model annual cumulative distribution of 1-min rainfall rate in the range percentage of exceedance 0.1-0.001% by using the Moupfama distribution with empirical parameters.

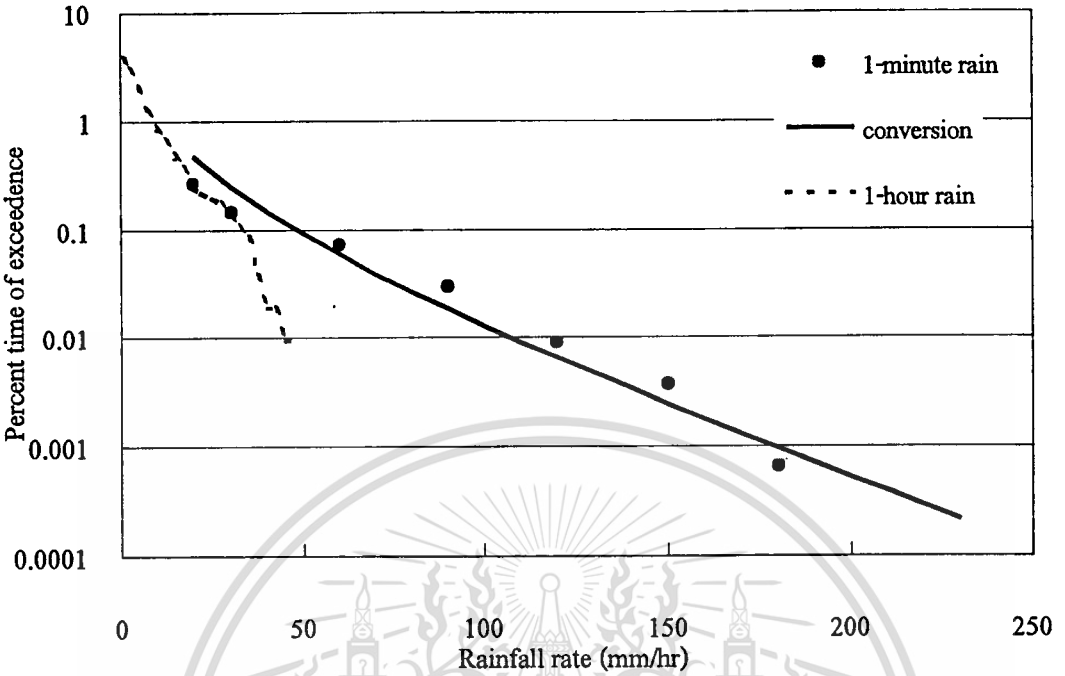

Fig. 4.14 Conversion of 1-hour to 1-min rainfall rate of average 2 years data at KMITL

4.5 Conclusions

With the proposed methods of determining the correlation between rain attenuation and rainfall rate based on the cumulative distributions of attenuation and rainfall rate data, some unreasonable correlation are filtered out. Therefore, the obtained correlation considerably agrees with the predicted model of ITU-R.

In each of rainfall events, probability for both time duration and times of single exceedance of thresholds can be represented by the conditional distribution. Then, conditional distributions of number of single exceedance of each rainfall rates are characterized by log-normal function with mean and standard deviation as $\overline{\ln D}$ and $\sigma_{\ln D}$, respectively. It can be seen that log-normal function can not fit with fading duration distribution of 1-minute rainfall rate data at rainfall rate higher than 30 mm/hr. The interval 1-minute might be larger than most duration of those high rainfall rates. The higher rainfall rate, the shorter fading duration they are. Therefore, if we need to model fading duration at high rainfall rate with log-normal function, shorter interval of observation data is required. This conclusion was support by 10-second rainfall rate data. Even though, they are available only 4 months, they give good fitting with log-normal function.

To determine 1-hour to 1-minute rainfall rate conversion method as proposed in this chapter, one-hour and 1-minute rainfall rate data are required at least 1 year in ordering to determine the coefficients of Moupfama distribution function. It was seen that the proposed method is simple calculation scheme and good accuracy. Even though, Bangkok and Trad are not too far distance, their data are quit different. Therefore, to development of such propagation prediction methods, it is necessary to grasp accurate rainfall rate characteristics for all the areas where the installation of radio communication equipment is planed. In addition, rainfall rate cumulative distribution can also be modeled by the conversion method.

CHAPTER 5

SATELLITE CHANNEL UTILIZATION IN THE PRESENCE OF RAIN ATTENUATION

For satellite links, the attenuation factors involved include scintillation, multipath fading, and the most dominant factor of all, rain attenuation. In the design of such a link maintaining a fixed, large fading margin to combat occasional deep rain fading as done in rain compensation algorithms, results in severe reduction in communication capacity [6]. Traditional fading countermeasures concentrate on the use of power, bandwidth, and site diversity. In this chapter, we use the adaptive rain fading counter measure, based on the effective utilization of the cannel capacity proposed in [6,7] to study the performance of satellite communication links for ground terminal locations in the experiment site.

5.1 Rain Attenuation on Satellite Links

A detailed information of the attenuation statistics for each ground terminal locations is needed in order to evaluate the effects of rain attenuation on satellite links. Even though the obtained data are considerably short-term statistics data, they provide importantly empirical parameters of each ground terminal location. In addition, rain statistics of each terminal locations are different, especially in tropical zone such terminal locations in this study. For a conventional frequency translation satellite, the total system carrier-to-noise density ratio $(C/N_o)_{s,c}$ for clear air (no attenuation) is given by [7]

$$\left(\frac{C}{N_o}\right)_{s,c} = \frac{\left(\frac{C}{N_o}\right)_u \cdot \left(\frac{C}{N_o}\right)_d}{\left(\frac{C}{N_o}\right)_u + \left(\frac{C}{N_o}\right)_d} \tag{5.1}$$

where $(C/N_o)_u$ and $(C/N_o)_d$ are the carrier-to-noise density ratio for the uplink and downlink transmission for clear air, respectively. Note that the quantities in (5.1) are not in units of dB. The above quantities can be converted to dB by

$$S_u = 10\log\left(\frac{C}{N_o}\right)_u, \quad S_d = 10\log\left(\frac{C}{N_o}\right)_d \tag{5.2}$$

then the total equivalent attenuation due to rain fading for the system (up&downlink) is given by

$$A(dB) = \left(\frac{C}{N_o}\right)_{s,c|dB} - \left(\frac{C}{N_o}\right)_{s,att|dB} \tag{5.3}$$

$$\left(\frac{C}{N_o}\right)_{s,c|dB} = 10\log\left(\frac{10^{\frac{S_u}{10}} \cdot 10^{\frac{S_d}{10}}}{10^{\frac{S_u}{10}} + 10^{\frac{S_d}{10}}}\right) \tag{5.4}$$

where

$$\left(\frac{C}{N_o}\right)_{s,att|dB} = 10\log\left(\frac{10^{\frac{S_u - A_u}{10}} \cdot 10^{\frac{S_d - A_d}{10}}}{10^{\frac{S_u - A_u}{10}} + 10^{\frac{S_d - A_d}{10}}}\right) \tag{5.5}$$

in (5.5), A_u and A_d (in dB) are the uplink and downlink attenuations in dB due to rain, respectively. The over-all system attenuation expressed in dB given in (3) can be shown to be

$$A(dB) = \left(\frac{C}{N_o}\right)_{s,c|db} - 10\log\left(\frac{1}{10^{\frac{S_u - A_u}{10}}} + \frac{1}{10^{\frac{S_u - A_d}{10}}}\right)^{-1} \tag{5.6}$$

It is well known that the attenuations A_u, A_d and A are approximately lognormally distributed random variables [6]. Therefore, the probability density function (pdf) of rain atttenuation along the link has the from

$$P_A(a) = \frac{1}{a\sigma\sqrt{2\pi}} \exp\left(-\frac{(\ln a - m)^2}{2\sigma^2}\right) \quad ; a>0$$

$$P_A(a) = 0 \quad ; a \le 0 \tag{5.7}$$

The mean and standard deviation of A can be determined by the methods described in [6] or by lognormal function fitting the obtained rain attenuation data, using the Mathcad software. For three experiment sites, mean and standard deviation of observed attenuation data on satellite-to-ground links of experiment location are given in Table 5.1.

Table 5.1 Mean and standard deviation estimated from experimental data

Experiment Site/Available data	Mean $\left(\overline{\ln A}\right)$	Standard deviation (μ)
KMITL (JCSAT-Bangkok), 2000-2001	-2.79	1.82
Klong Yai (Thaicom3-Trad), 2000	-3.60	1.85
KMITL (Thai com3-Bangkok), 1999	-3.82	1.95

Fig. 5.1 illustrates the example of cumulative distribution of rain attenuation and fitting curve modeled by a log-normal distribution with empirical parameters estimated by experimental data. It can be seen that rain attenuation is well modeled by a log-normal distribution.

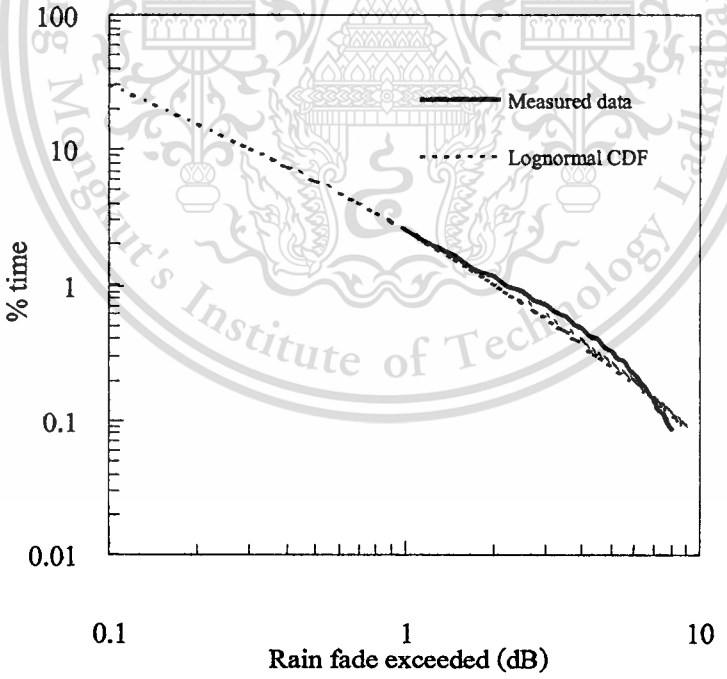

Fig. 5.1 Example of cumulative distribution of rain attenuation at Klong Yai and fitting curve of lognormal distribution.

These parameters, mean and standard deviation of log-normal function, are manipulated in the following section for considering channel capacity.

5.2 Channel Capacity

Due to particular constraints of modulation, coding and throughput, and the absence of onboard processing, in most cases satellite communications system designers implement a fixed link margin. For very small aperture (VSAT), this implies insufficient utilization of channel capacity for a considerably high percentage of time, especially for satellite communications system operating higher frequency band which subject to severe performance degradations due to rain attenuation [7]. A good performance measure of such a communications system is channel capacity which gives the maximum rate of signal transmission over the channel.

For continuous channel with additive white gaussian noise, Shannon defines the channel capacity in bit per sec. (b/s) by

$$C = B\log_2\left(1+\frac{S}{N}\right) \tag{5.8}$$

where B is the channel bandwidth in Hz, and S/N is the signal-to-noise ratio in the channel in dB. The capacity per unit bandwidth may be written as

$$\frac{C}{B} = \log_2\left(1+\frac{S}{N}\right) \quad \text{(bps/Hz)} \tag{5.9}$$

Due to propagation fading, the term S/N in (5.9) is a random variable with arbitrary but known distribution which depends on the characteristics and type of the fading process. This implies that the channel capacity is also a random variable and therefore imposes performance degradation on the system. Using standard transformation of random variables, the pdf of C/B can be written in term of S/N [6]

In the presence of rain attenuation, the received signal-to-noise power level is given by

$$\left(\frac{S}{N}\right) = \left(\frac{S}{N}\right)_{s,c} - A \quad \text{(dBW)} \tag{5.10}$$

where $(S/N)_{s,c}$ is unfadingd signal-to-noise power level (in dB) for clear air condition, and A is the total equivalent rain attenuation on the link. The cumulative distribution function (cdf) of channel capacity is given by

$$\begin{aligned} F_{C/B}(y) &= \Pr ob\left(\frac{C}{N} \le y\right) = \Pr ob\left(\frac{S}{N} \le 2^y - 1\right) \\ &= \Pr ob\left(A \ge \left(\frac{S}{N}\right)_{s,c} - 10\log\left(2^y - 1\right)\right) \\ &= \Pr ob\left(\ln A \ge \ln\left[\left(\frac{S}{N}\right)_{s,c} - 10\log\left(2^y - 1\right)\right]\right) \\ &= Q\left(\frac{1}{2}(\lambda)^2\right) \end{aligned} \tag{5.11}$$

where

$$\lambda = \frac{\ln\left[\left(\frac{S}{N}\right)_{s,c} - 10\log\left(2^y - 1\right)\right] - m}{\sigma}$$

In (5.11) the variables $y=C/B$, $(S/N)_{s,c}$, A are all expressed in the units of dB, and

$$Q(x) = \int_x^{\infty} \frac{1}{\sqrt{2\pi}} e^{-\frac{t^2}{2}} dt \tag{5.12}$$

By using Mathcad software, the cdf of channel capacity in the presence of rain attenuation, for the various unfaded signal-to-noise ratio values is plotted as shown in Fig. 5.2 and 5.3.

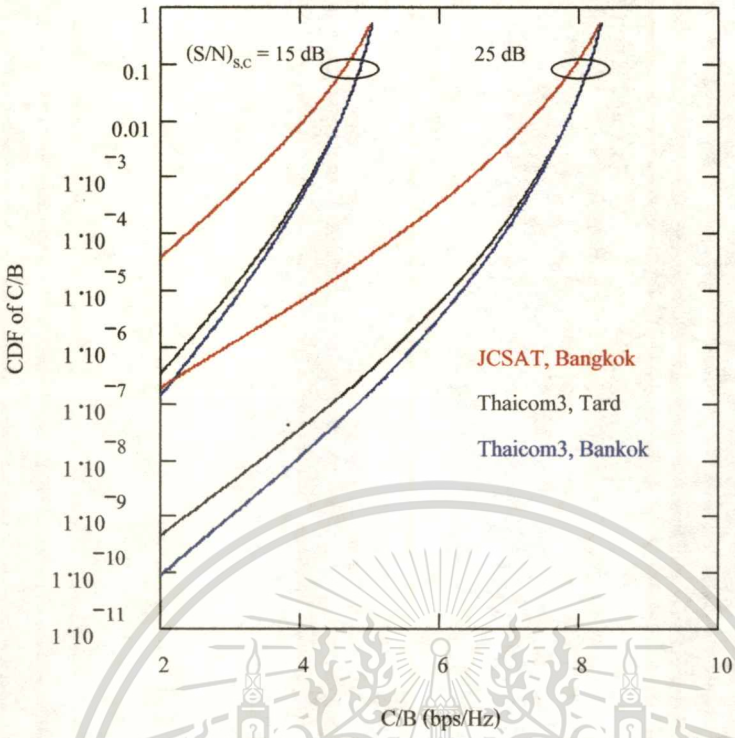

Fig. 5.2 Cumulative distribution of channel capacity in the presence of rain attenuation on the Bangkok-JCSAT, Bangkok-Thaicom3 and Tard-Thaicom3 links

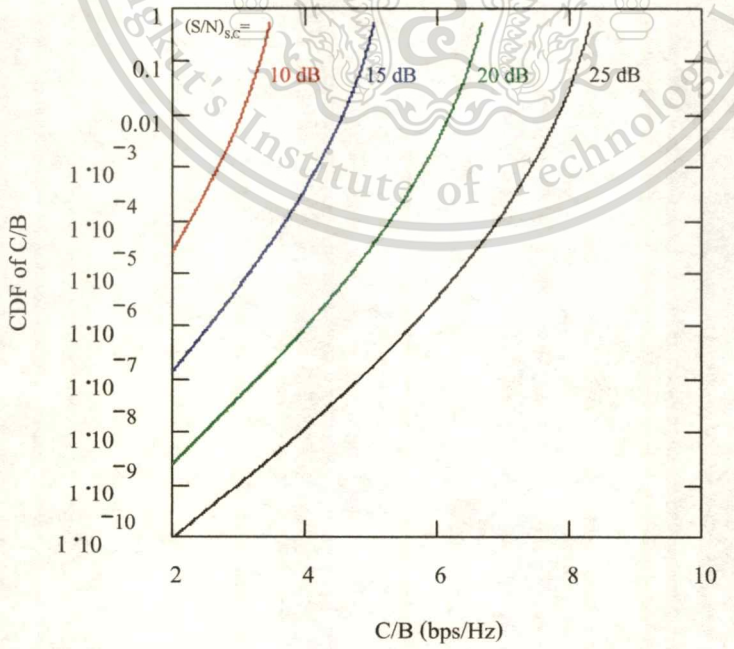

Fig. 5.3 Cumulative distribution of channel capacity in the presence of rain attenuation on the Bangkok-Thaicom3 link

5.3 BER Degradations

The bit error rate (BER) is one of the measures of the performance of satellite communication system. For a given modulation scheme, the system BER is a function of *S/N*, and the presence of fading, is also a random variable. By following procedure similar to the channel capacity analysis presented in previous section, it is possible to determine the cdf of BER performance in the presence of propagation fading. This gives the measure of the availability of the communication link, since it gives the percentage of the time for which the specified BER will be exceeded. For a digital communications system using M-PSK modulation scheme, the probability that any M-ary symbol will be received in error, for $P_s<10^{-3}$, can be approximated by [32]

$$P_s = 2Q\left[\left(\sin\frac{\pi}{M}\right)\sqrt{\frac{2E_s}{N_o}}\right] \tag{5.13}$$

where E_s is the energy per M-ary symbol, and N_o is one-sided power spectral density. Since block of k input data bits is encoded into M-ary symbol, the equivalent energy per data bit E_b is given by

$$E_b = \frac{E_s}{k} = \frac{E_s}{\log_2 M} \tag{5.14}$$

Furthermore, if the data bits input to the modulator are encoded by Gray code, then adjacent carrier phase angle in the signal constellation differ only by one bit, and therefore the relationship between probability of bit-error and signal-to-noise may be denoted by [32]

$$P_b = f\left(\frac{S}{N}\right) \tag{5.15}$$

The cdf of BER in the presence of overall rain attenuation A is given by

$$\Pr ob(BER > x) = \Pr ob\left[\left(\frac{S}{N}\right)_{s,c} - f^{-1}(x) > A\right]$$
$$= 1 - Q\left(\frac{1}{2}(\beta)^2\right) \tag{5.16}$$

where

$$\beta = \frac{\ln\left[\left(\frac{S}{N}\right)_{s,c} - 10\log\left(f^{-1}(x)\right)\right] - m}{\sigma} \tag{5.17}$$

where $f^{-1}(x)$ is the inverse function of BER versus *S/N*.

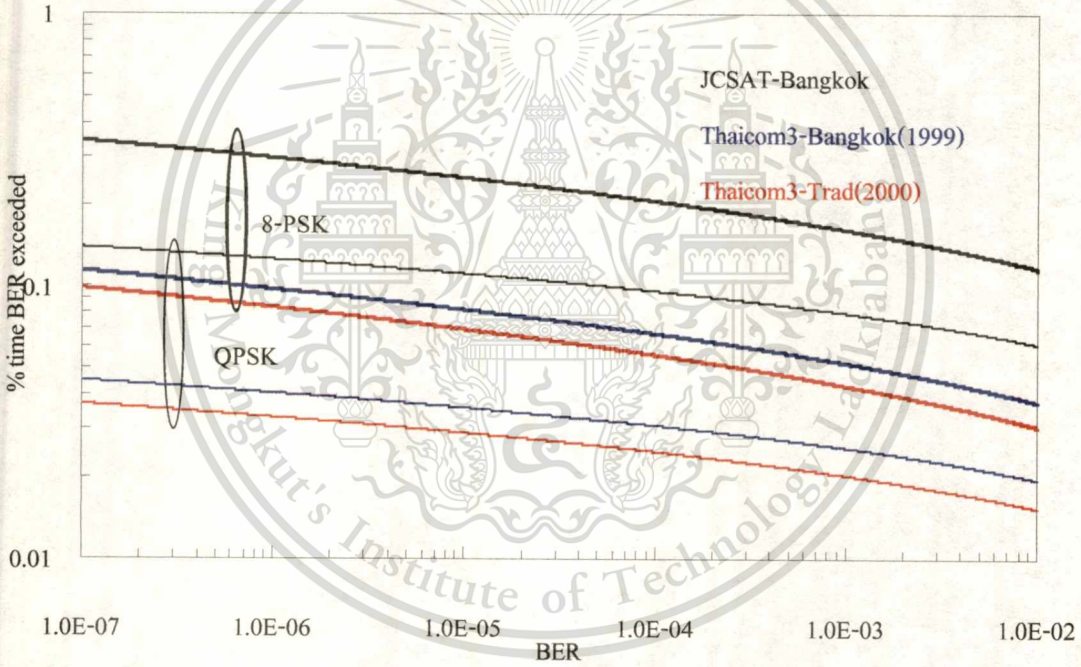

Fig. 5.4 Complementary cdf of BER for uncoded M-PSK scheme in the presence of rain attenuation on JCSAT-Bangkok, Thaicom3-Trad and Thaicom3-Bangkok links

Fig. 5.4 and 5.5 illustrate the annual cdf of BER in the presence of over-all rain attenuation for a given M-ary modulation scheme, for 3 experiment locations. It can be seen that for a given unfaded signal-to-noise ratio value, by relaxation of the BER for more error tolerant applications, the capacity of the communications can be increased drastically. For example, Fig. 5.5 provides of how the relaxation of the BER requirement reflects on improvement in

overall availability of the modulation techniques considered. We can see that by reducing the BER requirement to 10^{-3}, it would be possible to operate at 32 PSK for a considerably high percentage of the time. With 32 PSK, even more data can be transmitted than with 16 PSK (5/4 ratio), which is good to have in mind for applications that are more error-tolerant. As with the channel capacity, such an analysis can performed independently for particular fading processes, but the results obtained will always be more realistic when a more complex global process is considered.

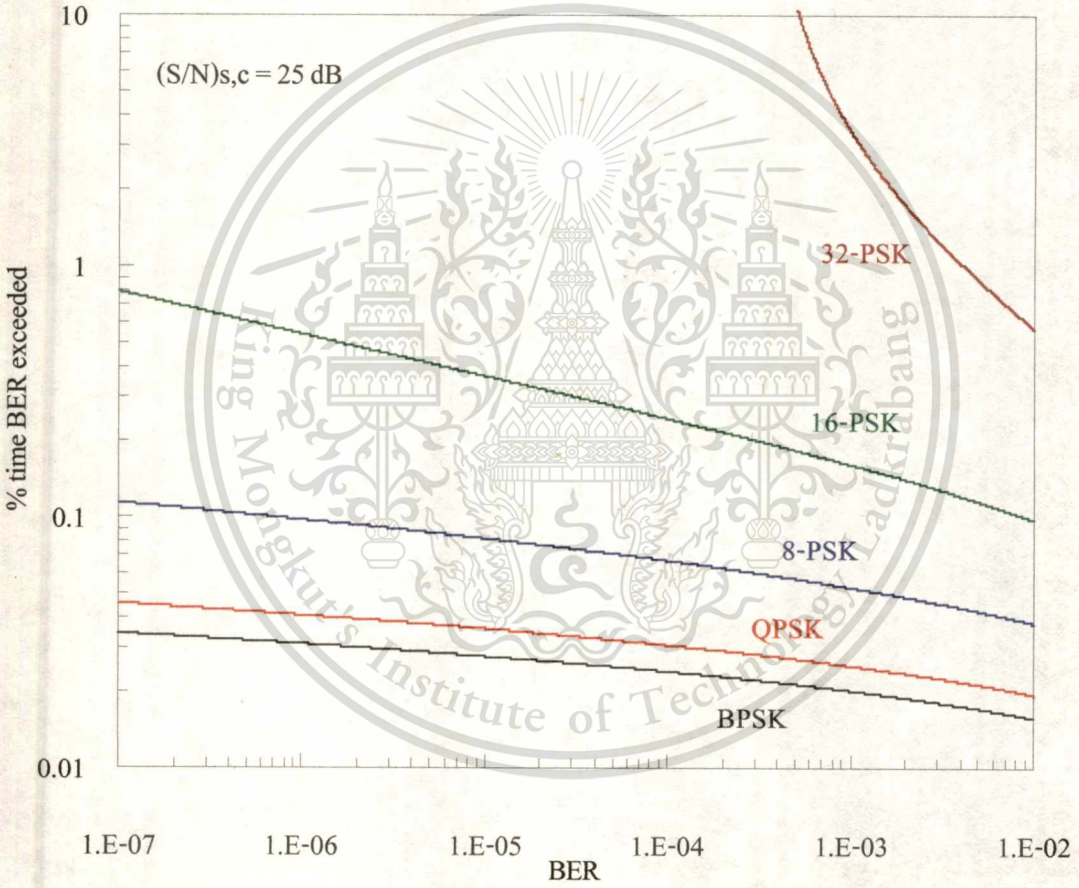

Fig. 5.5 Complementary cdf of BER for uncoded M-PSK scheme in the presence of rain attenuation on the Thaicom3-Bangkok link

5.4 Conclusions

Satellite channels at Ku band and 20/30 GHz, in particular, are subject to severe performance degradations due to the propagation effects that prevail in these frequencies. The

need for cost-effective communications systems precludes the implementation of large fixed link power margins, and thus adaptive techniques are required instead. Adaptive systems are step towards more efficient channel utilization and closely relate to the fading countermeasure design philosophy. However, in both fixed margin and fading countermeasure design approaches, the channel itself has so far been neglected, and both concentrate on fading and seek away to avoid them. Furthermore, both approaches consider only the phase process, which is dominant and is usually rain attenuation. A more satisfactory way of designing of communications systems is to consider the capacity of satellite channel and it statistics in the light of the global fading process. Although it may at first appear that there is no difference in the design approach between fading and channel capacity considerations, channel offer a wider view of what the system can achieve. One can look for what can be gained from the channel rather than what has to be given away in order to compensate to the fading. Channel capacity should help the designer of a communications system with the selection of potentially suitable modulation/coding techniques. This aspect has also been addressed in this paper by showing how to determine the statistics of BER for various M-ary PSK modulation schemes. Other modulation schemes can, of course, be considered.

CHAPTER 6

CONCLUSIONS

6.1 Summaries

This thesis represents rainfall rate and rain attenuation characteristics based on the short-term observation data of 2 experimental location in Thailand, Klong Yai, Trad and KMITL, Bangkok. One of concepts of manipulating on such short-term obtained data is to find optimum and highly effective process in order to illustrate the detailed characteristics of study as much as possible. In addition, some limitations of equipment and instrument affect on the analyzed methodologies, for example, intervals of sampling time of observed data, small receiving antenna, power electric off, etc.

Average annual cumulative distribution of point rainfall rate of Klong Yai and KMITL at 0.01% of rainfall rate exceeded $R_{0.01}$ are 120 and 144 mm/hr, respectively. While the attenuation at 0.01% could not be presented because of the small antenna and the high rainfall rate, the maximum of observed attenuation are 7.5, 8 and 23 dB on Thaicom3-Trad, Thaicom3-Bangkok and JCSAT-Bangkok links at percentages of time exceeded 0.11475, 0.15059 and 0.0388%, respectively. On monthly cumulative distribution of Klong Yai, based on the intensities of rainfall rate, 12 months can be classed into 3 groups, (May-August), (March, April, September and October) and (January, February, November and December). Then, worst-month statistics can be acceptably estimated by the conversion proposed by ITU-R with conversion parameters of both global and Indonesia.

The correlation between rainfall rate and signal attenuation can be obtained by the proposed methods in order to neglect some uncorrelated conditions, for example, the unidentical GMT of rainfall rate and signal attenuation data, rainfall on the slant path, etc. Based on the same percentage time of exceedance of rainfall rate and signal attenuation cumulative distributions, the coordinates of rain attenuation are obtained.

For each threshold R exceeded, the "number" probability $P_n(D/R)$ which gives the fractional number of single exceedances with duration D, and the "time" probability $P_t(D/R)$ which gives the probability that durations may exceed a specified value D. For each threshold R both P_n and P_t are found to be well modeled by lognormal distribution with mean and standard deviation as $\overline{\ln D}$ and $\sigma_{\ln D}$, respectively.

The 1-hour to 1-minute conversion model for experiment location is proposed. Firstly, empirical parameters, a and b, are obtained from $R_{0.01}$ and $R_{0.1}$ of 1-hour and 1-minute annual rainfall rate data. Then, the parameters of adopted Mopfama distribution, u_m and r_m are evaluated from some high-ranking of 1-hour rainfall rate data and obtained a and b. Moreover, this distribution can be used as a model for cumulative distribution of rainfall rate for observation location. The conversion gives a good fit with the range 0.001-0.1% time of exceedances.

Finally, satellite channel utilization in the presence of rain attenuation is presented. Rain attenuation is proposed to be modeled by the log-normal distribution. Even though, obtained rain attenuation range is limited by the condition of the receiving terminal, the log-normal distribution shows good fitting in that range. The measures of the performance of satellite communication system in the presence of rain attenuation are discussed. Channel capacity gives the maximum rate of signal transmission over the channel. In this thesis, channel capacity is illustrated as the cumulative probability versus capacity per unit bandwidth (bps/Hz). Another, BER degradation is indicated the cumulative distribution of percentage time of BER exceeded on the satellite-to-ground links.

6.2 Further Work Discussions

For the annual statistics to worst-month statistics conversion, it is probably possible to define the conversion parameter for the observation location that it needs more long-term statistics of observation data.

1-minute rainfall rate data can not indicate the distribution of fading duration as log-normal function at the rainfall rate higher than 30 mm/hr. Whereas 10-second rainfall rate data, even though 4 months available, give fading duration distributions considerably modeled by log-normal function. Therefore, if fading duration distributions are needed, 10-second interval of observation data is requires.

Even though, the locations of experiment are considerably not so far, the different of elevation angle less than 1 degree, but the conversion parameters of 1-hour to 1-minute conversion are quit different. It might be depending on others conditions of observation location, for example, topography, distance from sea, etc. Therefore, to develop this prediction as mentioned process, it is necessary to grasp accurate rainfall rate characteristics for interesting areas at least 1 year. As Morita said that a better prediction is made by using only mean annual rainfall as the meteorological data depending on the area.

Thus, 10-second interval observation has been installed at Satellite Communication Laboratory, KMITL since October 2001. Rainfall rate observation instrument and measurement have also been installed at meteorology station at Ranong in the South of Thailand, one of the highest rainfall regions in Thailand.

REFERENCES

[1] Robert K. Crane. **Electromagnetic wave propagation through rain**. New York : John Willey&Sons. Inc., 1996.

[2] K. Morita and I. Higuchi. "Statistical studies on rain attenuation and site diversity effect on Earth to satellite links in microwave and millimeter wavebands," Trans. IEICE Japan, vol. E61, pp. 425-432, June 1978.

[3] Enric Villar et al. "Analysis of joint rainfall rate and duration statistics : micorwave system design implications," IEEE Trans. Commun., vol. 36, no.6, June 1988.

[4] Y. Karasawa and T. Matsudo. "One-minute rain rate distributions in Japan derived from AMeDAS one-hou rain rate data," IEEE Trans. Commun., vol. 29, no. 6, pp. 256-262, Nov. 1991.

[5] Y. Karasawa and T. Matsudo. "Ka-band Earth-space propagation research in Japan," Proc. IEEE, vol. 8, no. 6, pp. 821-842, June 1997.

[6] M. Filip and E. Vilar. "Optimum utilization of the channel capacity of a satellite link in the presence of amplitude scintillation and rain attenuation," IEEE Trans. Commun., vol. 38, no. 11, pp. 19581965, Nov. 1990.

[7] K. Karimi, V. Aalo and H. Helmken. "A study of satellite uitilization in the presence of rain attenuation," A Global Affair., Proc. IEEE, pp. 196-200, 1944.

[8] M. P. M. Hall, L. W. Barclay and M.T. Herwitt. **Propagation of radiowaves.** UK : The institute of electrical engins.,1996.

[9] C. W. Ulbrich. "Natural variations in the analytical form of the rain drop size distribution," J. Clim. Appl. Meteorol., pp. 1764-1774, 1983

[10] B. N. Harden, J. R. Norbury and W. J. K. White. "Use of a log-normal distribution of raindrop sizes in millimetric radio attenuation studies," IEE Conf. Publ. 169, part 2, pp. 87-91, 1978.

[11] H. C. Van Der Hult. **Light scattering by small particles.** New York : Dover, 1981.

[12] A. R. Holt, N. K. Ozunoglu and B. G. Evan. "An integral equation solution to the scattering of electromagnetic radiation by dielectric spheroids and ellipsoids", IEEE Trans., AP-26, (5), pp. 706-712, 1976.

[13] J. Louis And Jr. Ippolito **Radiowave propagation in satellite communications.** New York: Van Nostrand Reinhold Company Inc., 1986.

[14] P. L. Rice and N. R. Holmberg. "Cumulative time statistics of surface point-rainfall rates," IEEE Trans. Commun., vol. com-21, no. 10, Oct. 1973.

[15] E. J. Dutton and H. T. Dougherty. "Modeling the effects of cloud and rain upon satellite-to-ground system performance," OT report 73-5, Office of Telecommunications, Boulder, CO, March 1973.

[16] S. H. Lin. "Nationwide long-term rain statistics and empirical calculation of 11 GHz microwave rain attenuation," The Bell System Technical Journal, vol. 56, no. 9, Nov. 1981.

[17] Frank Gergione et al. "Services, technologies, and systems at Ka band and beyond-a survey," IEEE Journal on Selected Areas in Commun., vol. 17, no. 2, Feb. 1999

[18] John Austin et al. "Analysis of moderate and intense rainfall rates continuously recorded over half a century and influence on microwave communications planning and rain-rate data acquisition," IEEE Trans. Commun., vol.com-35, no. 4, April 1987.

[19] P. Nakonrat, P. Phodpong and N. Hemmakorn. "Ku band attenuation statistics in tropical zone," 2000 Asia-Pacific Symposium on Broadcasting and Communications, Bangkok, Thailand, pp. 175-180, Dec. 2000.

[20] ITU-R, Rec. ITU-R P.618-6, "Propagation data and prediction methods required for the design of Earth-space telecommunication systems," Geneva, 1999.

[21] CCIR, Rec. and report of the CCIR, "Propagation in non-ionized," vol. 5, Geneva, 1990.

[22] ITU-R, Rec. ITU-R PN.837-1, "Characteristics of precipitation for propagation modeling," Geneva, 1994.

[23] ITU-R, Rec. ITU-R P.838-1, "Specific attenuation for rain for use in prediction methods," Geneva, 1999.

[24] ITU-R, Rec. ITU-R P.841-1, "Conversion of annual statistics to worst month statistics," Geneva, 1999.

[25] Z. Zhenw-wei, Z. Ming-gao and W. Zhen-sen. "An analytic model of specific attenuation due to rain," Infrared and Millimeter Wave, 2000. Conference Digest. 2000 2th International Conference, pp. 471-172, 2000.

[26] K. S. Paulson and C. J. Gibbins, "Rain models for the prediction of fade durations at millimeter wavelengths," IEE Proc.-Microw. Antennas Propag., vol. 147, no. 6, pp. 431-436, Dec. 2000.

[27] B. N. Harden, J. R. Nobury and W. J. K. White. "Measurements of rainfall for studies of millimetric radio attenuation," Peoc. IEE, Microwave Opt. Acoust., vol. 1, pp 197-202, 1977.

[28] G. O. Ajayi and E. B. C. Ofoche. "Some tropical rainfall rate characteristics at Iie-Ife for microwave and millimetric applications," J. Clim. Appl. Meteor., vol. 23, pp. 562-567, 1984.

[29] E. Vilar and A. Burgueno. "Analysis and modeling of time intervals between rain rate exceedances in the context of fade dynamics," IEEE Trans. Commun., vol. 39, no. 9, pp.1306-1312, Sep. 1991.

[30] M. Yamada et al. "Rain depolarization measurement using INTELSAT IV satellite in 4 GHz band at low elevation angle," Ann. Teleconm., vol. 32, 11-12, pp. 524-529, 1977.

[31] F. Fedi, "Rainfall characteristics across Europe," Alta Frequenza, XLVII, vol. 4, pp. 158-166, 1979.

[32] Bernard Sklar. **Digital communications fundamentals and applications.** New Jersey : Prentice-Hall International, Inc., 1988.

APPENDICS

APPENDIX A

RAIN CLIMATE ZONE MAPS

The statistics of precipitation intensity is needed for the prediction of attenuation and scattering cause by precipitation for all locations on the globe. The ITU recommendation has proposed the model of rain climate zone maps to provide the precipitation intensity. Table A.1 gives rainfall intensity exceeded (mm/hr) for specific rain climate zone referring to Fig. A.1 to A.3 that are illustrated the specific rain climate zones covering the continents of the Earth.

Table A.1 Rainfall rate intensity exceeded (mm/hr) (referring to Fig. A1 to A.2

Percentage of time (%)	A	B	C	D	E	F	G	H	J	K	L	M	N	P	Q
1.0	<.1	0.5	0.7	2.1	0.6	1.7	3	2	8	1.5	2	4	5	12	24
0.3	<.8	2	2.8	4.5	2.4	4.5	7	4	13	4.2	7	11	15	34	49
0.1	2	3	5	8	6	8	12	10	20	12	15	22	35	65	72
0.03	5	6	9	13	12	15	20	18	28	23	33	40	65	105	96
0.01	8	12	15	19	22	28	30	32	35	42	60	63	95	145	115
0.003	14	21	26	29	41	54	45	55	45	70	105	95	140	200	142
0.001	22	32	42	42	70	78	65	83	55	100	150	120	180	250	170

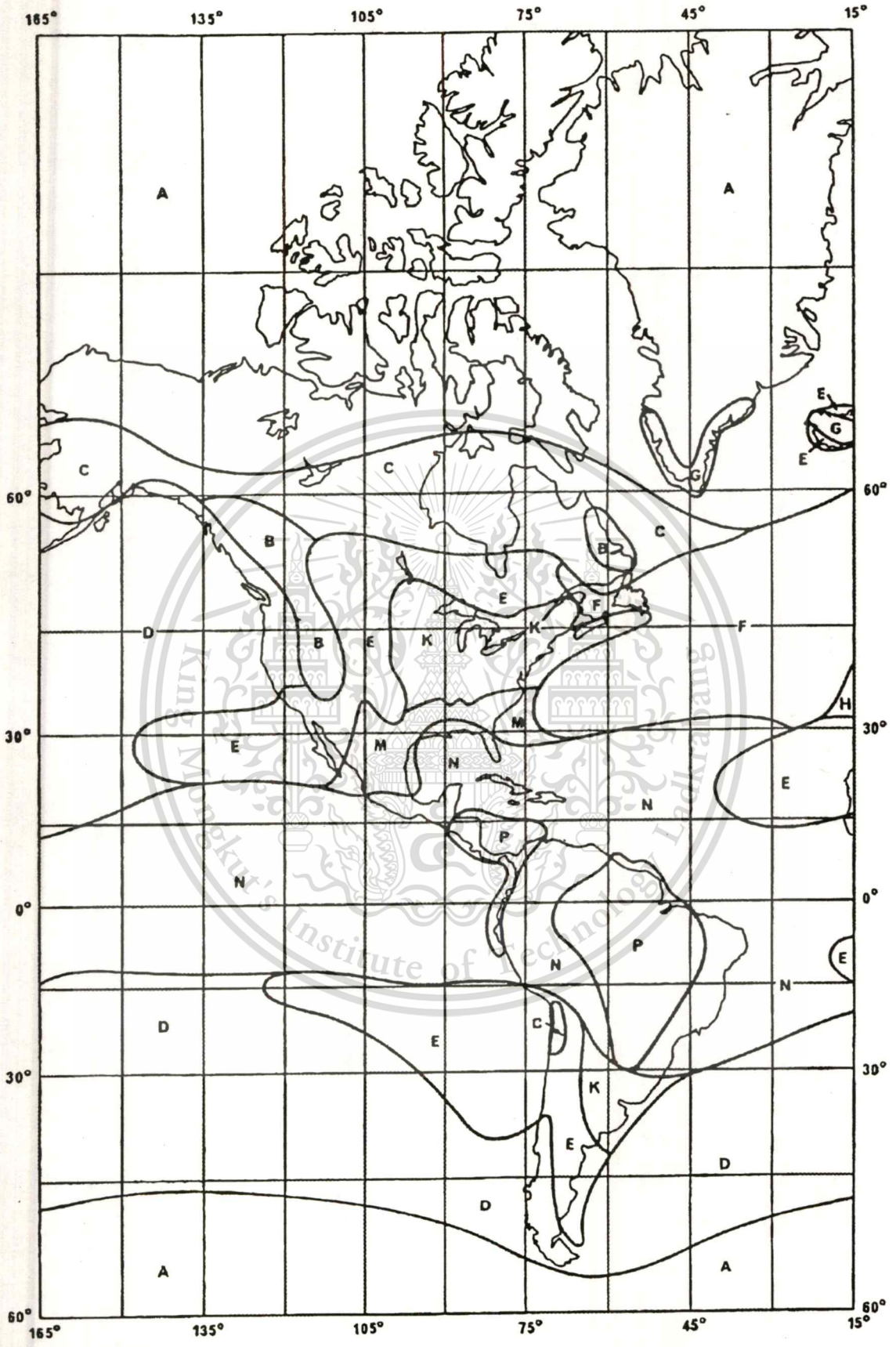

Fig. A.1 Rain climate zone map of American continent

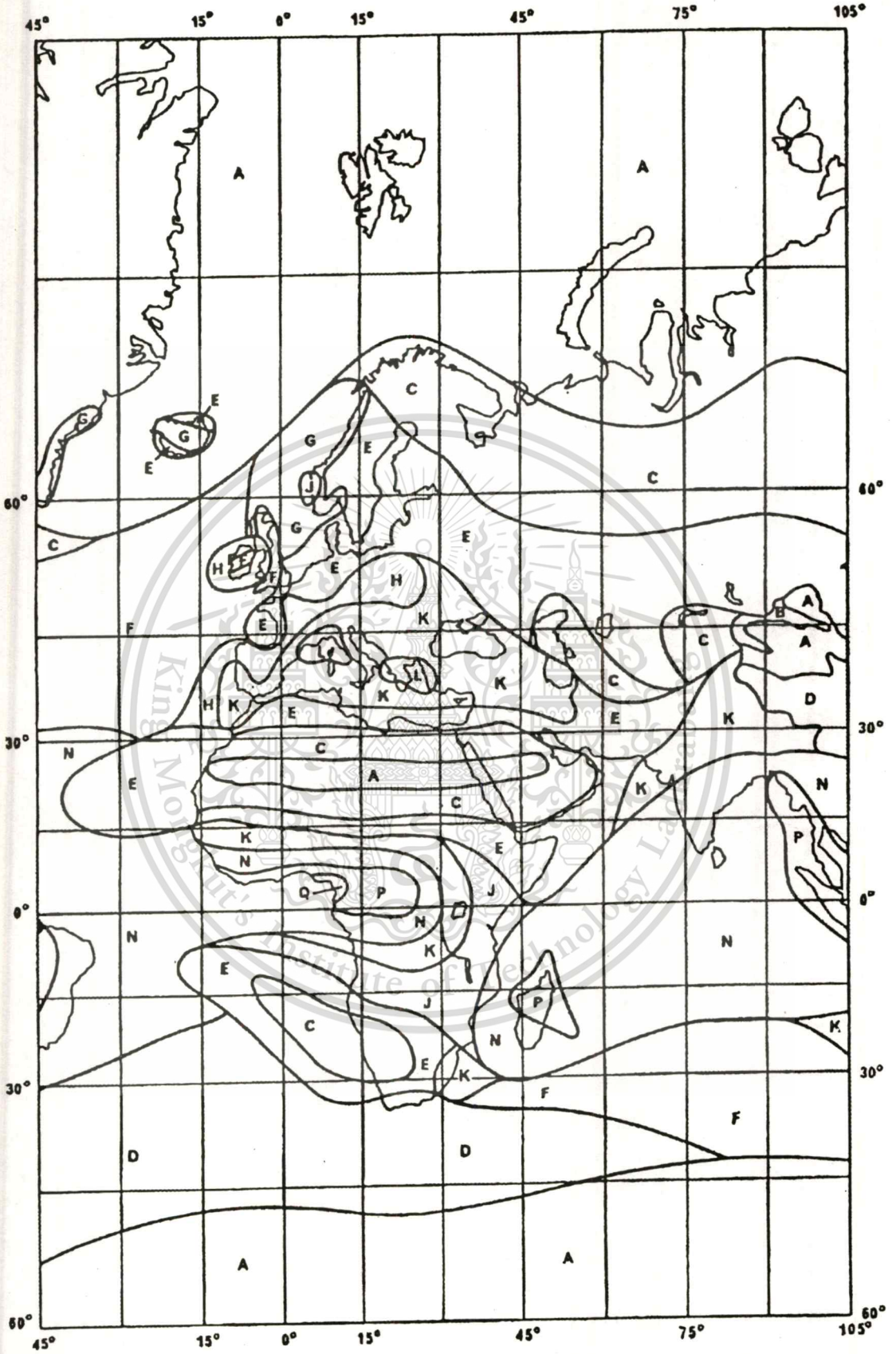

Fig. A.2 Rain climate zone map of European and African continents

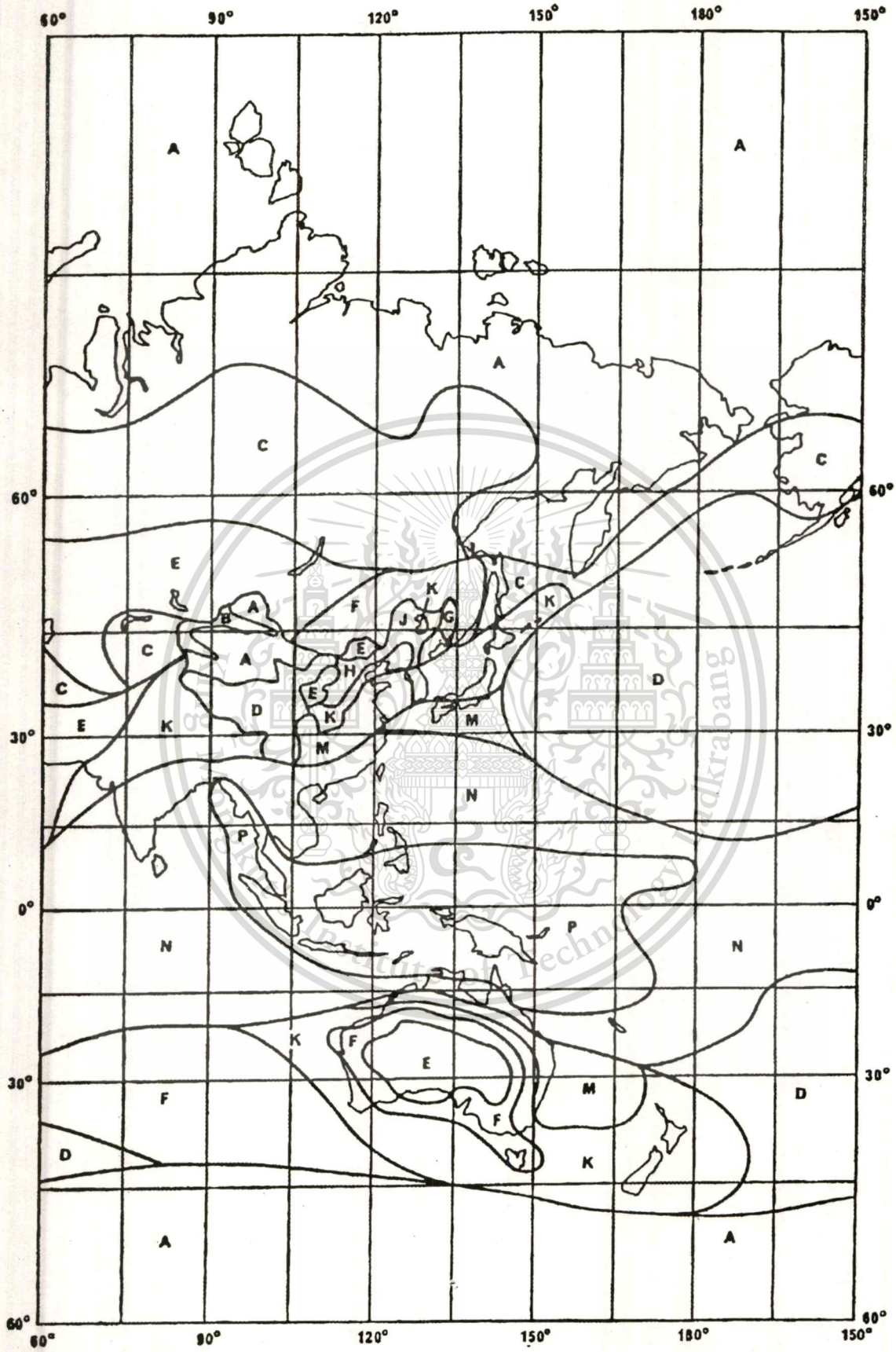

Fig. A.3 Rain climate zone map of Asian and Australian continents

APPENDIX B

COEFFICIENTS FOR SPECIFIC RAIN ATTENUATION

The values in Table B.1 have been tested and found to be sufficiently accurate for attenuation prediction up to frequencies of 55 GHz. For linear and circular polarization, and for all path geometries, the coefficients k and α can be calculated from the values in Table 1 using the following equations:

$$k = \left[k_H + k_V + (k_H - k_V)\cos^2\theta\cos 2\tau\right]/2 \quad \text{(B.1)}$$

$$a = \left[k_H a_H + k_V a_V + (k_H a_H - k_V a_V)\cos^2\theta\cos 2\tau\right]/2k \quad \text{(B.2)}$$

where θ is the path elevation angle and τ is the polarization tilt angle relative to the horizontal (τ=45° for circular polarization).

Logarithm scale interpolation

Given the frequency/coefficient pairs f_1/y_1 and f_2/y_2 from the table, we desire to determine the coefficient y_0 at frequency f_0 in the interval of f_1 and f_2.

Note that,

$$\log y_2 = m \log f_2 + b' \quad \text{(B.3)}$$

and

$$\log y_1 = m \log f_1 + b' \quad \text{(B.4)}$$

Solving for m an b',

$$m = \frac{\log\left[\left(y_1 / y_2\right)\right]}{\log\left[\left(f_1 / f_2\right)\right]} \quad \text{(B.5)}$$

$$b' = \log y_2 - m \log f_2 \quad \text{(B.6)}$$

The coefficient y_0 at frequency f_0 is then found from

$$\log y_0 = m \log f_0 + b' \qquad \text{(B.7)}$$

Table B.1 Regression coefficients for estimating specific attenuation

Frequency (GHz)	k_H	k_V	α_H	α_V
1	0.0000387	0.0000352	0.912	0.880
2	0.000154	0.000138	0.963	0.923
4	0.000650	0.000591	1.121	1.075
6	0.00175	0.00155	1.308	1.265
7	0.00301	0.00265	1.332	1.312
8	0.00454	0.00395	1.327	1.310
10	0.0101	0.00887	1.276	1.264
12	0.0188	0.0168	1.217	1.200
15	0.0367	0.0335	1.154	1.128
20	0.0751	0.0691	1.099	1.065
25	0.124	0.113	1.061	1.030
30	0.187	0.167	1.021	1.000
35	0.263	0.233	0.979	0.963
40	0.350	0.310	0.939	0.929
45	0.442	0.393	0.903	0.897
50	0.536	0.479	0.873	0.868
60	0.707	0.642	0.826	0.824
70	0.851	0.784	0.793	0.793
80	0.975	0.906	0.769	0.769
90	1.06	0.999	0.753	0.754
100	1.12	1.06	0.743	0.744
120	1.18	1.13	0.731	0.732
150	1.31	1.27	0.710	0.711
200	1.45	1.42	0.689	0.690
300	1.36	1.35	0.688	0.689
400	1.32	1.31	0.683	0.684

APPENDIX C

COEFFICIENTS FOR CONVERSION OF ANNUAL TO WORST-MONTH STATISTICS

Table B.1 β and Q_i values for various propagation effects and locations

	Rain effect terrestrial attenuation	Rain effect slant path attenuation	Rain rate	Multipath	Trans-horizon land	Trans-horizon land
Global	0.13, 2.85	0.13, 2.85	0.13, 2.85	0.13, 2.85	0.13, 2.85	0.13, 2.85
Canada Prairie and North	0.08, 4.3					
Canada Coast and Great Lake	0.10, 2.7					
Canada Coast and Great Lake	0.13, 3.0					
United States of America Virginia		0.15, 2.7				
Australia Temperate/coastal			0.21, 2.25			
Australia Subtropical/coastal			0.15, 3.01			
Australia Tropical/arid			0.11, 4.35			
Japan Tokyo	0.20, 3.0					
Japan Yamaguchi		0.15, 4.0				
Japan Kashima		0.15, 2.7				
Congo	0.25, 1.5					
Europe North West	0.13, 3.0	0.16, 3.1		0.13, 4.0	0.18, 3.3	
Europe North West 1.3 GHz						0.11, 4.9
Europe North West 11 GHz						0.19, 3.7
Europe Mediterranean	0.14, 2.6	0.16, 3.1				
Europe Nordic	0.15, 3.0	0.16, 3.8		0.12, 5.0		
Europe alpine	0.15, 3.0	0.16, 3.8				
Europe Poland	0.18, 2.6					
Europe Russia	0.14, 3.6					
Indonesia	0.22, 1.7					

APPENDIX D

EXAMPLE OF CACULATION FOR LOG-NORMAL TEST OF FADE DURATION DISTRIBUTION

Import arranged data file N=

:=

C:\Kmitlthesis\Bfade.xls

Determine mean and standarddeviation

$$\mu := \frac{1}{n} \cdot \sum_{i=1}^{n} \ln(x_i) \qquad \mu = 1.982$$

$$\sigma := \sqrt{\frac{1}{n-1} \cdot \sum_{i=1}^{n} (\ln(x_i) - \mu)^2} \qquad \sigma = 0.913$$

Test-of-fit

$$w_i := \text{cnorm}\left(\frac{\ln(x_i) - \mu}{\sigma}\right)$$

$$A := \left[-n - \frac{1}{n} \cdot \left[\sum_{i=1}^{n} (2 \cdot i - 1) \cdot (\ln(w_i) + \ln(1 - w_{n-i+1})) \right] \right] \cdot \left(\frac{2.25}{n^2} + 1 + \frac{0.75}{n} \right)$$

$$A = 0.761$$

Probability plot

$$p_i := \frac{(i - 0.3)}{n + 0.4} \qquad t := 0 \qquad z_i := \text{root}(\text{cnorm}(t) - p_i, t)$$

$$y_i := 0.5 + 0.21 \cdot z_i \qquad r_i := 0.5 + 0.21 \cdot \frac{(\ln(x_i) - \mu)}{\sigma}$$

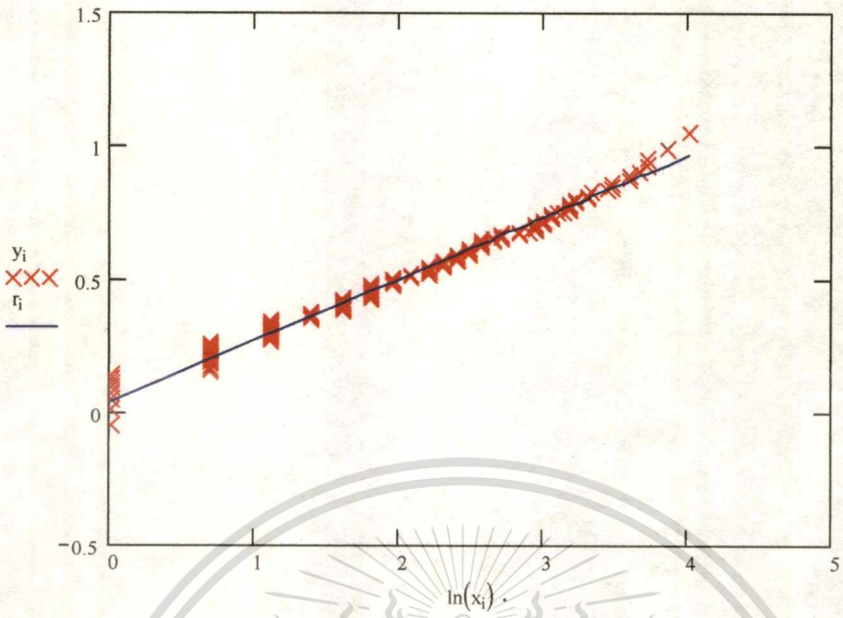

Fig. D.1 Example plot of log-normal function test fitting for fade duration

The above process is used to test log-normality of fade duration. For test of the fit at 5% level of significance, 5% critical value is 0.752. The sample value, A, is close to the critical value, so the estimated model is approximately excepted. Moreover, the data plot looks linear and the model fit looks reasonable; thus, a log-normal model appears reasonable.

AUTHOR BIOGRAPHY

Author: Prasit Nakonrat

Date of Birth: June 10, 1973

Place of Birth: Yasothon Province, Thailand

Bechelor Degree: B.Eng of Electrical Engineering

Institution: Department of Electrical Engineering

Faculty of Engineering

Khon Khean University

Year of Graduation: 1995

Experience during doing master degree :

2000-2001 Participating 1 year exchange student in JUSST (Japanese University Studies in Science and Technology) program at the University of Electro-Communications, Tokyo, Japan

June 2000 Short-term researching in Prof.Yoshiaki MORIYA's Lab. at Tokai University, Japan

Interested Reseaches:

Radiowave propagation on satellite communication

Radio software, adaptive array antenna

Related Publications:

1. P nakonrat, P. Phodpong and N. Hemmakorn. "Ku band attenuation statistics in tropical zone," 2000 Asia-Pacific Symposium on Broadcasting and Communications, Bangkok, Thailand, pp. 175-180, Dec. 2000.
2. P. Nakonrat, T. Boonchuck and N. Hemmakorn, "Rain and rain attenuation in unique high rainfall region in tropical zone," PIERS 2001, Osaka, Japan, 2001.
3. P Nakonrat, T Taniguchi and Y Karasawa, "Estimation of Near-Field Interfernce Source Position for Satellite Communications by Using MUSIC Algorithm," 2001 IEICE General Conference, the University of Electro-Communications, Tokyo, Japan, Nov. 2001.